VLÁKNA a TEXTIL

3

Volume 26.
September
2019

FIBRES AND TEXTILES

STU FCHPT

TECHNICAL UNIVERSITY OF LIBEREC
Faculty of Textile Engineering

Trenčianska univerzita Alexandra Dubčeka v Trenčíne
Fakulta priemyselných technológií v Púchove

VÚCHV

VÚTCH CHEMITEX

Spoločnosť priemyselnej chémie

CHEMOSVIT FIBROCHEM

Indexed in:
SCOPUS
Chemical Abstracts
World Textiles

ISSN 1335-0617
print version

ISSN 2585-8890
online version

Fibres and Textiles
Vlákna a textil

Published by

- Slovak University of Technology in Bratislava, Faculty of Chemical and Food Technology
- Technical University of Liberec, Faculty of Textile Engineering
- Alexander Dubček University of Trenčín, Faculty of Industrial Technologies
- Slovak Society of Industrial Chemistry, Bratislava
- Research Institute of Man-Made Fibres, JSC, Svit
- VÚTCH – CHEMITEX, Ltd., Žilina
- Chemosvit Fibrochem, JSC, Svit

Vydáva

- Slovenská technická univerzita v Bratislave, Fakulta chemickej a potravinárskej technológie
- Technická univerzita v Liberci, Fakulta textilní
- Trenčianska univerzita Alexandra Dubčeka v Trenčíne, Fakulta priemyselných technológií
- Slovenská spoločnosť priemyselnej chémie, Bratislava
- Výskumný ústav chemických vlákien, a.s. Svit
- VÚTCH – CHEMITEX, spol. s r.o., Žilina
- Chemosvit Fibrochem, a.s., Svit

Editorial office and distribution of the journal
(Redakcia a distribúcia časopisu)

Ústav prírodných a syntetických polymérov
Fakulta chemickej a potravinárskej technológie
Slovenská technická univerzita v Bratislave
Radlinského 9, 812 37 Bratislava, SK
Tel: 00 421 2 59 325 575
e-mail: marcela.hricova@stuba.sk

Order and advertisement of the journal
(Objednávka a inzercia časopisu)

Slovenská spoločnosť priemyselnej chémie,
člen Zväzu vedecko-technických spoločností
Radlinského 9, 812 37 Bratislava, SK
Tel: 00 421 2 59 325 575
e-mail: marcela.hricova@stuba.sk

Order of the journal from abroad – excepting Czech Republic
Objednávka časopisu zo zahraničia – okrem Českej Republiky

SLOVART G.T.G, s.r.o. EXPORT-IMPORT
Krupinská 4, P.O.Box 152, 852 99 Bratislava, SK
Tel: 00421 2 839 471-3, Fax: 00421 2 839 485
e-mail: info@slovart-gtg.sk

Typeset and printing *(Sadzba a tlač)*

FOART, s.r.o., Bratislava

Journal is published 4x per year
Subscription 60 EUR

Časopis vychádza 4x ročne
Ročné predplatné 60 EUR

Evidenčné číslo MKCR SR Bratislava EV 4006/10

IČO vydavateľa 00 397 687

Fibres and Textiles (3) 2019
Vlákna a textil (3) 2019
September 2019

Special issue venue the 22nd International Conference STRUTEX 2018
"Structure and Structural Mechanics of Textiles"
held on December 5.- 7. 2018 in Liberec, Czech Republic

Content

Předložená publikace je souhrnem odborných prací předních textilních odborníků z celého světa, Fakulty textilní a také studentů doktorských studijních programů na Fakultě textilní Technické univerzity v Liberci.
Práce jsou tematicky rozděleny do dvou kapitol dle sekcí konference. Kapitola první obsahuje práce k tématu Struktura a strukturní mechanika textilií. Kapitola druhá se týká inovací a aplikací textilního výzkumu.
Všechny příspěvky byly vybrány odbornou komisí, která zajistila jejich vysokou odbornou úroveň.

prof. Ing. Bohuslav Neckář, DrSc.

THE STRUCTURE OF ARCHAEOLOGICAL TEXTILES FROM THE EARLY AND HIGH MIDDLE AGES IN FINDS FROM THE CZECH REPUBLIC (PART 2)

Helena Březinová, Milena Bravermanová and Jana Bureš Víchová

Institute of Archaeology of the Czech Academy of Sciences, Prague, Czech Republic
brezinova@arup.cas.cz, milena.bravermanova@seznam.cz, JVichova@seznam.cz

The Part 1 was published in the issue 1/2019.

1 PROTO-LAMPAS

Proto-lampas is a weave composed of a main warp, a binding warp and two weft systems - a ground weft and a pattern weft which, depending on the demands of the pattern, run either on the obverse or reverse of the fabric. The warp threads are often grouped in the ratio of two main warp threads to one binding warp thread. The ground is in an extended tabby weave and is composed of all warp threads and the ground weft, the pattern weft lies beneath the main warp and interlaces with the binding warp in a 1.2 twill S on the face. The pattern is composed of the pattern weft, which lies above the main warp and is connected by a binding warp in a 1.2 twill S on the face; the ground weft is in a tabby weave. The proportion of ground wefts to the pattern wefts in the following order is characteristic: one ground weft, one pattern weft, one ground weft, two pattern wefts (see 1.1). Other variants also exist (see 1.2).

Proto-lampas weaves appear at the turn of the 11th century, when in the Byzantine Empire, in a historical region in West Asia situated within the Tigris-Euphrates river system and in Persia, interest in monochrome patterned fabrics grew. Several weaving techniques emerged differentiating the ground and pattern structure, thus making it possible to emphasise the decorative motifs on monochrome fabrics. Proto-lampas was one of these techniques, as the grainy surface of tabby alternates here with the glossy surface of twills [1].

1.1 Fabric with pointed ovals (?) [2, pp. 461-462, 479]

Find circumstances: Prague Castle, St. Vitus Cathedral, graves of the Prague bishops, probably Bishop Cosmas (†1098)
Storage; inventory number: Church treasury at St. Vitus (held by the Prague Castle Administration); K 441
Dating: 11th century (?)
Provenance: Byzantine Empire (?), Syria (?)
Technical analysis (Figure 1)
Textile type: proto-lampas
Warp proportion: 2 main warps to 1 binding warp
- main: silk, z-twist, brown colour
- binding: silk, z-twist, brown colour
découpure: 1 main warp
count: 32 threads per cm (main warp), 16 threads per cm (binding warp)

Weft proportion (pass): 2 ground wefts to 3 pattern wefts (1 ground weft, 1 pattern weft, 1 ground weft, 2 pattern wefts)
- ground: silk, no visible twist, brown colour
- pattern: silk, no visible twist, brown colour
count: 30 passes per cm
découpure: 4 passes (?)

Characteristics of the weave: ground - extended tabby; pattern - 1.2 twill S; classic proto-lampas
Pattern: indeterminable, it is possible that it was conceived as pointed ovals
Pattern rapport: indeterminable
Original use: burial vestment

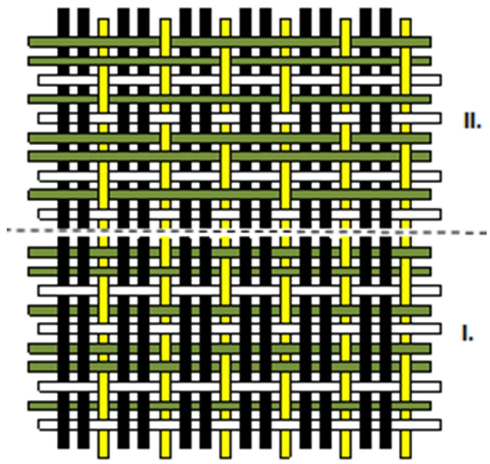

Figure 1 Fabric with pointed ovals (?): weave diagram: I. - ground; II. - pattern

1.2 Fabric with two patterns - birds in medallions and small connected medallions [2]

Find circumstances: Prague Castle, St. George's Basilica, reliquary tomb of St. Ludmila
Storage; inventory number: Prague Castle collection; PHA 35/03, HS 10999

Dating: about 1000 - first third of the 11th century
Technical analysis (Figure 2a, b)
Textile type: proto-lampas
Provenance: Byzantine Empire (?), Byzantine province in contact with the Islamic countries

Warp proportion: 1 main warp to 1 binding warp
- main: silk, z-twist, natural colour
- binding: silk, z-twist, natural colour
découpure: 1 main warp
count: 18-22 threads per cm (main warp), 18-22 threads per cm (binding warp)

Weft proportion (pass): 1 ground weft to 1 pattern weft
- ground: silk, no visible twist, natural colour
- pattern: silk, no visible twist, natural colour
count: 50-58 passes per cm
découpure: 3 passes

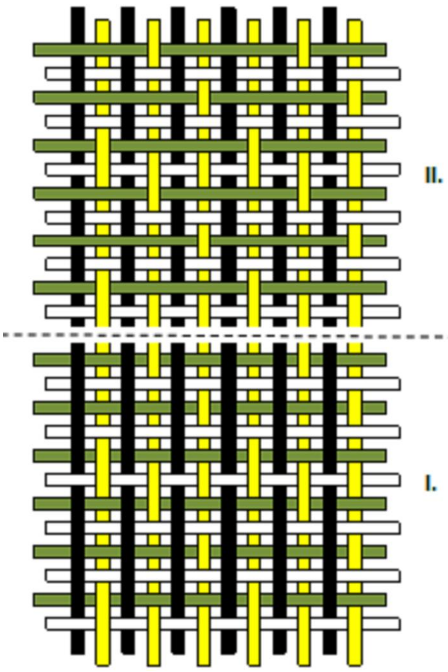

a)

b)

Figure 2 Fabric with two pattern: a) weave diagram: I. - ground; II. - pattern; b) fabric detail © Prague Castle Administration, photo: J. Gloc

Characteristics of the weave: ground - extended tabby; pattern - 1.2 twill S; unlike classic proto-lampas, there is a different ratio of warps and wefts in passes; an early variant of proto-lampas
Pattern (large): much of the preserved fabric is decorated with a large pattern with touching medallions formed by double rings; the space between the two lines is filled with tendrils; inside the medallions, birds sit in trees along the sides with their feet touching the pedestal in the shape of leaves; the connecting discs between the medallions form a double circle with pearl roundel; a flower is inside the circle; the spaces between the medallions are filled with flowers
Pattern (small): a smaller pattern in the lower strip of the preserved fabric features one row of medallions made from double circles filled with four small birds standing opposite each other in pairs; the second strip features medallions made from double lines with obliquely placed diamonds with inscribed squares; this octagon is filled with four birds standing opposite one another with flowing ribbons around their neck; in the upper and lower corner of the octagon are small discs; in the side corners are anchored crosses, and the round and octagonal medallions are continuously interconnected by loops
Pattern rapport (large): height 18-24.2 cm, height 24.3-28.2 cm
Pattern rapport (small): the full height is not preserved, the width is half the width of the large pattern
Original use: originally a dalmatic that was one of the wrappings for the relics of St. Ludmila

2 LAMPAS

Lampas is a term used for figured textiles in which a pattern composed of weft floats bound by a binding warp is added to a ground fabric formed by a main warp and a ground weft. The ground may be tabby, twill, satin, etc. The weft threads forming the pattern may be main, pattern or brocading wefts. They float on the face as required by the pattern and are bound by the ends of the binding warp in a binding ordinarily tabby or twill and which is supplementary to the ground weave.

Lampas was developed sometime in the 11th century, presumably in Iran or Iraq, from where production expanded around the year 1100 to the entire eastern Mediterranean, to Sicily and Islamic Spain. The application of this technique began in northern Italy in the 13th century. Lampas was the predominant weave in the 14th century [3, 4].

2.1 Fabric with a small medallion between larger medallions (?) [5]

Find circumstances: Prague Castle, St. Vitus Cathedral, graves of the Prague bishops, probably Bishop Bernard Kaplíř (†1240)

Storage; inventory number: Church treasury at St. Vitus (held by the Prague Castle Administration); K 435
Dating: 12th century (?)
Provenance: Byzantine Empire, Syria
Technical analysis (Figure 3a, b)

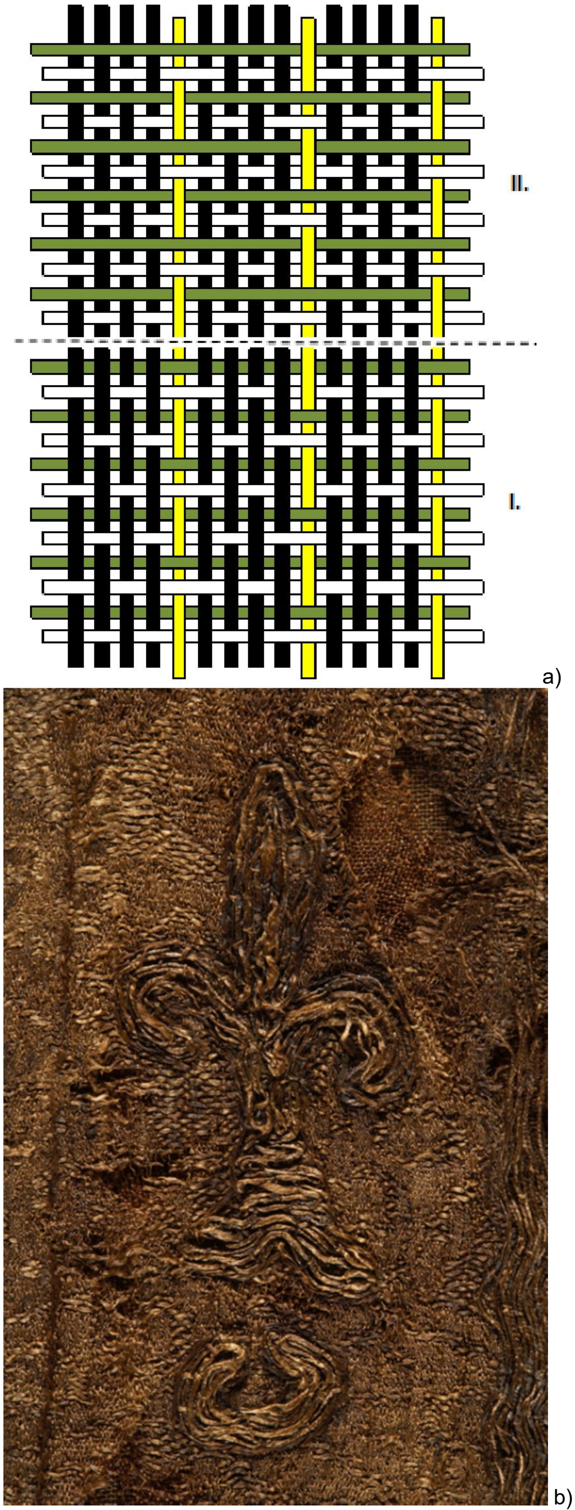

Figure 3 Fabric with small medallion between larger medallions: a) weave diagram: I. - ground; II. - pattern; b) fabric detail © Prague Castle Administration, photo: J. Gloc

Textile type: lampas
Warp proportion: 4 main warps to 1 binding warp
- main: silk, z-twist, light brown colour
- binding: silk, z-twist, light brown colour
découpure: 4 main warps
count: 68 threads per cm (main warp),
17 threads per cm (binding warp)

Weft proportion (pass): 1 ground weft to 1 pattern weft
- ground: silk, no visible twist, light brown colour
- pattern: silk, no visible twist, light brown colour
count: 24 passes per cm
découpure: 1 pass

Characteristics of the weave: ground - tabby (main warp and ground weft); pattern - tabby (binding warp and wefts in passes)
Pattern: the ground is composed of vertically placed round medallions demarcated by two lines; the space between them is filled with pearl roundel; the centre of the medallions is a flower; two bands made of two lines are always connected to the medallion, again filled with pearl roundel and assembled in an angle who peak always touches the next round medallion
Pattern rapport: indeterminable
Original use: mitre stitched with gold thread

2.2 Fabric with palmettes and a diamond mesh [6]

Find circumstances: Prague Castle, Cathedral of St. Vitus, Royal crypt, possible coffin of Charles IV (†1378)
Storage; inventory number: Prague Castle collection; PHA 41/06, HS 25847
Dating: first half of 14th century
Provenance: Central Asia or north China
Technical analysis (Figure 4a, b)
Textile type: lampas
Warp proportion: 3 pairs of main warp to 1 binding warp
- main, paired: silk, z-twist, blue-green colour
- binding: silk, no visible twist, ochre colour
découpure: 3 pairs of main warp
count: 42 pairs thread per cm (main warp),
14 threads per cm (binding warp)

Weft proportion (pass): 1 ground weft to 1 pattern weft I. to 1 pattern weft II.
- ground: silk, no visible twist, blue-green colour
- *I. pattern*, *interrompu*: silk, no visible twist, ochre colour
- *II. pattern*: gold-plated animal substrate; preserved in minute remnants
count: 12 passes per cm
découpure: 1 pass

Characteristics of the weave: ground - warp-faced 5-end satin (interruption 2; main paired warp and ground weft); pattern - tabby (binding warp and wefts in passes)
Pattern: composed of wide horizontal strips filled with grid ornament; the background features rows of two alternating types of palmette blossoms moved by half of their spacing
Pattern rapport: height 12.6 cm, width 25 cm
Original use: perhaps a dalmatic (only one sleeve and several small fragments are preserved)

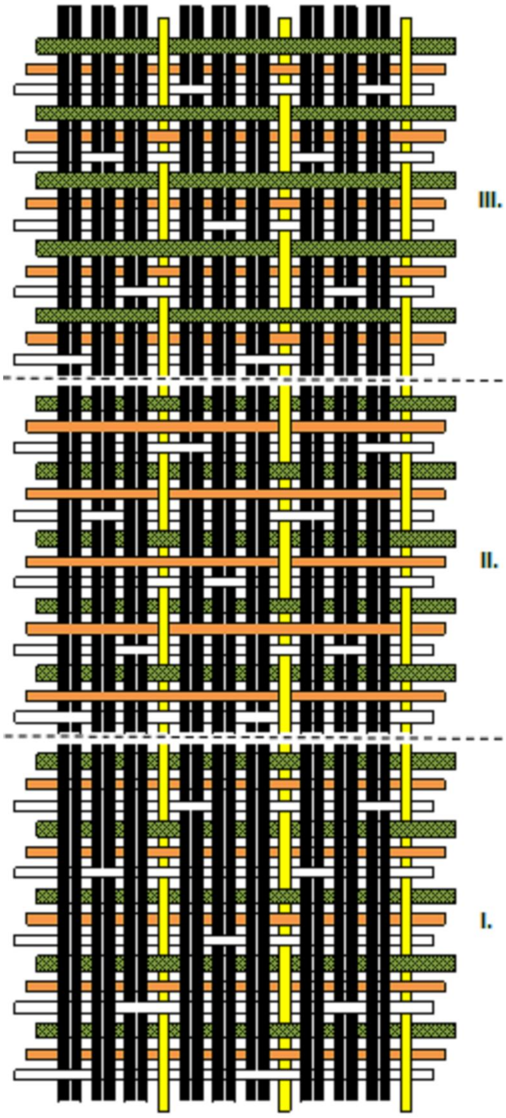

a)

b)

Figure 4 Fabric with palmettes and diamond mesh: a) weave diagram: I. - ground; II. - pattern - effect of weft I.; III. - pattern - effect of weft II.; b) fabric detail © Prague Castle Administration, photo: J. Gloc

2.3 Fabric with pairs of Chinese dogs, birds and a pseudo-Islamic inscription [7]

Find circumstances: Prague Castle, St. Vitus Cathedral, Royal crypt, coffin of Charles IV (†1378) or George of Poděbrady (†1471)
Storage; inventory number: Prague Castle collection; PHA 41/04, HS 21142
Dating: second half of the 14th century
Provenance: Italy
Technical analysis (Figure 5a, b)
Textile type: lampas, double weave in ground

Warp proportion: 3 pairs of main warp to 1 binding warp
- main, paired: silk, z-twist, green colour
- binding: silk, no visible twist, ochre colour

découpure: 2 pairs of main warp
count: 45 pairs of thread per cm (main warp), 15 threads per cm (binding warp)

Weft proportion (pass): 2 ground wefts to 1 pattern weft
- ground: silk, weak z-twist, green colour
- pattern: gold-plated metal strip wound around a silk core (S twist, ochre colour),

assembly S, couvert
count: 24 passes per cm
découpure: 1 pass

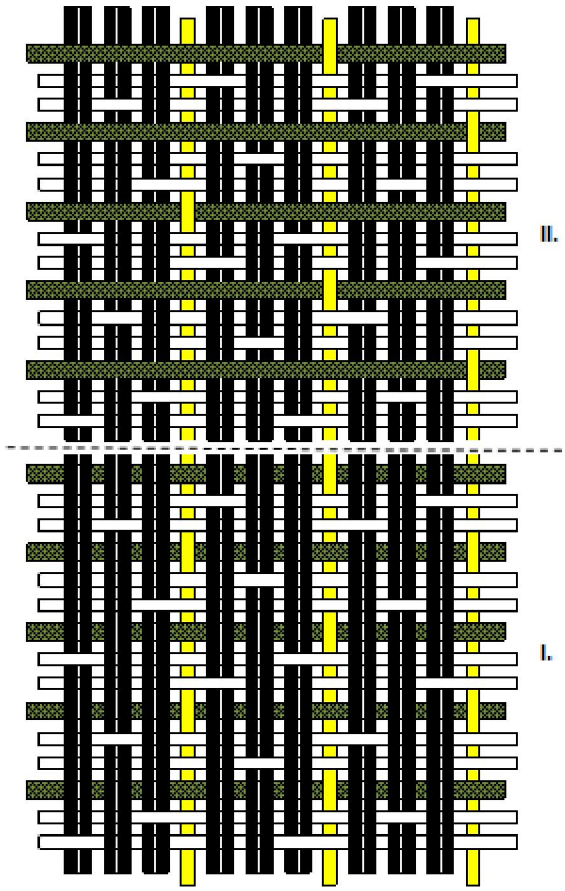

a)

Figure 5a Fabric with a pair of Chinese dogs, birds and pseudo-Islamic inscription: weave diagram: I. - ground; II. - pattern

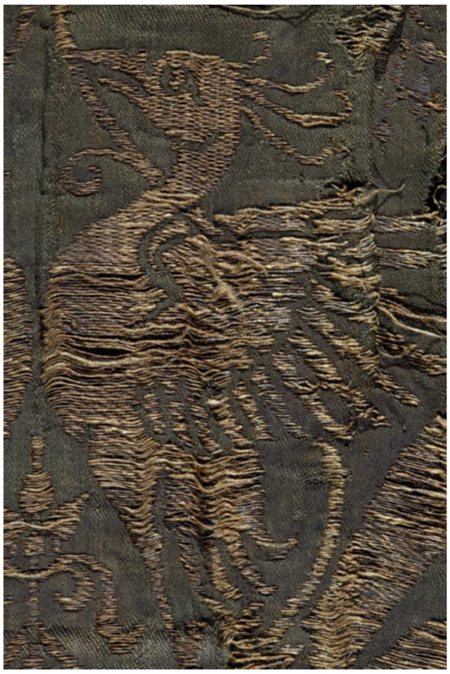

b)

Figure 5b Fabric with a pair of Chinese dogs, birds and pseudo-Islamic inscription: fabric detail © Prague Castle Administration, photo: J. Gloc

Characteristics of the weave: ground - warp-faced 5-end satin (interruption 2; main paired warp and ground weft); pattern - 1.2 twill S (binding warp and pattern weft); where the pattern weft on the reverse is beneath the ground, it is connected to the binding weft in a tabby weave, but not connected in satin weave; in places with the pattern, the binding warp also runs beneath the ground wefts, thus binding the otherwise separate layers of the fabric
Pattern: a pair of Chinese birds flying towards one another from incomplete lotus palmettes connected below by a band with pseudo-Islamic characters; in their beak, the birds are carrying stalks from which a pair of leaves are growing, and between them is a pair of Chinese dogs
Pattern rapport: height 36.3 cm, width c. 9.2 cm
Original use: dalmatic

3 VELVET

Velvet is a pile weave in which the pile is produced by a pile warp which, by the introduction of thin metal rods during weaving, is raised in loops above a ground weave. Velvets can be classified based on the nature of the pile, e.g. in cut velvet the loops formed by the pile warp are cut, in uncut velvet the loops formed by the pile warp are left uncut.

The real velvet was woven in China and the Near East in the 13th and 14th centuries, despite the fact that knowledge of the loop pile warp technique is much older. The first European town to produce velvet was Lucca, Italy, at the end of the 13th century. Production then spread to other Italian towns, to Spain, France, Germany and England. Velvet was initially monochrome; polychrome velvet and velvet with patterns were introduced later [3, 4, 8].

3.1 Unpatterned velvet [9]

Find circumstances: Prague Castle, St. Vitus Cathedral, Royal crypt, coffin of John of Görlitz (†1386)
Storage; inventory number: Prague Castle collection; PHA 53/09, HS 25824
Dating: second half of 14th century
Provenance: Italy
Technical analysis (Figure 6a, b)
Textile type: velvet
Warp proportion: 3 main warps to 1 pile warp
- main: silk, z-twist, brown colour
- pile: silk, no visible twist, brown colour
count: 45 threads per cm (main warp), 15 threads per cm (pile warp)

Weft proportion (pass): 3 wefts to 1 rod
silk, no visible twist, brown colour
count: 45 threads per cm

Characteristics of the weave: ground - extended tabby; cut velvet; cut pile warp interlaces with one ground weft identically over one and beneath two weft threads
Pattern: unpatterned; pile covers the entire surface of the fabric
Original use: cloak with a long and free cut composed of trapezoidal segments - 'houppelande'

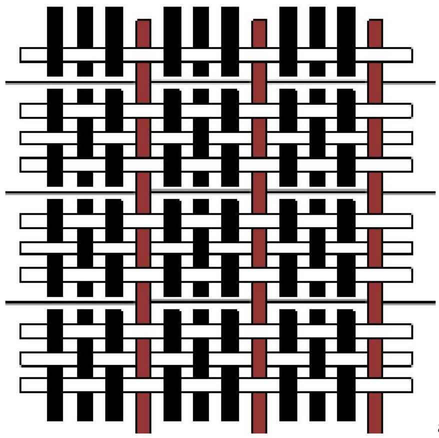

a)

b)

Figure 6 Unpatterned velvet: a) weave diagram; b) fabric detail © Prague Castle Administration, photo: J. Gloc

3.2 Velvet with a grape motif [7]

Find circumstances: Prague Castle, Cathedral of St. Vitus, Royal crypt, coffin of Charles IV (†1378)
Storage; inventory number: Prague Castle collection; PHA 41/03, HS 21141
Dating: second half of the 14th century
Provenance: Italy
Technical analysis (Figure 7a, b)
Textile type: velvet
Warp proportion: 6 main warps to 1 pile warp
- main: silk, z-twist, brown colour
- pile: silk, no visible twist, brown colour

count: 78 threads per cm (main warp), 13 threads per cm (pile warp)
découpure: 1 pile warp (pile warp effect), 1 main warp (brocading weft effect)

Weft proportion (pass): ground and pile warp effect – 3 ground wefts to 1 rod
ground and brocading weft effect - 3 ground wefts to 2 brocading wefts (2 ground wefts, 1 brocading weft, 1 ground weft, 1 brocading weft)
- ground: silk, no visible twist, brown colour
- brocading: gold-plated metal strip wound around a silk core (S twist, brown colour), assembly S, *couvert*

count: 39 threads per cm (ground weft), 26 threads per cm (brocading weft)
découpure: 1 brocading weft (brocading weft effect), 1 rod (pile warp effect)

Characteristics of the weave: ground - warp-faced 6-end satin (interruption 3-2-3-2-0-2); pattern - a) cut pile warp interlaces with one ground weft identically over one and beneath two weft threads; b) brocading weft binds in 1.3 weft-faced twill Z with each fifth main warp thread
Pattern: small, S-shaped twigs in oblique rows; each twig has two leaves turned to the opposite side (in cute pile) and one grape-shaped flower from a brocading weft
Pattern rapport: height 15.5 cm, width 15 cm
Original use: semi-circular cloak composed of either horizontally or vertically placed bands

4 CONCLUSION

In the period from the Early to Late Middle Ages, a wide variety of weaves and techniques were used to weave textiles. While only a small number have been preserved in archaeological contexts in the Czech environment, basic weaves, more complicated techniques and their variations testify to the advanced level of medieval textile production. Available finds document common household textile production as well as the ability of ruling dynasties, Church dignitaries and nobles to acquire luxury imported goods.

Acknowledgements: *This work was accomplished with institutional support RVO:67985912. For their assistance in producing this article, we thank the Archaeological Institute of the Czech Academy of Science and the Prague Castle Administration.*

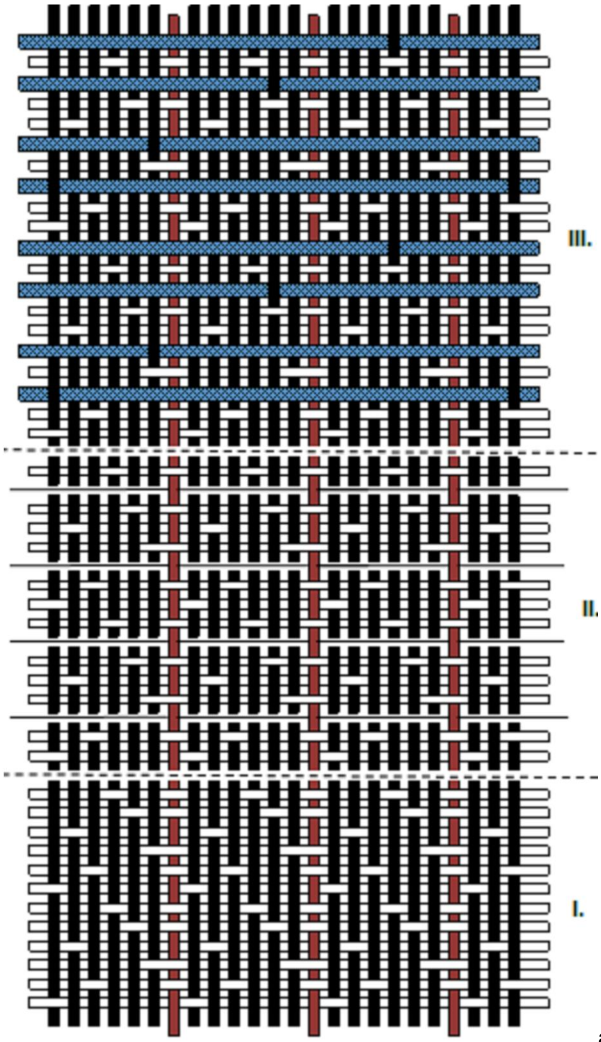

a)

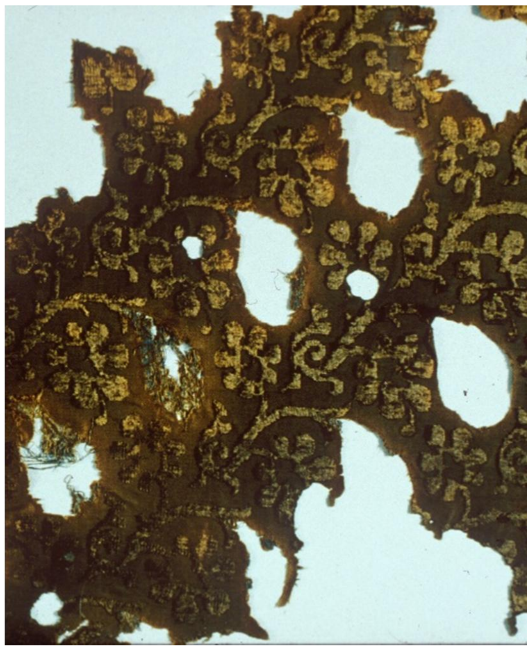

b)

Figure 7 Velvet with a grape motif: a) weave diagram: I. - ground; II. - pattern - pile warp effect); III. - pattern - brocading weft effect; b) fabric detail © Prague Castle Administration

5 REFERENCES

1. Schorta R.: Monochrome Seidengewebe des hohen Mittelalters (Monochrome silk fabric of the high Middle Ages), Deutscher Verlag für Kunstwissenschaft Berlin, 2001, pp. 34-41, ISBN 3871571830
2. Bravermanová M., Otavská V., Sliwka A., Beneš J., Kopecká I., Mazura I.: Nové poznatky o nejstarších textiliích z hrobu sv. Ludmily. Neue Erkentnisse von den ältesten Textilien aus dem Relikviengrab der Heiligen Ludmila (New knowledge about the oldest textiles from the grave of St Ludmila), Archaeologia historica 26(1), 2001, pp. 447-486, http://hdl.handle.net/11222.digilib/140436
3. von Wilckens L.: Die textilen Kunste. Von der Spätantike bis um 1500 (The textile arts. From late antiquity until 1500), Verlag, München, 1991, ISBN 3406353630
4. Geijer A.: A History of Textile Art, Pasold Research Fund in association with Sotheby Parke Bernet, London, 1979
5. Bravermanová M., Foltýn D., Sliwka A.: Mitra z hrobu 'ctihodného Bernarda, biskupa pražského' (The mitre from the grave of 'venerable Bernard, the Prague bishop'), Medievalia historica Bohemica 13(1), 2010, pp. 7-45
6. Bravermanová M., Brabcová T., Odstrčilová S., Prajzlerová A., Vrabcová A.: Nové poznatky o pohřebním rouchu Karla IV. z královské krypty v katedrále sv. Víta. Neue Erkenntnisse über das Begräbnisgewand Karl IV. aus der königlichen Krypta in der St.-Veits-Kathedrale (New knowledge about the funeral vestments of Charles IV. from the royal crypt in st. Vitus), In: Nachtmannová, A., Klapetková, O. (Eds.): Oděv a textil v životě člověka doby lucemburské (Clothing and Textiles in the Life of a Man of Luxembourg Time), Praha, 2017, pp. 17-40
7. Bravermanová M., Kloudová R., Otavská V., Vrabcová A.: Pohřební roucho Karla IV. z královské krypty v katedrále sv. Víta. Das Beerdigungsgewand des Karl IV aus der königlichen Krypta in der Kathedrale des Hl. Veit (Funeral robe of Charles IV. from the royal crypt in st. Vitus), Archaeologia historica 30(1), 2005, pp. 471-496, http://hdl.handle.net/11222.digilib/140639
8. Zhao F., Li W., Chen J., Huang N., Peng H.: Chinese Silks (The Culture and Civilization of China), Watt J.C.Y., Kuhn D. (Eds), Yale University Press, 2012, pp. 399-402, ISBN 0300111037
9. Bravermanová M., Kloudová R.: Pohřební oděv Jana Zhořeleckého z královské hrobky v katedrále sv. Víta na Pražském hradě. Begräbnisgewand von Jan Zhořelecký aus der königlichen Gruft im Sankt -Veits -Dom in der Prager Burg (Funeral clothing of Jan Zhořelecký from the royal tomb in the Cathedral of Sts. Vitus Cathedral at Prague Castle), Archaeologia historica 31(1), 2006, pp. 403-412, http://hdl.handle.net/11222.digilib/140682

Footnotes:

1) Illustrations of weave diagrams are processed according to the following key:

- main warp
- binding warp
- pile warp
- ground weft
- ground weft II.
- pattern weft
- pattern weft – metal thread
- brocading weft
- brocading weft – metal thread
- weft
- weft II.
- weft *interrompu*
- weft *interrompu* – metal thread
- rod

IMPACT OF HEAT ON RECOVERY EFFICIENCY OF CAR SEATS FABRICS

Viera Glombikova, Petra Komarkova and Zdenek Kus

Technical University of Liberec, Faculty of Textile Engineering, Department of Clothing Technology
Studentska 1402/2, Liberec, Czech Republic
petra.komarkova@tul.cz

Abstract: *This paper deals with investigating performance of car seat fabrics in terms of their compression and recovery properties influenced by heat degradation. Polyurethane foam, nonwoven and 3D knitted spacer fabrics are commonly used as padding (in middle layer) in car seats cover. The current work presents an alternative approach to evaluate effectivity of car seat fabrics, namely behaviour of their middle layers before and after heat degradation which simulates hot summer condition. In summary, results show that 3D spacer is the most appropriate middle layer for car seat cover because of its recovery properties is very good at both before and after heat degradation (about 94% from original thickness) on the contrary PU foam. The PU foam is very good at recovery behaviour under standard ambient conditions (temperature about 25°C) on the other hand PU foam recovery significantly decreases (about 40% against 3D spacer) after impact of high temperature.*

Keywords: *car seats cover, compression, recovery, heat degradation.*

1 INTRODUCTION

There are approximately 3-5 kg car seat cover fabrics used in each car [1]. Car seat covers are often composed of several layers of different materials, usually polyester fabric (or leather or synthetic leather) laminated to polyurethane foam (or 3D knitted spacer or nonwoven) backing by an adhesive. Each part of car seat cover brings different properties which affect both their durability and comfort in automotive seating. One group of researchers prefer polyethylene terephthalate (PET) fibres for automotive application (both for top and middle layers) due to their superior properties, like a high tenacity, abrasion, light, heat and chemical aging, UV resistance, dimensional stability, recyclability etc. [2-5]. The others are in favour of modified PU foam (in middle layer) because of their excellent elasticity and very good recovery to compression [4]. Study on comparison of quality for different types of seat cover padding was carried out from aspects of physiological properties and relaxation behaviour after static and dynamic loading [6]. The result of this study showed that warp knitted spacer fabrics demonstrate better recovery to compression, better thermal properties and better breathability as compared to PU foam [6]. The other research found out that fabrics using monofilament as spacer yarn generally have higher compression resistance than multifilament yarns [2, 7]. Major car manufacturers evaluate degree of car seat durability, including relaxation behaviour after cyclic loading by special equipment, which uses the robot. This robot allows realistic simulation, of someone getting into and out of the seat (ingress/egress test), or of strong pulsation or vibration during driving [8]. The current study is focused on investigating performance of car seat fabrics in terms of their compression and recovery properties influenced by heat degradation which simulates hot summer condition.

2 EXPERIMENTAL

2.1 Materials

Tested materials were designed in order to understand the role of middle layer of textile sandwich car seats from point of view of their compression and relaxation behaviour. There were used different middle layers (polyurethane foam, nonwoven and 3D spacer) in the tested samples. Material in top layer was the same – PES woven fabric. Basic characteristics of all tested car seat fabrics are shown in Table 1.

The Figures 1a-1c show 3D structures of all tested middle layers by means of micro tomography system. Before being tested, the samples had been washed and conditioned for 24 hours. The measurement was carried out in an air-conditioned room under constant relative humidity of 65% and the temperature of 21°C. Measurements of thickness were performed under 100 Pa.

Table 1 Basic characteristic of the tested samples

Code	Structure	Raw material	Thickness [mm]	Weight [g/m²]
		Top layer		
	woven fabric, twill	100% PES, twill	0.7	203
		Middle layer		
A	3D warp knitted spacer	100% PES	6.2	408
B	nonwoven	70% PES / 30% wool	5.7	230
C	foam	100% PUR	4.1	247

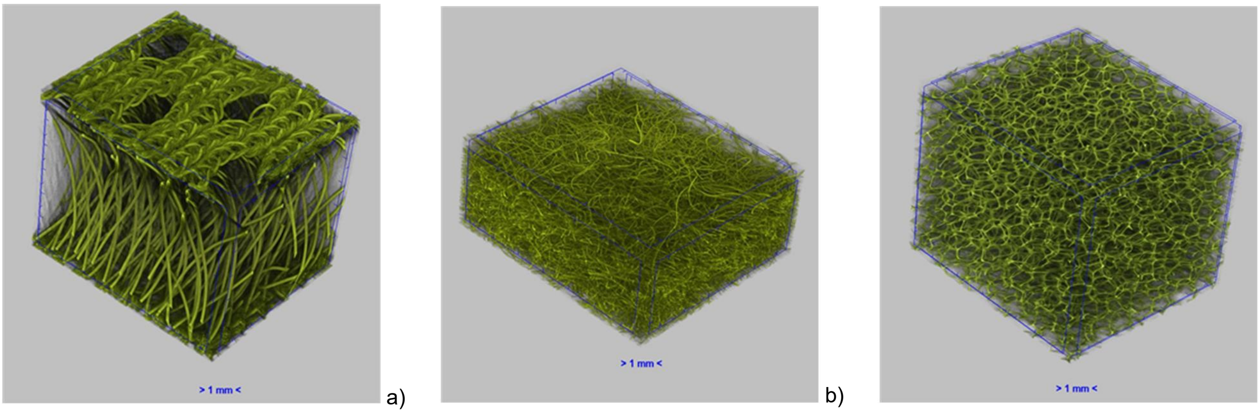

Figure 1 a) 3D spacer, b) nonwoven, c) foam

2.2 Methods

The compression and relaxation behaviour were investigated before and after degradation of tested samples in autoclave which simulates hot summer conditions. It is important to uncover how cyclic compressive loading combined with above mentioned degradation influence recovery of car seat cover for the lifetime period.

The results were compared and discussed in order to understand the real performance of tested materials. Final values (means) of all tested parameters correspond to five measurements on average. The coefficients of variation for all tests do not exceed 10% and therefore not statistically significant.

Simulation of sample degradation by heat

Generally, the autoclave is a piece of equipment used for sterilizing various requirements in the lab by wet sterilization method. Car producer very often use this device for testing car seat fabric to simulate accelerated degradation by high temperature corresponds to hot summer conditions.

Principle autoclave is following. When water is heated in a closed container, saturated steam is produced under pressure. According to Boyle's Law, when volume of the steam is kept constant, the temperature is directly proportional to pressure. If the pressure is reduced, it boils at a lower temperature. If the pressure rises, it boils at a greater temperature. The autoclave Sano LA-MCS was used for degradation of samples, see Figure 3. Applied conditions for degradation were: 120°C during 20 hours.

Compression and relaxation behaviour

Repeated compression - recovery test was carried out by the device developed by Technical University of Liberec [9] as shown in Figure 2. This simple device consists of transparent Perspex cylinder (diameter of base is 14 cm) and pressure plate for set of required compression. Loading time was set to 24 hours and the pressure of static loading was 12 kPa. Value of pressure corresponds to maximum real loading of car seat during sitting of driver [10]. Relaxation behaviour given by the thickness recovery of samples was investigated after above mentioned compression test, when load was removed The measurement of recovery was carried out immediately, 10 min, 20 min, 40 min, 1 h, 2 h and 3 h after test. The referred compression - recovery test was repeated 5 times for each sample. The thickness of tested samples was measured by compression tester SDL M 034A according to EN ISO 5084 both before and after loading (pressure 1000 Pa). The recovery R [%] were determined by means of equations (1), see below. Recovery is given as the degree which a sample mass recovered to its original height upon unloading.

$$R = \left(\frac{h_2}{h_1}\right) * 100 \quad [\%] \tag{1}$$

where h_1 is the original height of the samples,
h_2 is the height of samples after removal of load.

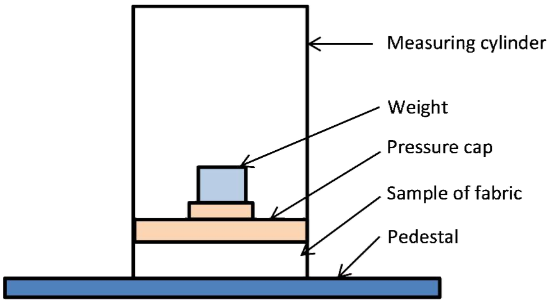

Figure 2 Schema of recovery measurement

Figure 3 SanoClave LA MCS

3 RESULTS AND DISCUSSION

The results of the recovery tests are presented in Figure 4 and Figure 5.

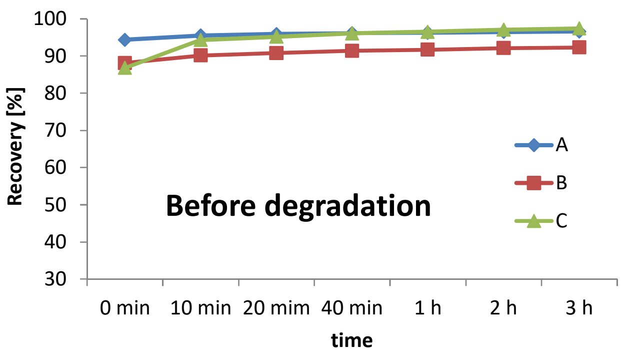

Figure 4 Recovery of tested samples before degradation

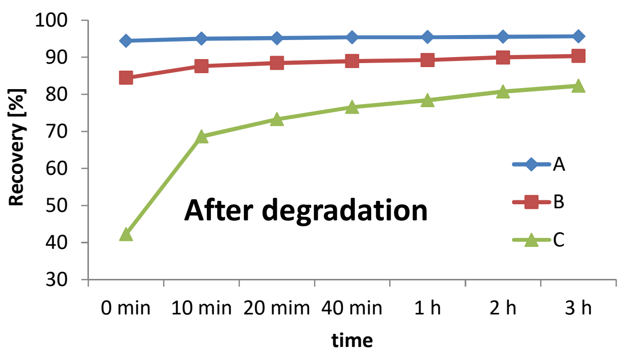

Figure 5 Recovery of tested samples after degradation

The results, as shown in Figures above, indicate that the difference between the groups was significant. The recovery before degradation of Group A (3D warp knitted spacer in middle layer) was equal to recovery after degradation, i.e. 94.4% immediately 96.2% after 40 min and 96.6% after 3 hours. Group B (nonwoven) reports decrease of recovery after degradation about 2% than before degradation. The impact of degradation was most pronounced in Group C (foam) when recovery before degradation was 86.8% immediately, 96.1% after 40 min and 97.4% after 3 hours and recovery after degradation was 42.2%, 76.6% and 82.3%.

4 CONCLUSIONS

The results of this study are consistent with data obtained in other researches which studied using of 3D spacer in car seat cover. The most obvious finding to emerge from this study is that 3D spacer is the most appropriate middle layer for car seat cover in view of the fact that its recovery properties is very strong in both before and after heat degradation (about 94% from original thickness) on the contrary PU foam. The PU foam is very good at recovery behaviour under standard ambient conditions (temperature about 25°C). On the other hand PU foam recovery significantly decreases (about 40% against 3D spacer) after impact of high temperature. PU foam is degraded by combination of hydrolysis and thermal oxidation, which causes shortening of the polymer chains. Further research could usefully explore compression and relaxation behaviour of tested materials using not static but dynamic loading. A further study might also focus on determining relaxation behaviour after lower degradation temperature than standardized 120°C.

ACKNOWLEDGEMENTS: *This work was supported by the Ministry of Education, Youth and Sports of the Czech Republic and the European Union – European Structural and Investment Funds in the frames of Operational Programme Research, Development and Education – project Hybrid Materials for Hierarchical Structures (HyHi, Reg.No.CZ.02.1.01/0.0/0.0/16_019/0000843).*

5 REFERENCES

1. Fung W., Hardcastle J.M.: Textiles in automotive engineering, Woodhead Publishing limited Cambridge, England, UK, 2000, 384 p., ISBN 9781855734937
2. Yip J., Ng S.P.: Study of three-dimensional spacer fabrics: Physical and mechanical properties, Journal of Materials Processing Technology 206(1-3), 2008, pp. 359-364, https://doi.org/10.1016/j.jmatprotec.2007.12.073
3. Koc K.S., Mecit D., Bozaci B., Ornek M., Hockenberger A.: Effect of filament cross section on the performance of automotive upholstery fabric, Journal of Industrial Textiles 46(3), 2015, pp. 1-15, https://doi.org/10.1177/1528083715598652

4. Jerkovic I., Pallares J.M., Capdevila X.: Study of the abrasion resistance in the upholstery of automobile seats, Autex Research Journal 10(1), 2010, pp. 14-20
5. Glombikova V., Komarkova P., Havelka A., Kolinova M.: Approach to evaluation of car seats fabrics performance, Industria Textila 69(2), 2018, pp. 96-103, ISSN 1222-5347
6. Ye X., Fangueiro R., Hu H., de Araujo M.: Application of warp - knitted spacer fabrics in car seats, Journal of the Textile Institute 98(4), 2007, pp. 337-343, https://doi.org/10.1080/00405000701489677
7. Chen S., Long H.R.: Investigation on compression properties of polyurethane-based warp-knitted spacer fabric composites for cushioning applications, Part II. Theoretical and experimental verification, Industria Textila 65(6), 2014, pp. 340-344
8. Stewart R., O'Bannon T., Müller M., Beeh F.: Creating the Next Generation Ingress/Egress Robot, SAE Technical Paper 1999-01-0628, 1999, https://doi.org/10.4271/1999-01-0628
9. Glombikova V.: Apparatus for measuring compressibility of volume textile structures, national utility model application, 2013, Application number: 2013-27589, Registration number: 25543, Website: http://isdv.upv.cz/webap/webap.pts.det?xprim=1949313&lan=cs&s_majs=&s_puvo=%25Glomb%C3%ADkov%C3%A1%2%20viera&s_naze=&s_anot=
10. Mazari F.B., Havelka A.: Pressure distribution of car seat at different angle of backrest, Vlákna a textile (Fibres and Textiles) 22(3-4), 2015, pp. 33-39

THE EFFECT OF RIBS ON COOLING ABILITY OF WETTED SHIRT KNITS AT LOW AIR VELOCITY

Lubos Hes[1] and Monika Boguslawska-Baczek[2]

*[1]Technical University of Liberec, Faculty of Textiles, Department of Textile Evaluation
Studentska 2, 461 17 Liberec, Czech Republic,
[2]Katowice School of Technology, Faculty of Architecture, Civil Engineering and Applied Art, Department of Design
43 Rolna Street, 40-555 Katowice, Poland
lubos.hes@gmail.com*

Abstract: *In hot-wet countries, a possible way to increase thermophysiological comfort of sweating dressed humans is to wear elastic shirts with larger surface, like rib fabrics. In the paper, the cooling ability of 6 various wetted fabrics with surface ribs subject to parallel air flow was investigated. It was found that at low air velocity the ribs did not provide the expected enhanced cooling effect. In the last part of the study, the cooling effect of thin wetted woven fabrics was investigated.*

Keywords: *thermal comfort, rib shirts, wet state, cooling flow.*

1 INTRODUCTION

At high body activity, typical for running sportsman, the body generates up to 1000 W of metabolic power, from which more than 80% should be transferred away from the body in the form of heat. At low outside air temperatures t_A, most of this heat Q [W] is transferred from the human skin of temperature t_{sk} and surface S by simple convection, characterized by the heat transfer coefficient α, as follows:

$$Q_{conv} = \alpha.S.(t_{sk} - t_{out}) \qquad (1)$$

However, when the air temperature exceeds 25-30°C, the convection cooling is not sufficient. Then, body starts to generate sweat. In some body parts the partial pressure of the evaporated sweat/water reaches the saturate level p_{sat}. If the partial pressure of the water vapour (wv) in the outside air p_{out} is low enough, then the convection cooling flow generated by water evaporated from the active area $S.w$ (w lies between 0 and 1) is given by the relationship:

$$Q_{conv\ evap} = ß.L.w.S.(p_{sat} - p_{out}) \qquad (2)$$

where L (2 500 000 J/kg) presents the latent heat of evaporation and $ß$ is the mass transfer coefficient.

The evaporative cooling is extremely efficient, provided the difference of the wv partial pressure is big enough. However, in hot/wet countries the mentioned driving force is too low. The only theoretical way to increase the cooling flow from the body of a moving person is to increase the mass transfer area (surface) of the shirt tightly covering the body of the person exposed to these extreme climatic conditions. The only way to increase this area is the use of relatively large ribs vertically outstanding from the fabric surface.

2 MATERIALS AND METHOD

Vertical ribs were prepared by sewing on 8 various single jersey knits made of 100% PES Coolmax and its blends with PES Thermocool, Modacryl and Lycra. Square mass extended from 169 to 213 g/m^2. The ribs dimensions were: height 5 and 10 mm, distance between the ribs was 10 and 15 mm.

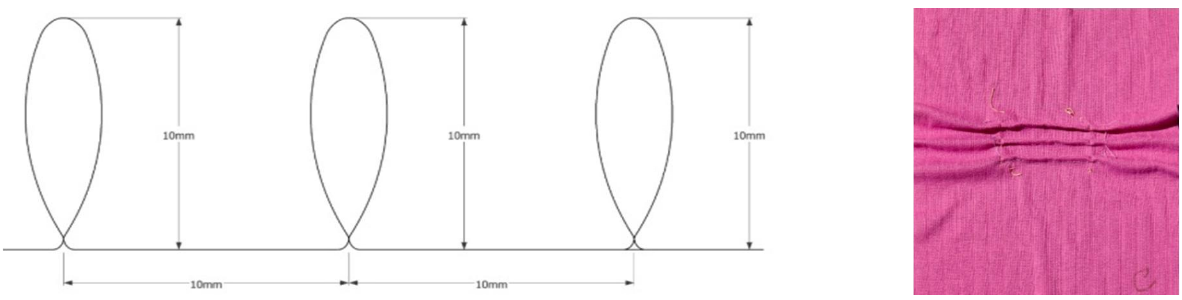

Figure 1 Geometry and appearance of vertical ribs on fabrics

2.1 Calibration of the 100% cooling flow

The Eq. 2 presents the level of cooling flow, where the parameter β is the convection mass transfer coefficient – see in [2]. This coefficient β can be determined by means of the dimensionless Sherwood *Sh* and Schmidt *Sc* numbers defined by the next relations (*b* is the dimension, *v* is the viscosity of the humid air):

$$Sh = \beta.b/D_u \quad (3)$$

$$Sh = 0.664\ Re^{1/2}.Sc^{1/3} \text{ (for air flow parallel to a plane)}$$

$$Re = v.b/\nu$$

where the term D_u is the coefficient of water vapour diffusion into air for t = 20°C and for p = 0.1013 MPa it reaches the value $1.136.10^{-5}$ $m^2.s$. The term *Re* is another dimensionless number, reaching here the value of 4970, for the velocity v = 1 m/s used in the PERMETEST instrument.

Having completed all the calculations we obtain the level of the Sherwood number:

$$Sh = 0.664\ Re^{1/2}.Sc^{1/3} = 39.48 \quad (4)$$

$$Sc = 0.60 \text{ (for air at room temperature)}$$

As $\beta = Sh.D_p/v$ then (for w = 1, S = 1 m^2) from the above theory and Eq. (2) follows:

$$\begin{aligned} Q_{conv\ evap} &= \beta.L.[(p_{sat} - p_{out}) = \\ &= L.0.664\ Re^{1/2}.Sc^{1/3}\ D_p^{2/3}\ (p_{sat} - p_{out}).M_D/R.T = \\ &= L.1.161.10^{-7}(p_{sat} - p_{out}) \end{aligned} \quad (5)$$

where the term $M_D/R.T$ presents a conversion parameter enabling the use of difference of wv partial pressure instead of dimensionless wv concentration drop.

$$\begin{aligned} Q_{conv\ evap} &= 2.5.\ 10^6.1.161.10^{-7}.1250 = \\ &= 362.8\ W/m^2 \end{aligned} \quad (6)$$

The determined cooling flow presenting in the PERMETEST instrument the 100% cooling effect is quite high. However, in real situations, when a person is wearing a wetted dress under identical climatic conditions, this level of cooling is never achieved, as sweating coefficient *w* characterising the relative distribution of zones with intensive sweating is mostly lower than 0.4. Thus, the effective cooling flow around 200 W/m^2 already presents a realistic value.

3 EXPERIMENTAL RESULTS

Relative water vapour permeability *P* of the tested samples meaning the relative cooling flow Q_{cool} was determined by means of the Czech commercial PERMETEST instrument, which was in Czech Republic recently certified as satisfying the ISO 11092 standard. During the initial test on dry samples, the samples were (over the semi-permeable membrane) placed on the wetted microporous surface, which well simulates a human skin with 100% relative cooling flow. The lowest relative cooling effect, 59% exhibited sample No. 4 (modacryl + Thermocool), whereas the higher cooling effect, 72%, offered the sample No. 5 (PES Thermocool). Beside the measurement of cooling flow on dry smooth samples, also the cooling flow from dry rib samples was determined. All these values were determined for the air flowing with the velocity 1 m/s along the ribs.

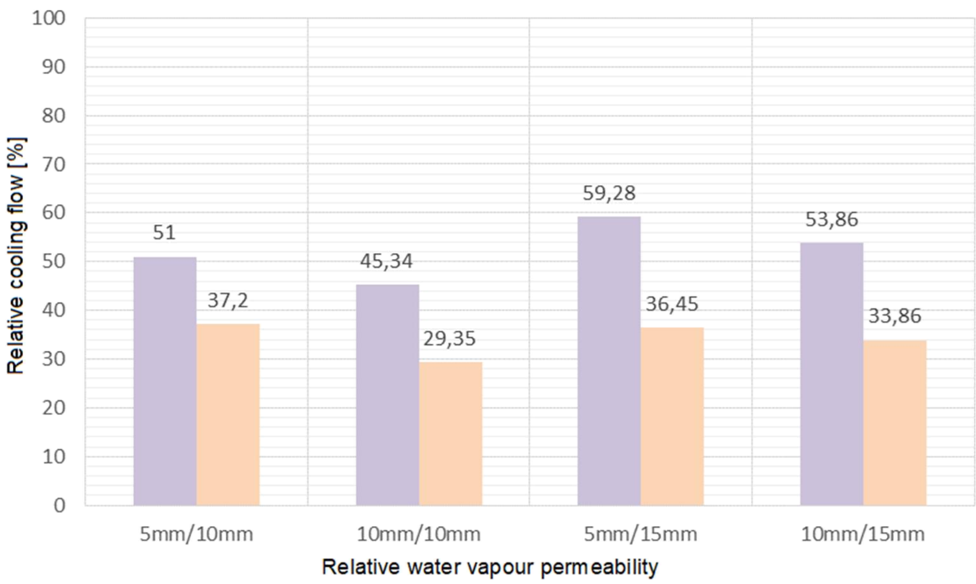

Figure 2 Relative cooling flow / Relative water vapour permeability of fabrics in dry state. Higher levels present the results for ait flow parallel with the ribs, then in case of the air flow across the ribs. It is evident, that the ribs provide lower wv permeability then smooth fabrics

Next experiments were focused on the objective of this study: investigation of the influence of the size of mass (heat) transfer area, executed by forming the surface ribs on the studied fabrics, on the cooling effect given by evaporation of moisture from these rib fabrics enhanced by convection heat transfer from the fabrics.

From the Figure 4 follows that against expectation, the rib fabrics under the applied experimental conditions exhibit lower heat and mass transfer of water vapour than smooth fabrics. Explanation of this observation may depend in the possibility that at low air velocity the thermal boundary layer is quite thick, runs above the ribs and does not create thermal contact with the bottom area between the ribs. Second explanation may take into consideration that cooling effect generated on the upper parts of the ribs is not properly conducted toward the basic level of the fabric, which is in direct contact with the simulated skin. The amendment of the limited heat conduction along the height of ribs may depend in the use special fibres (carbon fibres) with very high thermal conductivity in the design of the ribs. However, carbon fibres are stiff and do not conduct moisture as well as the COOLMAX fibres used in this research.

As long as the smooth textile surfaces provide the highest cooling effect, it will be important to investigate the effect of the fabric structure and composition. This research should respect the same experimental conditions as in the above study: the wetted fabrics will be placed (over the semi-permeable porous membrane) on the wetted surface which simulates sweating human skin.

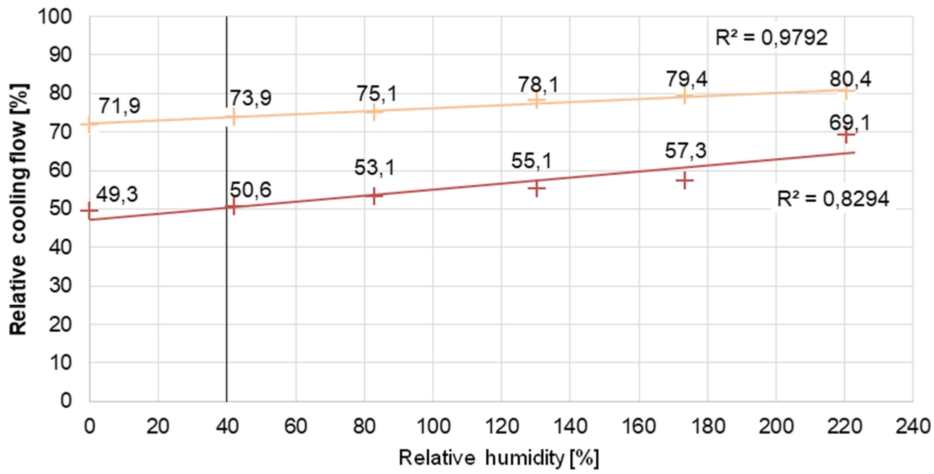

Figure 3 The effect of the sample relative humidity on the relative cooling flow released from the sample No. 5 (PES Thermocool). The higher levels were determined for the air flow parallel with the ribs. Height of the ribs 5 mm, distance 15 mm

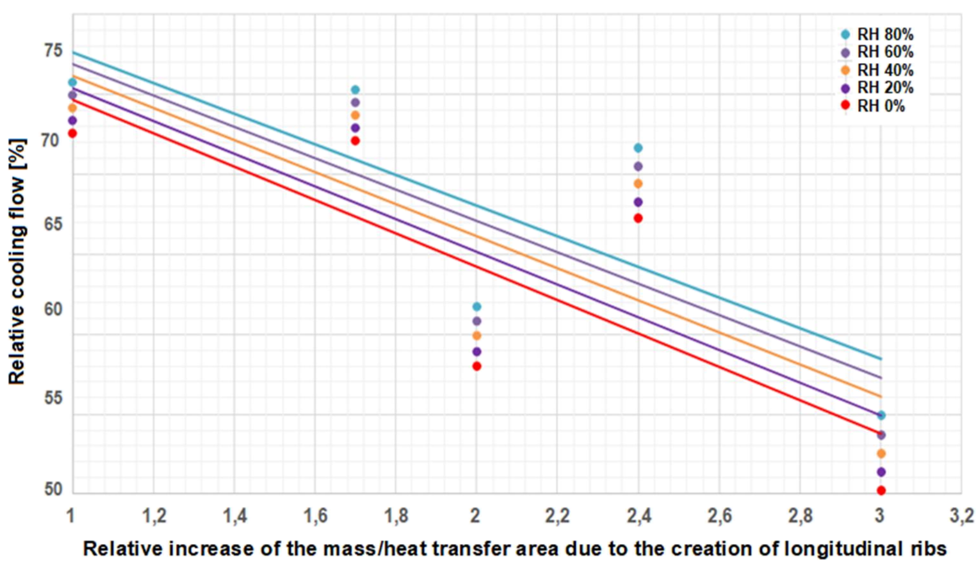

Figure 4 The effect of fabric relative humidity and heat transfer area on the relative cooling flow of the most efficient fabric No. 5 from the Themocool fibres, when the air passes along the ribs (better case)

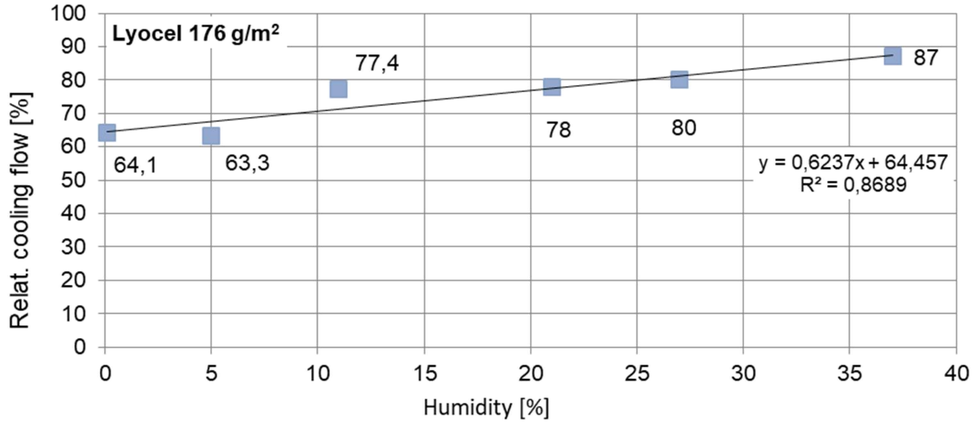

Figure 5 The effect of the fabric relative humidity on the relative cooling flow of the most efficient smooth Lyocel fabric

3.1 *Cooling effect of selected smooth fabrics in wet state*

Five thin woven fabrics in a plain structure made of cotton (square mass 163 and 95 g/m^2), Lyocel viscose (square mass 175 and 96 g/m^2), PES (square mass 92 g/m^2) and PA nanofibre layer (square mass 5.3 g/m^2) were stepwise wetted and relative cooling flow generated by evaporation water from their surface in the PERMETEST instrument was registered. The 100% relative cooling flow was caused by evaporation of water from the porous surface which simulates human skin.

The objective of this study was the determination of a fabric with the highest cooling effect in wet state, which should be used for design of a comfortable sport dress. As the reference value of the relative moisture *U* of the fabric was 40%, which presents the moisture level when the increased friction between a skin and a fabric starts to cause sensorial discomfort.

The highest relative cooling flow 90% was observed when testing the Lyocel fabric with the square mass 176 g/m^2. The lowest cooling flow 63% was registered for the cotton fabric with the square mass 163 g/m^2. Other fabrics provided the cooling flow in the range from 72 to 79%.

4 CONCLUSION

In the paper, the cooling ability of 6 various knitted fabrics with 4 different surface ribs subject to air flow was investigated. The stepwise wetted samples were inserted into the PERMETEST Skin model with ribs oriented parallelly and perpendicularly to the air flow and the relative cooling flow was recorded. This relative heat flow was then converted (calibrated) into the real cooling flow.

It was found that at low air velocity the ribs did not provide the expected enhanced cooling effect. In the last part of the study the cooling effect of thin wetted woven fabrics was investigated. The highest level was observed for the relatively thick Lyocel woven fabric.

5 REFERENCES

1. Hes L., Dolezal I.: A new portable computer-controlled skin model for fast determination of water vapour and thermal resistance of fabrics, Asian Textile Conf. (ATC 7), New Delhi, 2003
2. Bogusławska-Bączek M., Hes L.: The Effective water vapour permeability of wet wool fabric and blended fabrics, Fibres & Textiles in Eastern Europe 21(1), 2013, pp. 67-17
3. Slancova M.: Knits with enhanced cooling (in Czech), MSc Thesis, TU Liberec, 2018
4. Karakoc Y.: Cooling efficiency of selected fabrics, Research Report, TU Liberec, 2017

HYDROPHOBIC AND ANTIBACTERIAL TREATMENT OF TEXTILES USING ORGANIC-INORGANIC HYBRID LAYERS PREPARED BY SOL-GEL

Vojtěch Miller[1], Hana Šourková[2], Irena Lovětinská Šlamborová[1], Petr Exnar[1] and Jiří Škach[3]

[1]Faculty of Science, Humanities and Education; Department of Chemistry; Technical University of Liberec Studentska 2, 461 17 Liberec, Czech Republic,
[2]The Institute for Nanomaterials, Advanced Technology and Innovation; Technical University of Liberec Studentska 2, 461 17 Liberec, Czech Republic,
[3]Hernia Center, Regional Hospital of Liberec, Husova 357, 460 63 Liberec, Czech Republic
vojtech2miller@gmail.com, hana.sourkova@tul.cz, irena.slamborova@tul.cz, petr.exnar@tul.cz, jiri.skach@nemlib.cz

Abstract: *The sol-gel method allows the preparation of organic-inorganic layers with the possibility of adjusting the resulting properties to a relatively wide range. Potentially very interesting treatments are hydrophobic or antibacterial layers that can be applied to practically all types of textiles. Their main advantage is, in addition to their excellent adhesion to the fabric surface, their high resistance to both mechanical and chemical attack. On non-polar textiles, the increase in layer adhesion is supported by surface plasma treatment. Resistance of layers on fabrics has been confirmed by functionality even after repeated washing.*

Keywords: *Sol-gel method, hydrophobicity, antibacterial layer, textile, organic-inorganic hybrid material, plasma treatment.*

1 INTRODUCTION

The sol-gel process is a chemical method for preparing nanolayers and is mainly used in the synthesis of the oxidic layers. Its utilization increases due to its universality and simplicity, without the need for expensive laboratory equipment for the vacuum processes. Other advantages include cleanliness and homogeneity of the final product.

The principle of the sol-gel process rests in the preparation of the sol – mainly from the alkoxides. Prepared sol is afterwards applied onto the surface of the substrate (by wetting, spraying, etc.). Evaporation of the remaining solvent and placing the sol in contact with the air humidity leads to an exponential increase in hydrolysis and rapid transformation of the sol into a gel and further to a xerogel. In the case of hybrid inorganic-organic materials, the final step is to polymerize the coating material either by the heat or by the UV light if there are any photo-initiators built into the nanolayer [1-3].

The research that includes the undertaken experiments in this paper targets the development of hydrophobic or antibacterial coating for the textile materials.

2 EXPERIMENTAL

2.1 Materials

Pure cotton (further referred as Ba) and pure polyester (further referred as PE) were chosen for the first series of experiments that compares microbiological behavior of the textiles with antibacterial or hydrophobic (also antifouling) layers.

AMANDA (100% PE), CARLTON (100% Ba) and TAURUS (mixed Ba/PE 50/50) textiles were chosen for the second series of the experiments that deals with the optimization of the hydrophobic coating.

Monofils for the medical hernia nets Bard Mesh (polypropylene monofil, further referred as PP monofil), manufacturer C. R. Bard, Inc. and Parietex Hydrophobic 3-Dimensional Mesh (PE monofil), manufacturer Covidien were chosen for the third series of the experiments that test possibilities of the treatment of the medical materials.

<u>Preparation of sols and their application</u>

All of the sols for the surface treatment of the tested textiles were prepared by the sol-gel method from 3-(trimethoxysilyl)propyl methacrylate and tetraethoxy-silane in the isopropyl alcohol solvent by an acid catalysis.

The sol marked as AD30 was used for the antibacterial treatment – bounded cations of silver, copper and zinc were added to the basic composition and the acid catalysis was secured by adding a small amount of nitric acid. Composition of this sol and its preparation are protected by patents [4-6].

Hydrophobic treatments were applied by the sol AE10 and further by the sols from series AF (AF8-2, AF10-2 and AF12-2), all of them with added catalytic amount of a hydrochloric acid. As a hydrophobic agent in sols AE10, AF10-2 and AF12-2 was used trialkoxyalkylsilane with alkyl-hexadecyl in this case. The sols AE10 and AF10-2 were different only in the details of the preparation. The sol AF12-2 had enhanced volume of hexadecyl groups. The hexadecyl was substituted with a dodecyl in the sol AF8-2. The detailed process of synthesis of the hydrophobic sols is described in publication [7].

All of the layers are characterized by an excellent chemical resistance against all organic solvents and water solutions except highly concentrated alkali hydroxides and hydrofluoric acid. The thickness of the layers can be adjusted from 80 to 200 nm according to the dilution of the sols and the way of the application of the sol.

All of the samples of the textiles were cleaned by repeated soaking into the isopropyl alcohol or by a plasmatic treatment (in the case of the hernia nets) prior to the application of the sols. The application of the sols onto the surface of the tested textiles was done by foulard (pressure 5 bars, velocity of cylinders 3 m/min). The application of the sols onto the hernia nets was done by soaking the nets in the sol followed by pulling out – this process was chosen due to the structure of the material – knitwear. The application of the sols was followed by the heat polymerization, which was done in 85°C/3 h (in the case of materials with PE or PP) or in 150°C/2 h (in the case of pure Ba).

Plasmatic treatment of hernia nets

For enhancing adhesion of antibacterial layers onto the hernia nets and similar substrates it was necessary to treat the surface by plasma with a vacuum aperture by application of the oxygen plasma (device LA400, flow of oxygen 200 sccm with pressure 100 Pa, 10 s for PP monofil, 60 s for PE monofil) in the company SurfaceTreat Turnov. The adhesion of the applied layers especially onto the PP monofil without this treatment was insufficient. There was also tested an atmospheric plasma treatment of the surfaces but the results were inconvenient (worse adhesion of the layers with the low intensity, destruction of monofils with higher intensity).

2.2 Methods

Determining of antibacterial properties

Following pathogenic bacterial strains from the Czech collection of microorganisms of Masaryk University Brno were used to test the antibacterial properties.

1. *Escherichia coli* (E.C.) - CCM 2024 (ATCC 9637), gram-negative bacteria (G-).

2. *Staphylococcus aureus* (S.A.) - CCM 2260 (ATCC 1260), gram-positive bacteria (G+).

AATCC Test Method 147-2016 [8]

This method is qualitative, tentative and it should be done prior to the method AATCC 100-2012. The antibacterially treated sample is placed on the agar which is standardly applied with the bacterial inoculum in several lines. A modification of this method was used in this case where the bacterial inoculum was applied to the whole surface of the agar. After 24 hours of incubation there was rated grow of the bacteria under the tested sample as well as the inhibitory (halo) zone around the sample.

Specific conditions of the tests: There was cut a square sample of 18x18 mm (according to the norm). 1 ml of the bacterial inoculum with a concentration of 10^5 CFU/ml was inoculated individually on a Petri dish with the blood agar. Tested sample was put in the middle of the dish and firmly pressed to the agar. The incubation took place in a thermostat with 37°C for 24 hours. After the specified incubation there was the halo zone rated (its area) and the inhibition of bacteria under the sample (place of a sample).

AATCC Test Method 100-2012 [9]

This method is quantitative and there is rated a reduction factor which states the reduction (in percent) of the inoculated concentration of the bacteria due to the effect of the sample. The result is a number of survivor bacteria colonies (CFU) and from this number there is calculated inhibition degree (in %). It is always necessary to compare the treated sample with an untreated one (standard).

Specific conditions of the tests: There was cut a square sample of 18x18 mm which was placed into a sterile container. There was applied 100 µl of the respective bacterial strain with a concentration of 10^5 CFU/ml. Incubation took place in the thermostat with 37°C for 24 hours. After incubation there was added 10 ml of a physiological solution. After vortexing there was pipetted 1 ml and it was inoculated on the Petri dish with the blood agar (there were inoculated triplets from each sample). The result is a sum of number of colonies on all three dishes.

Determination of hydrophobicity

Krüss Drop Shape Analyser DSA30 device in Surface Treat Turnov was used to determine the wetting angles of water. The wetting angle was measured by measuring a small exactly-defined drops placed on the surface of the textile, with a defined volume of 3 µl. The results are calculated as the average of the 10 measurements with the corresponding standard deviation.

3 RESULTS AND DISCUSSION

3.1 Microbiological behavior of textiles with layers

The sol AD30 was used as an antibacterial treatment for the tested textiles (pure cotton Ba and pure polyester PE). Next to the antibacterial treatment based on the effect of cations Ag, Cu and Zn in the active layer there was also tried a treatment of the textiles with the hydrophobic sol AE10 where it was assumed an antifouling effect will take place [10-11]. The antifouling effect restricts the adhesion and the number of bacteria and subsequent creation of the biofilm on the surface of the textile.

The details about the used sols and their application on the tested textile are mentioned in the paragraph 2.1. Testing of the antibacterial properties on the prepared samples of the textiles together with the untreated samples was done both by the qualitative AATCC Test Method 147-2016 and by the quantitative AATCC Test Method 100-2012. The results are summarized in Tables 1 and 2.

Table 1 The results of the antibacterial testing of the textiles by the AATCC Test Method 147-2016

Bacterial strain	Sample	Inhibition zone, inhibition
Escherichia coli	Ba - US	0% inhibition zone, 0% inhibition under the sample
	PE - US	0% inhibition zone, 0% inhibition under the sample
	Ba - AE10	0% inhibition zone, 0% inhibition under the sample
	PE - AE10	0% inhibition zone, 0% inhibition under the sample
	Ba - AD30	Inhibition zone d = 1.3 mm, 100% inhibition under the sample
	PE - AD30	Inhibition zone d = 2.9 mm, 80% inhibition under the sample
Staphylococcus aureus	Ba - US	0% inhibition zone, 0% inhibition under the sample
	PE - US	0% inhibition zone, 0% inhibition under the sample
	Ba - AE10	Inhibition zone d = 5.5 mm, 100% inhibition under the sample
	PE - AE10	0% inhibition zone, 0% inhibition under the sample
	Ba - AD30	0% inhibition zone, 100% inhibition under the sample
	PE - AD30	Inhibition zone d = 5.5 mm, 100% inhibition under the sample

US – untreated standard

According to the acquired results it is visible that the effects on the used bacterial strains differ in partial parameters. In both cases it can be said that the results are greatly positive.

The qualitative method with the hydrophobic treatment of AE10 with the bacterial strain *Escherichia coli* has not showed any inhibitory effect in any of the materials used. On the other hand, with the bacterial strain *Staphylococcus aureus* there has been noted an inhibition zone and 100% inhibition under the sample on the cotton sample. This means that the treatment on the cotton limits the adhesion and the growth of the bacteria *Staphylococcus aureus.* There has been no inhibitory effect noted on the polyester samples.

Table 2 The results of the antibacterial testing of the textiles by the AATCC Test Method 100-2012

Bacterial strain	Sample	Result	% of inhibition
Escherichia coli	Ba - US	UQ	0
	PE - US	UQ	0
	Ba - AE10	28	100
	PE - AE10	300	99.9
	Ba - AD30	2	100
	PE - AD30	2	100
Staphylococcus aureus	Ba - US	UQ	0
	PE - US	450	Sample stops compact growth of test strain
	Ba - AE10	1	100
	PE - AE10	0	100
	Ba - AD30	2	100
	PE - AD30	0	100

US – untreated standard; UQ – unreadable quantity

The quantitative method with the antibacterial treatment of AD30 showed the inhibition under the samples (that means the treatment stopped the growth of the bacteria under the material with a treatment) for both materials (Ba, PE) and there also appeared inhibition zones which indicates that the components of the final layer (cations Ag, Cu and Zn) partially release themselves into the surroundings and inhibit the bacterial strain.

The quantitative method proved excellent or very good inhibitory effect to all of the tested samples with layers. The number of cultivated bacterial colonies of *Escherichia coli* on the materials with the hydrophobic treatment AE10 has been larger than on the other treated samples. Nevertheless, even these results can be rated as good when compared with the standards.

The really important aspect is a stability of the antibacterial layer on the textile substrate which has been verified by repeated washing of cotton socks with the layer AD30. Still suitable antibacterial properties have been observed even after 50th washing by a standard washing cycle [2].

3.2 Hydrophobic treatment of textiles

The hydrophobic treatment of the textiles is interesting for a number of practical uses, mainly for outdoor finishes of sportswear and working cloth. Next to stopping the liquid water penetration, great penetration of water vapors and a long-term preservation of mechanical and utility properties of textiles it has also important ecological aspect. In contrary to commonly used impregnations with the addition of fluorine compounds nor the tested sols nor the final layers contain any ecologically problematic components while keeping all the necessary requirements for the outdoor usage. Table 3 summarizes the results of test with three different test sols. As you can see in the results all of the textiles with the treatment have outstanding hydrophobic properties and there are basically no differences between the tested sols.

Table 3 The results of the water wetting angle measurement on the treated textiles (n = 10)

Textile	Sol	Water	
		Angle [°]	**s_x [°]**
AMANDA (PE)	US	Soaking	
AMANDA (PE)	AF8-2	124.5	4.0
AMANDA (PE)	AF9-2	125.8	2.5
AMANDA (PE)	AF12-2	126.3	2.6
CARLTON (Ba)	US	Soaking	
CARLTON (Ba)	AF8-2	122.8	5.3
CARLTON (Ba)	AF9-2	124.1	4.1
CARLTON (Ba)	AF12-2	124.0	3.2
TAURUS (Ba/PE)	US	Soaking	
TAURUS (Ba/PE)	AF8-2	135.3	4.1
TAURUS (Ba/PE)	AF9-2	132.5	3.0
TAURUS (Ba/PE)	AF12-2	135.1	4.6

s_x – standard deviation; US – untreated standard

3.3 Hernia nets

The hernia implants (nets) are used for a surgical solution of hernias which is a bag-like exit of a peritoneal cavity where part of the abdominal organs moves to. Although there is applied the latest knowledge and used modern materials in the surgical solution, one of the post-operative complication is an inflammation. In the material which are the hernia nets made of can occur so called hiding of the microorganisms from the effects of the immune system and persistence of inflammation or delay of break out in the range from several months to several years [12].

The most promising strategy in the present is the usage of an implant material with added antibacterial properties which stops the bacterial adhesion and creates a biofilm on its surface. The design of these resistant implants [13] is based on a modification of their surface by anti-adhesive substance, antimicrobial agents, antiseptic, antibiotic, metals or their ions or inhibitors of bacterial adherence coatings. These treatments should be nontoxic in the case of releasing controllably-degradable non-affecting original biomechanical properties of the material and non-obstructing integration of the implant to the organism.

Currently there are no hernia nets with the antimicrobial treatment which would meet all the requirements of the nontoxicity. Greatly promising treatment is the applied layer summarized below which contains ions of Ag, Cu, and Zn and very effectively stops growth of the pathogenic bacteria. The results of the testing in this work are summarized in Table 4.

Table 4 The results of antibacterial testing of the hernia nets by the AATCC Test Method 147-2016

Sample	*Escherichia coli*	*Staphylococcus aureus*
PP monofil-US	0% inhibition under the sample	0% inhibition under the sample
PE monofil-US	4% inhibition under the sample	2% inhibition under the sample
PP monofil-AD30	25% inhibition under the sample	100% inhibition under the sample
PE monofil-AD30	100% inhibition under the sample, inhibition zone d=2 mm	100% inhibition under the sample, inhibition zone d=1.5 mm

US – untreated standard

The applied antibacterial treatment to the surface of hernia implants enhanced their antibacterial effect in the comparison with the standards. Even the standard PE monofil proved inhibition under the sample for both the bacterial strains but after the application of the sol the inhibition improved and showed itself as inhibition zones with the material PE. This effect is, especially in the case of the hernia nets, requested because it will not only kill the bacteria in the application spot but also in the near surroundings and prevent creation of the inflammation which could appear as an after-effect of an operation.

4 CONCLUSIONS

The organic-inorganic hybrid layers based on 3-(trimethoxysilyl)propyl methacrylate and tetraethoxysilane prepared by the sol-gel method have great adhesion and long-term durability on the surface of the polar textiles. When the application to the non-polar textile is needed it is necessary to treat the surface of the textile with the low-pressure oxygen plasma.

Significant modification of the properties of the prepared layers can be achieved by adding the proper additions (nitrates of Ag, Cu and Zn for the antibacterial layers, trialkoxyalkylsilanes with alkyl with 12 to 16 carbons for the hydrophobic layers) to the basic composition of the sols.

By using the both standardized methods it was confirmed the antibacterial effectiveness of the layer AD30 on all of the tested textiles and the hernia nets. According to the achieved results it is noticeable that the effects on the used bacterial strains differ in partial parameters but in all of the cases, it can be said that the results are quite positive.

The really important aspect is a durability of the antibacterial layer on the textile substrate which has been verified by repeated washing of the cotton socks with the layer AD30. Still suitable antibacterial properties have been observed even after 50th washing by a standard washing cycle.

In the case of the hydrophobic layer AE10 there have been anticipated just a lesser antifouling effect during the antibacterial tests. The expectation has been confirmed. The qualitative method on the bacterial strain *Escherichia coli* did not show any inhibition effect on neither of the tested materials. On the other hand, the bacterial strain *Staphylococcus aureus* on the cotton showed the inhibition zone plus 100% inhibition under the sample. That means the treatment on the cotton limits the adhesion and the growth of bacteria *Staphylococcus aureus.* There was no inhibitory effect observed on the polyester. The quantitative method on the other hand showed excellent or great inhibitory effect on all of the samples with the hydrophobic layers AE10. The number of the bacterial colonies of *Escherichia coli* on the materials with this treatment has been larger than on the other treated samples. Nevertheless, even these samples can be classified as great when compared with the untreated samples.

The measuring of the water wetting angles on the textiles with all of the types of hydrophobic treatments confirmed that all the textiles with treatment have excellent hydrophobic properties and among both the used sols and the textiles there were no real differences.

The antibacterial treatments of the textiles (both the classical and the hernia nets) are greatly perspective for a medical usage. This treatment causes antibacterial effect that leads to the death of tested bacteria. The hydrophobic treatment had significantly lower effectiveness during antibacterial tests. Still, for a number of usages in common life is it enough to stop adhesion and further bacterial growth (bacterial-static effect).

The hydrophobic treatment of the textiles is interesting for a number of practical uses, mainly for the outdoor finishes of sportswear and working cloth. In contrary to the commonly used impregnations with addition of fluorine compounds nor the tested sols nor the final layers contain any ecologically problematic components while keeping all the necessary requirements for the outdoor usage.

Acknowledgement: *This publication was written at the Technical University of Liberec as part of the project TAČR TH02020145 "Hydrophobic UV-lacquers and nano-layers protecting substrates against bio-attack" and the SGS project no. 21176/11 by the Ministry of Education of the Czech Republic.*

5 REFERENCES

1. Zajícová V., Exnar P., Staňová I.: Properties of hybrid coatings based on 3-trimethoxysilylpropyl methacrylate, Ceramics – Silikáty 55(3), 2011, pp. 221-227
2. Šlamborová I., Zajícová V., Karpíšková J., Exnar P., Stibor I.: New Type of protective hybrid and nanocomposite hybrid coatings containing silver and copper with an excellent antibacterial effect especially against MRSA, Material Science and Engineering C 33(1), 2013, pp. 265-273, https://doi.org/10.1016/j.msec.2012.08.039
3. Exnar P., Lovětinská-Šlamborová I., Veverková I., Danilová I.: Antimicrobial hybrid nanolayers prepared by sol-gel method, In: NANOCON 2015, Conference Proceedings, Brno, Oct.14-16.2015, Ostrava: Tanger, pp. 525-529, ISBN 978-80-87294-63-5
4. Šlamborová I., Zajícová V., Exnar P.: Antibacterial layer active against pathogenic bacteria, particularly against the MRSA bacterial strain, and the method of its production, CZ 303 250, 7.4.2011, 9.5.2012
5. Šlamborová I., Zajícová V., Exnar P., Stibor I.: Antibacterial layer active against pathogenic bacteria, particularly against the MRSA bacterial strain, and the method of its production, CZ 303 861, 23.5.2012, 18.4.2013; WO 2013174356, 28.11.2013; EP 2852630, 1.4.2015
6. Lovětinská-Šlamborová I., Zajícová V., Exnar P., Stibor I.: Antibacterial hybrid layer operating against pathogenic bacterial strains, particularly against the bacterial strain MRSA, and a method for its preparation, CZ 305 045, 28.8.2013, 25.2.2015; EP 2843019, 12.8.2014
7. Miller V., Bakalova T., Exnar P., Lovětinská Šlamborová I., Louda P.: Mechanical resistance of hydrophobic inorganic-organic nanolayers with antifouling effect, Manufacturing Technology, 2018, in press
8. AATCC Test Method 147-2016, Antibacterial Activity Assessment of Textile Materials: Parallel Streak Method
9. AATCC Test Method 100-2012, Antibacterial Finishes on Textile Materials: Assessment of
10. Yebra D.M., Kiil S., Dam-Johansen K.: Antifouling technology - past, present and future steps towards efficient and environmentally friendly antifouling coatings, Progress in Organic Coatings 50(2), 2004, pp. 75-104, https://doi.org/10.1016/j.porgcoat.2003.06.001
11. Nanoservice: Antifouling-Nano DS, Retrieved: September 5, 2018, Web site: http://nanoservice.cz/Antifouling-lode-/
12. Rastegarpour A., Cheung M., Vardhan M., Ibrahim M.M. et al.: Surgical mesh for ventral incisional hernia repairs: Understanding mesh design, Plastics Surgery 24(1), 2016, pp. 41-50
13. Mancino A.T., Lalani T.: Wound infection following repair of abdominal wall hernia, Retrieved: September 5, 2018, Web site: https://www.uptodate.com/contents/wound-infection-following-repair-of-abdominal-wall-hernia/print

ANALYSIS OF FORMATION OF MASS IRREGULARITY IN DRAFTING DEVICE DURING YARN SPINNING FROM SLIVER

Eva Moučková[1], Petr Ursíny[1], Petra Jirásková[1] and Martin Janoušek[2]

[1]Technical University of Liberec, Faculty of Textile Engineering, Department of Technologies and Structures Studentská 2, 461 17 Liberec, Czech Republic,
[2]Rieter CZ s.r.o, Moravská 519, 562 01 Ústí nad Orlicí, Czech Republic
eva.mouckova@tul.cz

Abstract: *This work deals with an analysis of formation of mass irregularity of fibrous product in a drafting arrangement of air-jet spinning machine. Sliver is supplied into the machine and attenuated in four-line double-apron drafting arrangements before formation into yarn. There, the total draft is realized within three zones: infeed draft, intermediate draft and main draft. In the work, the components of mass irregularity (limiting, systematic, additional and systematic developed from latent (immeasurable) irregularity), which form the structure of total mass irregularity of fiber strand in the output from the drafting unit, were defined. Transformation of mass irregularity of fibrous assembly by this drafting device was theoretically analyzed. The theoretical analysis of machine irregularity was realized too. Within the experiment, 100% Tencel yarns of count 23 tex were spun from the sliver of three various linear densities using the Rieter air-jet spinning machine J20. Three levels of intermediate draft ratio were also set. Proportionally to it, the level of main draft ratio was changed, while the both infeed draft ratio and other spinning parameters were kept constant. Sliver and yarn mass irregularity as well as number of yarn faults were measured and analyzed, machine irregularity was calculated. The results showed that the lowest value of yarn mass irregularity is achieved when the sliver with higher linear density in combination with the lowest level of intermediate draft ratio (both from the observed range) is used for air-jet yarn production. It confirmed the theoretical analysis that draft ratios in infeed and intermediate drafting zone has more significant importance for air-jet yarn mass irregularity compared to the level of main draft ratio. Sliver mass irregularity is also very important factor for total yarn mass irregularity. Similar results were also recorded for number of yarn faults (especially for thin places (-40%)).*

Key words: *Air-jet spinning, drafting, main draft ratio, intermediate draft ratio, yarn mass irregularity, components of yarn mass irregularity.*

1 INTRODUCTION

In the technology of staple spun yarn production, the draft is used for attenuation of supply fibrous product, fiber straightening and their aligning to a parallel position. The draft occurs usually in the drafting mechanism between pairs of roller, rotating at different speed. The principle of drawing is that fibers move relatively to each other to be distributed over a longer length of the product. It is generally known that drafting processes have significant effect on the yarn mass unevenness. Usually, higher draft ratio leads to higher total yarn irregularity and number of faults. A lot of research papers deal with analyses of drafting process and with a study of effect of drafting of yarn mass irregularity. Authors predominantly study the movement of fibers in the drafting zone, for example, in works [1, 2], or analyze drafting forces, for example, in works [3, 4]. The irregularity added by an apron drafting system on the ring spinning frame was studied in work [5]. During spinning from sliver, especially in the case of unconventional spinning systems such as a rotor spinning system, but also in the case of other spinning systems where a high-drafting device is used for given attenuation, it is necessary to apply a high draft ratio. The air-jet spinning system belongs to them. The process of forming the yarn on the air-jet spinning system comprises attenuation of supply sliver by the draft in the four-roller drafting device equipped with two aprons in the main drafting zone. Consequently, thin fibers strand is transformed into the yarn by means of vortex air in the nozzle houses [6]. Thanks to it, air-jet yarns are featured by a different, specific structure (so called fasciated yarn). The yarn consists of a core where fibers are parallel and without any twist, and of wrapper fibers twisted around the core. Although there are many research works focused on the air-jet yarns, they primarily deal with the influence of technological variables on the properties of air-jet yarns produced on Murata Vortex Spinning Machine (MVS) (for example [7-10]) or simulation of air flow field in the MVS nozzle chamber (for example [11]). In the year 2009, Rieter Company introduced also their air-jet spinning machine. It differs from the MVS by the machine concept, the nozzle geometry and fiber guide in the front of spinning tip placed in the nozzle house. Except for several works dealing with prediction of air-jet yarn tenacity [12], properties of plied air-jet yarn [13] or numerical simulation [14], there is a lack of research work about Rieter air-jet spinning system today. The effect of draft ratio on the properties of vortex spun yarn was investigated only in work [10]. Authors measured mass irregularity of yarn (15 tex) made of 100% VS fibres using the Murata Vortex spinning system. They spun set of yarns from slivers of three counts using two levels of intermediate draft ratio (2.3; 2.5). During results analysis, the authors limit on a two-way analysis of variance and statement that yarn samples spun with the lowest main draft ratio with highest used intermediate draft level achieved the worst irregularity. They concluded that it is a reason of out of optimum level of intermediate draft. However, for determination of the conditions ensuring optimal course of drafting process it is important to know the effect of the draft on the structure of mass unevenness. Therefore, the subject of our analysis is a high-drafting device (see Figure 1) used on the air-jet spinning machine. This device is characterized by three drafting zones that ensure the required total draft. Namely, it is a zone of infeed draft *P0*, a zone of intermediate draft *P1* and a zone of main draft *P2*. The infeed drafting zone and intermediate drafting zone consist in drafting rollers whereas in the main drafting zone also a pair of aprons controls fibers. In our case, the infeed draft ratio is constant for given fibrous material, the intermediate draft as well as the main draft is changed according to the experiment. Because of this, we assume that finally the main drafting zone and intermediate drafting zone form the total yarn mass irregularity. These zones will be a subject of theoretical analysis in the terms of their influence on the total mass unevenness of air-jet yarn. The analysis will be carried out also experimentally. At the same time, more general piece of knowledge about transformation of mass irregularity of linear fibrous product exposed to drafting processes in the given drafting device will be applied.

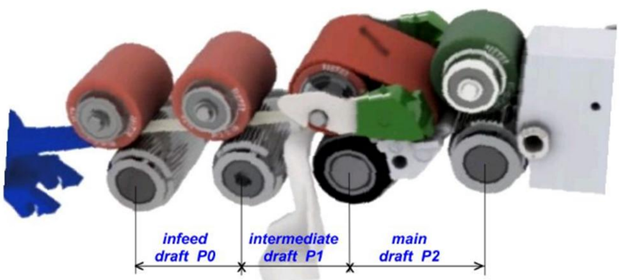

Figure 1 Scheme of drafting device of air-jet spinning machine (adapted and reproduced [17])

2 THEORY OF CHANGES OF MASS IRREGULARITY DUE TO DRAFT

2.1 General rules

The analysis of mass irregularity formation is performed on the basis of the laws of variation phenomena in random process. The total variation in the mass of short lengths of final product in a yarn manufacture can be regarded as the sum of the variations of individual components of mass irregularity (see equation (1)).

$$CV^2 = \sum_{i=1}^{k} CV_i^2 \tag{1}$$

where CV_i is i^th^ component of yarn square mass irregularity.

We consider following CV_i components [15, 16]:

CV_I - square limiting irregularity. It is determined by a random distribution of number of fibers in the sliver or yarn cross - sections. For better clarity, this component will be further referred as CV_{lim}.

CV_{II} - systematic square mass irregularity. It is caused by negative effects of technological stages before spinning system. For better clarity, this component will be further referred as CV_S. In the case of air jet spinning, CV_S includes also negative effect of infeed draft in the drafting arrangement of the air-jet spinning machine.

CV_{III} - additional square mass irregularity. It is induced only by the given technological stage (in our case by the spinning system). This component will be further referred as CV_P,

CV_{IV} - systematic square mass irregularity which is developed from a latent irregularity (immeasurable on very short lengths) due to drafting in given technological process (spinning). For better clarity, this component will be further referred as CV_{VS}.

We assume that the individual components of mass irregularity are mutually independent. As total variation in the mass of yarn short lengths we can use the parameter CV_m. It is a yarn total square mass irregularity obtained from Uster Tester and it will be further referred as CV_{yarn}. In our analysis, we start from above-mentioned components of mass irregularity. We determine the structure of mass irregularity of product in the input to the system and in the output from the system as well as resulting degree of mass irregularity using the effect of draft ratio and doubling (in general case) on the appropriate components of mass irregularity

2.2 Transformation rules of mass irregularity

Let us consider a general spinning system characterized by a certain draft *P* and doubling *D*. Due to different causes of the formation of individual components of total mass irregularity, the following expressions can be made:

$$CV_2^2 = CV_{lim2}^2 + CV_{S2}^2 + CV_P^2 + CV_{VS}^2 \tag{2}$$

and

$$CV_0^2 = CV_{lim0}^2 + CV_{S0}^2 \quad (3)$$

where quantities indexed by 0 express corresponding components of mass irregularity of fibrous product in the input into the spinning system and quantities marked by index 2 express corresponding components of mass irregularity in the output from the system.

Using the general transformation rules for limiting CV_{lim} and systematic CV_s square mass irregularity [15], we can express resulting total square mass irregularity of linear staple-spun product CV_2:

$$CV_2^2 = CV_{lim0}^2\left(\frac{P}{D}\right) + \frac{CV_{S0}^2}{D} + CV_P^2 + CV_{VS}^2 \quad (4)$$

We can express the contribution of given drafting system to the total square mass irregularity of output product by so called machine irregularity ($CV_{machine}$):

$$CV_{machine}^2 = (CV_2^2 - CV_{lim2}^2) - (CV_0^2 - CV_{lim0}^2) \quad (5)$$

Using equation (4), we can also express the resulting total square mass irregularity of linear fibrous product on the output from the drafting device CV_2 as:

$$CV_2^2 = CV_{lim0}^2 . P_c + CV_{S0}^2 + CV_P^2 + CV_{VS}^2 \quad (6)$$

where P_c is total draft, CV_p is additional square mass irregularity of fibrous product inducted in the drafting device and CV_{VS} is systematic square mass irregularity of fibrous product developed from latent irregularity by total draft in the drafting arrangements.

Substituting formulas (3) and (6) into the equation (5) we obtain:

$$CV_{machine}^2 = CV_P^2 + CV_{VS}^2 \quad (7)$$

From formula (7) it is evident that not only the additional irregularity but also the systematic square mass irregularity developed from the latent irregularity of input product influences the level of irregularity which the spinning system inserts into the final product.

Because the draft ratio in the infeed drafting zone is constant for given fibrous material, we will follow up relations in intermediate and main drafting zones of the given drafting device. For the intermediate drafting zone we can write:

$$CV_{PS}^2 = CV_{lim1}^2 . P1 + CV_{S1}^2 + CV_{P1}^2 + CV_{VS1}^2 \quad (8)$$

where CV_{PS} is total square mass irregularity of fibrous product after passing through the intermediate drafting zone; $P1$ means draft ratio in the intermediate drafting zone (intermediate draft ratio); CV_{lim1} is limiting square mass irregularity of fibrous product before entering into the intermediate drafting zone; CV_{S1} is systematic square mass irregularity of fibrous product before the intermediate drafting zone caused by both previous processes and infeed drafting zone; CV_{P1} is additional square mass irregularity caused by the intermediate drafting zone and CV_{VS1} is systematic square mass irregularity of fibrous product developed from the latent mass irregularity in the intermediate drafting zone.

For the main drafting zone we can write:

$$CV_{PH}^2 = CV_{lim2}^2 + CV_{S2}^2 + CV_{P2}^2 + CV_{VS2}^2 \quad (9)$$

where CV_{PH} is total square mass irregularity of fibrous product after passing through the main drafting zone, CV_{lim2} is limiting square mass irregularity of fibrous product after passing through the main drafting zone; CV_{S2} is systematic square mass irregularity of fibrous product before the main drafting zone caused by previous drafting processes; CV_{P2} means additional square mass irregularity of fibrous product induced in the main drafting zone and finally CV_{VS2} is systematic square mass irregularity of fibrous product developed from the latent irregularity in the main drafting zone.

Because of below mentioned formulas (10a) and (10b) hold:

$$CV_{lim2}^2 = CV_{lim1}^2 . P1 . P2 \quad (10a)$$

$$CV_{S2}^2 = CV_{S1}^2 + CV_{P1}^2 + CV_{VS1}^2 \quad (10b)$$

we can write:

$$CV_{PH}^2 = CV_{lim1}^2 . P1 . P2 + (CV_{S1}^2 + CV_{P1}^2 + CV_{VS1}^2) + CV_{P2}^2 + CV_{VS2}^2 \quad (11)$$

where $P2$ means main draft ratio.

From formulas (10b) and (11) it is obvious that with increasing draft ratio $P1$ in the intermediate drafting zone the component CV_{S2}^2 will have a significant effect on yarn mass irregularity. The component will increase irregularity of final yarn even if the main draft ratio will be reduced.

3 EXPERIMENT

Within the experiment, mass irregularity of 100% Tencel air-jet spun yarns as well as number of yarn faults were analyzed in dependence on the intermediate draft ratio as well as the main draft ratio.

3.1 Materials and methods

Tencel staple fibers (38 mm, 1.3 dtex) were used for production of air-jet spun yarns of nominal count 23 tex. Samples of yarns were spun on the Rieter Air-jet spinning machine J20 from a sliver which was processed in 3 passages of doubling and drawing after carding. Three different levels of sliver linear densities (see Table 1) were used for the experiment to analyze influence of main draft ratio on the yarn mass irregularity and yarn faults. Within each level of sliver linear densities, three levels of intermediated draft ratio were set to observe the influence of intermediate draft ratio on the yarn mass irregularity. The infeed draft and other spinning parameters were kept constant and they were set in accordance with the processed raw material and yarn count.

Table 1 Proposal of experiment

Trial Nr.	V1	V2	V3	V4	V5	V6	V7	V8	V9
Sliver linear density [ktex]	3.65	3.65	3.65	4.09	4.09	4.09	4.61	4.61	4.61
Infeed draft *P0*	1.78	1.78	1.78	1.78	1.78	1.78	1.78	1.78	1.78
Intermediate draft *P1*	1.97	2.30	2.64	1.97	2.30	2.64	1.97	2.30	2.64
Main draft *P2*	45.79	38.95	33.93	50.2	43.13	37.39	56.52	48.55	42.41
Total draft	160.6	159.46	159.45	176.06	176.6	175.69	198.19	198.79	199.3
Real average yarn count [tex]	22.72	22.89	22.89	23.23	23.16	23.28	23.26	23.19	23.13
Nozzle air pressure [MPa]	0.6								
Spinning nozzle	Z-1								
Spinning tip type	U1.2mm/A0.8								
Delivery speed [m.min^{-1}]	400								

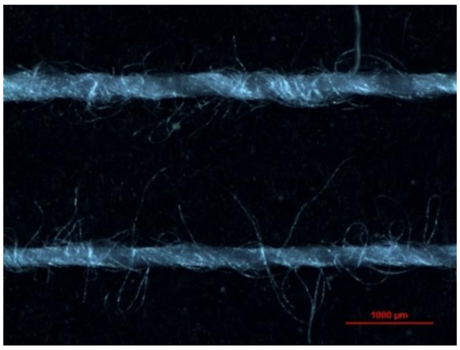

Figure 2a Longitudinal view on yarn samples (Trial Nr.8)

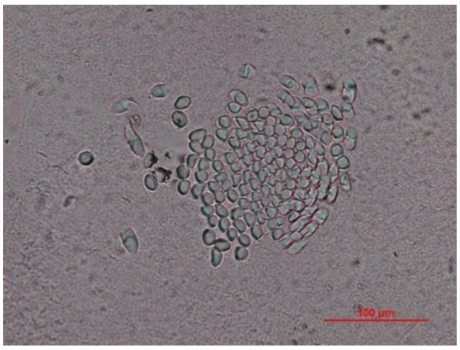

Figure 2b Cross-sectional view on yarn samples (Trial Nr.8)

For each trial, 5 bobbins were spun. For illustration of fasciated yarn structure, the longitudinal view on the yarn sample and yarn cross-section was made (see Figure 2a and 2b). The Uster Tester IV-SX was used for measuring yarns as well as slivers mass irregularity. Slivers were measured for 5 min with the speed of 25 m/min, whereas yarns were measured for 2.5 min with the speed of 400 m/min. For each yarn sample, 15 measurements were done.

To investigate the effect of main draft ratio on yarn mass irregularity (when the intermediate draft ratio is kept constant), it is necessary to analyze sliver mass irregularity and take it into account. The negative effect of measured sliver mass irregularity can be eliminated by calculating and comparing machine irregularity. Except for draft, all machine process parameters were constant for all tested yarn samples. Based on this, we can assume that square mass irregularity of yarn is the same as square mass irregularity of linear fibrous product in the output from drafting arrangements and thus we can calculate the machine irregularity using formula (5). The limiting mass irregularity is defined by the formula:

$$CV_{lim} = \frac{100}{\sqrt{n}} \tag{12}$$

where *n* is mean number of fibers in yarn (sliver) cross-section calculated as ratio of mean yarn (sliver) count and mean fiber fineness.

4 RESULTS AND DISCUSSION

4.1 *Square mass irregularity*

Table 2 shows results of square mass irregularity of sliver on various length sections. From the table, it can be seen that mean value of mass irregularity of sliver in the cross-section (CV_{sliver}) decreases with increasing linear density of slivers. This phenomenon is known. Finer sliver has a lower number of fibers in the cross-section and it expresses in growing of mass variability. Sliver mass irregularity on longer cut length has fluctuating tendency and it is caused by previous technological stages.

Table 2 Results of sliver mass irregularity

Sliver fineness [ktex]	CV_{sliver} [%]	CV_{sliver} (1m) [%]	CV_{sliver} (3m) [%]	CV_{sliver} (5m) [%]
3.65	6.96	1.01	0.63	0.5
4.09	6.28	1.15	0.72	0.6
4.61	5.82	0.96	0.67	0.5

Figure 3a demonstrates spectrogram of sliver. Significant higher harmonic components of mass irregularity at the wavelengths λ=50 cm and λ=1 m are probably caused by previous technological levels. Figure 3b shows the example of spectrogram of yarn mass irregularity. It can be seen that yarn has not any significant periodical irregularity. Spectrograms of slivers as well as yarns also show that higher periodical irregularity of sliver on long wavelengths does not fully transform into the yarn due to draft on the wavelength corresponding to the value equal to $\lambda * P_c$. The reason can be attributed to the relatively short length of measured yarn for this analysis and less statistical reliability of spectrogram results on the long wavelengths.

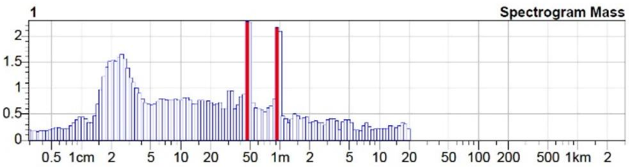

Figure 3a Spectrogram of sliver mass irregularity (Sliver fineness 4.09 ktex)

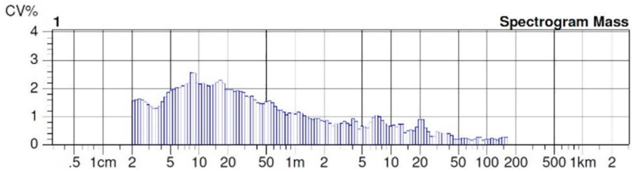

Figure 3b Spectrogram of yarn mass irregularity (Trial No. V8)

Figure 4 shows dependence of yarn square mass irregularity (CV_{yarn}) on the main draft ratio. Contrary to known theory, it can be seen that when keeping the intermediate draft ratio constant, the yarn mass irregularity decreases with growing the main draft ratio. The yarn mass irregularity also deteriorates with growing the intermediate draft ratio (or we can say with decreasing main draft ratio) when sliver mass density is kept constant. These results confirmed the theory mentioned above. When increasing the intermediate draft ratio, the component CV_{S2}^2 influences total yarn mass irregularity negatively. At increasing intermediate draft ratio $P1$, this component is affected by increase in components CV_{P1}^2 and CV_{VS1}^2. It is due to the character of the intermediate drafting zone and resulting friction force field in the longitudinal direction which corresponds to the drafting zone with missing a guiding (controlling) device. Due to its arrangements, the main drafting zone allows to minimalize the increase in additional mass unevenness.

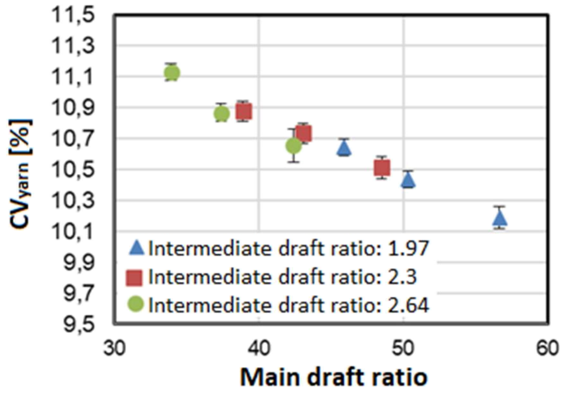

Figure 4 Dependence of yarn mass irregularity on main draft ratio and various intermediate draft ratios

Two-way variance analysis Anova confirmed a statistically significant effect of both intermediate draft ratio and sliver linear density on the yarn mass irregularity at the significance level of 5%. However, the significance of mutual interaction of these two factors was not statistically confirmed (see the results in Table 3).

4.2 Machine irregularity

Figure 5 presents machine irregularity in dependence on the main draft ratio for various intermediate draft ratio.

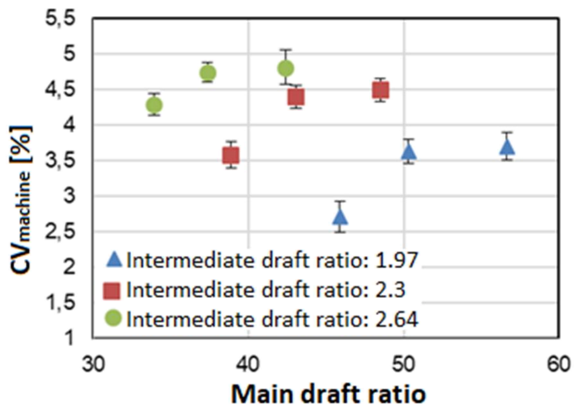

Figure 5 Dependence of machine irregularity on main draft ratio and various intermediate draft ratios

Table 3 Results of two-way Anova

Property	Source of variance	F-ratio	Critical quantile	Results	p-value
CV_{yarn} (CV_m)	Intermediate draft ratio	172.68	3.07	Significant	$3.55.10^{-36}$
	Sliver linear density	146.93	3.07	Significant	$4.22.10^{-33}$
	Interaction	1.30	2.45	Non-significant	0.27
Thin places (-40%)	Intermediate draft ratio	27.28	3.07	Significant	$1.61.10^{-10}$
	Sliver linear density	42.42	3.07	Significant	$1.03.10^{-14}$
	Interaction	2.62	2.46	Significant	0.04
Thick places (+50%)	Intermediate draft ratio	8.50	3.07	Significant	$3.48.10^{-4}$
	Sliver linear density	0.77	3.07	Non-significant	0.46
	Interaction	0.61	2.46	Non-significant	0.66
Neps (+200%)	Intermediate draft ratio	2.49	3.07	Non-significant	0.09
	Sliver linear density	1.25	3.07	Non-significant	0.29
	Interaction	0.95	2.46	Non-significant	0.43

The results showed that:

- When keeping the intermediate draft ratio constant, the main draft ratio is a significant factor which increases machine irregularity. This result is in accordance with theory presented above. Based on the theoretical analysis mentioned above, we can also say that systematic square mass irregularity developed from the latent irregularity by the draft probably contributes to the increase in machine irregularity. Based on this, we can conclude that when the intermediate draft is constant, decreasing values of measured yarn square mass irregularity (CV_{yarn}) with growing main draft ratio (due to higher sliver linear density) was caused by mass irregularity of input sliver which corresponds to the irregularity components CV_{lim0} and CV_{s0}. Finer sliver has higher measured valued of mass irregularity compared with course sliver. This irregularity transforms into the yarn and thus influences total square mass irregularity of yarn more than the drafting device itself.
- When sliver linear density is constant, the value of machine irregularity increases with increasing level of intermediate draft ratio (and thus with decreasing main draft). This result is in agreement with the previous one and verifies the higher importance of intermediate draft ratio on total yarn mass irregularity compared with the main draft ratio.

4.3 Yarn faults

Average values and corresponding 95% confidence intervals of yarn faults (thin places (-40%), thick places (+50%) and neps (+200%)) are presented in Figure 6a-6c. Number of thin places (-40%) was observed instead of thin places (-50%) because of zero number of faults in this category. Selected results of two-way analysis of variance are mentioned in Table 3. Results of numbers of thin places have the same trend as results of total mass irregularity of yarns. Number of thin places decreases with decreasing intermediate draft ratio and with increasing linear density of supplied sliver. Results of two-way Anova show that sliver linear density, the intermediate draft ratio as well as interaction of these two factors have a statistically significant effect on number of thin places (-40%). The linear density (and thus the main draft ratio at constant level of intermediate draft ratio) is a factor with a higher significant effect. However, it is clear from the graph in Figure 6a that, in the terms of overlapping confidence intervals, the statistically significant difference is only between the numbers of thin places of yarn sample spun from sliver of linear density 3.65 ktex at intermediate draft ratio of 2.64 and yarn sample made from a sliver of 4.61 ktex at intermediate draft ratio of 1.97. Number of thick places (+50%) shows similar results as in case of thin places, but in this case the effect of interaction of sliver linear density and level of intermediate draft ratio is a statistically insignificant. The results can be attributed to both mass variability of supply sliver, which is higher in the case of finer sliver, and negative effect of the intermediate drafting zone which is stronger with growing intermediate draft ratio. Based on results of two-way Anova, we can state that in the case of number of yarn neps (+200%) the effect of observed factors is statistically insignificant in significance level of 5%. However, we have to note that thanks to the specific yarn structure, the Uster Tester can also records as a nep the place where the ends of the wrapping fibers are not tightly twisted around the yarn core due to the air flow in the nozzle.

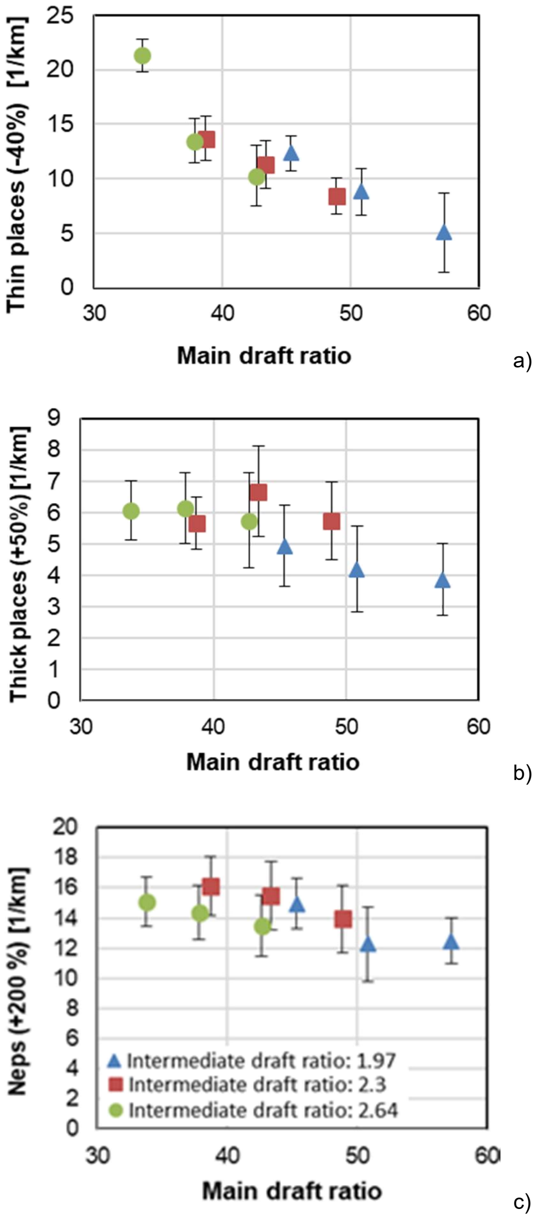

Figure 6 Dependence of yarn faults on main draft ratio and various intermediate draft ratios

5 CONCLUSIONS

In this work, the analysis of draft in the four-roller two-apron drafting device of air jet spinning machine was done together with theoretical analysis of transformation of mass irregularity of fibrous product by this drafting unit. The effect of intermediate and main drafting zones was observed. Within the experiment, mass irregularity of air-jet yarns of the same count, produced with various setting of intermediate and main draft ratio, was evaluated together with sliver mass irregularity and yarn faults. Based on theory, the mass irregularity of fibrous product is deepened by the draft mostly. Despite the fact that the main draft ratio is much higher compared with the intermediated draft ratio, this study shows that the intermediate draft ratio has more significant influence on the yarn mass irregularity than the main draft. It can be explained by the fact that fibers move in the intermediate drafting zone without aprons. The aprons are a part of the main drafting zone, and they control the fibers movement in the zone. Thus, in this zone, they minimalize the creation of the additional irregularity, which is one of a component of total yarn mass irregularity. The additional irregularity is probably highly deepened in the intermediate drafting zone due to the fact that various drafting force is applied on each fiber in the zone and change of speed of fiber movement does not occur at the same place. Also the irregularity of supplied sliver (limiting and so called systematic) has negative influence on the total yarn mass irregularity. The experiment shows that for achieving the lowest value of total mass irregularity of tested yarn samples it is suitable to use the lowest value of intermediate draft ratio (*P1* = 1.94) in combination with coarser supply sliver (4.61 ktex). Compared with finer sliver, the sliver with higher linear density (from the observed range) seems to be suitable because it has lower irregularity thanks to higher number of fibers in the sliver cross-section and due to lower draft ratios used in previous spinning processes. When observing number of yarn faults, the same trends were achieved. But the statistically significant differences were recorded only in the case of thin places (-40%). Finally, based on Uster Statistics, we have to note that tested samples of air jet yarns have lower irregularity. Also the differences between minimum and maximum *CVm* values were in the range up to 5%. For verification of results it is necessary to extend the experiment in terms of both wider draft range and raw material and to observe impact of yarn mass irregularity on various yarn properties.

6 REFERENCES

1. Grishin P.A.: Theory of drafting and its practical applications, Journal of the Textile Institute Transaction 45(3), 1954, pp. T167-T266, https://doi.org/10.1080/19447025408662644
2. McVitie J., De Barr A.E.: Fiber motion on roller and apron drafting system, Journal of the Textile Institute Transaction 51(4), 1960, pp. T147-T156, https://doi.org/10.1080/19447026008662681
3. Lin Q., Oxenham W., Yu C.: A study of the drafting force in roller drafting and its influence on sliver irregularity, Journal of the Textile Institute 102(11), 2011, pp. 994-1001, https://doi.org/10.1080/00405000.2010.529284
4. Audivert R., Viilaronga M., Coscolla R.: Drafting force in the front zone of a double apron drafting system, Textile Research Journal 37(1), 1967, pp. 1-10, https://doi.org/10.1177/004051756703700101
5. Balasubramanian N.: A study of the irregularities added in apron drafting, The Textile Research Journal, 39(2), 1969, pp. 155-165, https://doi.org/10.1177/004051756903900205
6. Stalder H.: The Rieter Manual of Spinning. Volume 6 - Alternative Spinning Systems, Wintherthur: Rieter Machine Works Ltd., 2014, ISBN 10 3-9523173-6-5
7. Basal G., Oxenham W.: Effects of some process parameters on the structure and properties of vortex spun yarn, Textile Research Journal, 76(6), 2006, pp. 492-499, https://doi.org/10.1177/0040517506064253
8. Kuthalam S.E., Senthilkumar P.: Effect of fibre fineness and spinning speed on polyester vortex spun yarn properties, Fibres & Textiles in Eastern Europe 21(5), 2013, pp. 35-39
9. Erdumlu N., Ozipek B., Oxenham W.: The structure and properties of carded cotton vortex yarns, Textile Research Journal 82(7), 2012, pp. 708-718, https://doi.org/10.1177/0040517511433150
10. Erdumlu N., Ozipek B.: Effect of the draft ratio on the properties of vortex spun yarn, Fibres and Textile in Eastern Europe 18(3), 2010, pp. 38-42
11. Zeng Y.C., Yu C.W.: Numerical simulation of air flow in the nozzle of an air-jet spinning machine, Textile Research Journal 73(4), 2003, pp. 350-356, https://doi.org/10.1177/004051750307300413
12. Eldeeb M., Demir A.: Optimizing the production process of Rieter air jet spun yarns and model form prediction of their strength, Fibres and Textiles in Eastern Europe 26(1), 2018, pp. 36-41, DOI: 10.5604/01.3001.0010.7794
13. Eldeeb M., Moučková E., Ursíny P.: Properties of viscose air-jet spun plied yarns, Indian Journal of Fibre and Textile Research 42(4), 2017, pp. 386-390, http://nopr.niscair.res.in/handle/123456789/43252
14. Eldeeb M., Moučková E.: Numerical simulation of the yarn formation process in Rieter air jet spinning, Journal of the Textile Institute 108(7), 2017, pp. 1219-1226, https://doi.org/10.1080/00405000.2016.1230000
15. Ursíny P.: Mass irregularity changes in spinning technology, Vlákna a textil (Fibres and Textiles) 10(2), 2003, pp. 62-65
16. Bowles A.H., Davies L.: The influence of drawing and doubling process on the evenness of spun yarn I, The Textile Institute and Industry 11, 1978, pp. 371-374
17. Rieter J 20 Air-Jet Spinning Machine Com4jet Yarn Formation original animations, animation made by Rieter, downloaded 10.3.2017 from: https://www.youtube.com/watch?v=rMYCb9ea11g

METHOD OF GENERATION ZONING AREAS IN PATTERN CONSTRUCTION NET OF SEAMLESS UNDERWEAR

Blažena Musilová, Alžbeta Hôrecká and Nareerut Jariyapunya

Technical University of Liberec, Faculty of Textile Engineering, Department of Clothing Technology
Studentská 2, 461 17 Liberec, Czech Republic
blazena.musilova@tul.cz

Abstract: *It is well known that in order to develop tight-fit seamless garment of satisfactory fit it is necessary to use shaping in order to achieve 3D shapes that relate to the shape of the body. This requires a sophisticated approach to create suitable pattern design. In this paper a method of generation zoning areas for 3D shaping has been designed within a 2D pattern construction net of the seamless underwear. To non-contact measure and display a three-dimensional body form the topography technique of the shadow moiré has been applied. To evaluate obtained 2D pictures of digitised zones of moiré fringe pattern the processing system NIS-Elements has been used. The size and location of the editing zoning areas has been compared with the corresponding place positions of zoning areas on the tubular knitted fabric which covers the pelvic part of the female figurine EU size 38. The geometry of the stretch pattern profile has been evaluated through understanding the dynamic effect of the fabric behaviour. Experimental results verify the effectiveness of the moiré topography to determine geometry of a 3D human body surface to achieve information of zoning areas for 3D design of seamless stretch underwear. Measured size and location of the zoning areas have been used as a pattern parameter for generation a 2D construction net of a seamless girdle.*

Keywords: *Seamless underwear, constructional net, non-contact body measurement, moiré, zoning area.*

1 INTRODUCTION

Currently there is a number of specialists knitted garment producers who are using type of seamless circular garments to create highly technical garments, using specific knit structures to map the body surface for comfort. These are mainly types of sportswear, therapy garments and others. In terms of fit, there is evidence to suggest that, although knitwear is stretchy and therefore there is an assumption it will fit a wide variety of body shapes and sizes; there is still need for fit improvements. Thus body mapping can be described as comfort mapping. The specific areas of the garment must map to specific areas of the body. It must be presumed that production technology development should include a sophisticated understanding not just of the functions of the body but also of body size, shape and proportion.

To create knitted garments that fit the body of 3D shape, it is important to have a suitable method of applying body measurement within product development processes. That can be one of non-contact contour mapping technics [1].

Research that is described in this paper has being focused on the development of pattern making method that is associated with seamless garments made by knit technology with the help of circular machinery.

2 EXPERIMENTAL

Experimental steps are concerned with the discovering the suitable way how to measure zoning areas of the female body surface geometry of the pelvic part and with the way how to determinate zoning areas within pattern construction net of seamless underwear.

2.1 Materials and methods

To target experimental strategy and define a female somatotype, the figurine AlvaForm (Figure 1) made from soft memory foam which simulates a soft human tissue, has been chosen. This AlvaForm of the European size code 38, which is in the half scale form (WAIST = 36 cm, HIP = 49 cm), is accurately shaped and proportioned physical characteristics derived from relevant consumer data based on Europe female population analysis.

For capturing 3D form of body and to found out input pattern construction parameters and position of zoning areas in a tubular knit structure of seamless product, the effective non-contact topography technique of a shadow moiré has been applied. This is a well-known technique commonly used in analysis of spiral deformities in human body. For clothing application of “Moiré” technique were found in the area of pattern construction of clothing [1]. This is the contour mapping technique, which has been involved positioning a grating close to the surface of figurine and observed its shadow on the figurine through the grating [1, 4].

To measure the size and place position of zoning areas on obtained 2D pictures of digitised moiré fringe pattern the image processing system NIS-Elements AR 40.00.8 has been used.

Figure 1 Figurine AlvaForm EU size code 38 (front, back and side view)

With regards of the research goal of this paper, to find out method for a design of a suitable seamless underwear shape including specific areas that must map specific areas of the body, a representative type of intimate apparel and an open bottom girdle has been selected. Thus it is necessary to create a suitable construction net. Its parameters should be determined as a dependent variable by computation using the regression equation and corresponding body measurement as an independently variable [5].

The quality of body contouring fit is inextricably linked with the stretch potential of fabric characteristics. Understanding the stretch behavior, visually and mechanically, is an essential part of predicting the pattern profile geometry and the optimum orientation of the pattern placement on the fabric to improve the fit-quality. This is achieved in part by maintaining the stretch extension of fabric within the lower modulus working range. The pattern orientation will affect the garment fit if the stretch fabric extension in the course and wale directions is different [1]. For this research a pattern profile is designed for (course) orientation on the fabric. Pattern grain line is situated in the vertical (wale) orientation.

The starting point of a research of a tight-fit garment pattern development is to use a law whereby the fabric tension, the radius of the part of the body being covered, determine garment pressure. Therefore a fabric circumference is of a smaller size than the body circumference. The suggested reduction of knitted fabric circumferences by 20-30% seams to by typical.

For this experiment the interlock knitted fabric (54% PA/46% EL, 319 g/m^2) of a tubular form is been used with the pattern dimensions reduction in weft direction by 26.5% [3].

3 RESULTS AND DISCUSSION

3.1 Non-contact body measuring method of the shadow moiré

Extensive pre-tests concerning to find out appropriate method to give high quality records of body morphology and also reliable cross-sectional measurements were carried out. The technique of a shadow moiré has been applied, which enable to map a human body and create picture with a topography effect. The experimental maps of the scanned figurine are given in Figure 2. Those moiré maps were the foundations for creating zoning areas in pattern constructional net of seamless circular garment.

For the non-contact shape measurement of the figurine the developed moiré topographic system (Figure 3) was placed close to the grid, enabling a sharp image of the moiré fringes to the be obtained (Figure 2). For capturing the size of a pelvic part of the figurine, a vertical wooden frame 0.594 m (*L*) x 0.420 m (*W*), was designed to mount the plane of grid lines in an exact parallel manner.

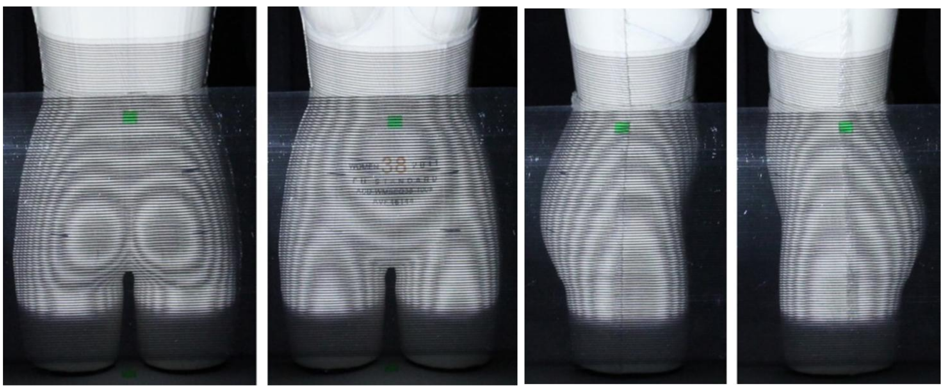

Figure 2 Moiré image of AlvaForm (back, front, right and left side view) [3]

The plane of the grid lines (1 mm line thickness and pitch size 2 mm) was translated in its own plane in a vertical position. The distance between the figurine surface and the grid (Figure 3) at a given position h = 0.08 m; the distance between the grid and light source l = 1.8 m; d = 0.5 m represents the distance between the light source and camera.

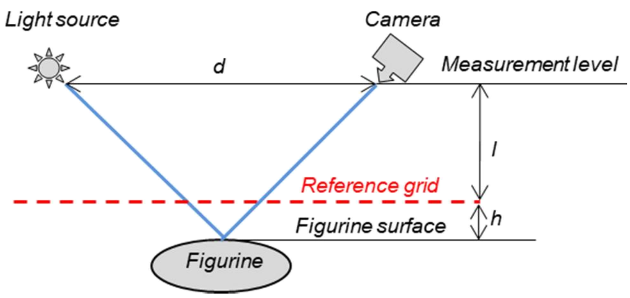

Figure 3 Schematic setup of the moiré system

3.2 Image processing of moiré fringe patterns

The contour map of the moiré fringes generates the required shape information across the pelvic part of the figurine body. A visual interpretation of the fringe pattern is a good means for assessing the shape conformity of three-dimensional seamless underwear (Figure 4).

For the objective measurement of a picture of the pelvic part of the figurine, a digital analysis of different sections of the back, front and side view was performed. The fringe pattern was then measured using tools of NIS-Elements system and a size of topography zones were determined. The shape and size characteristics of fringe zones were derived in the horizontal, vertical and bias direction. The profile of the zones was measured by evaluation of an intensity line profile distribution in Figure 4.

3.3 Evaluation of zoning areas position on the tubular knitted fabric

To evaluate the results of capturing 3D form of body mentioned in paragraph above the size and location of the editing zoning areas has being compared with the corresponding place positions of zoning areas on the tubular knitted fabric which covers the pelvic part of the female figurine.

The static width dimension of the tubular has been set according the WAIST = 36 cm. For static length dimensions of the tubular: UPPER HIP DEPTH = 5 cm (from waist to upper hip level); HIP DEPTH = 10 cm (from waist to hip); BODY RISE = 15 cm (from waist to hem edge). The elements of the size 10x10 mm have been marked on the tubular knit (Figure 5). Then a stretch behaviour of the knit has been tested dressed on a dummy. The dynamic dimensions have been evaluated.

The geometry of the stretch pattern profile has been evaluated through understanding the dynamic form of these elements. Dynamic effect “Δ” of the element dimensions was evaluated in horizontal (course) position. A digital calliper was used. The Table 1 lists “Δ” value of dynamic effect of the elements of the centre back part of the figurine.

These presented experimental results, highlighted in Table 1, show the similarity of the individual zoning area shape with the comparison with the digitised moiré fringe pattern in Figure 4. The same differences we can see in the intensity line profile of moiré map Figure 2.

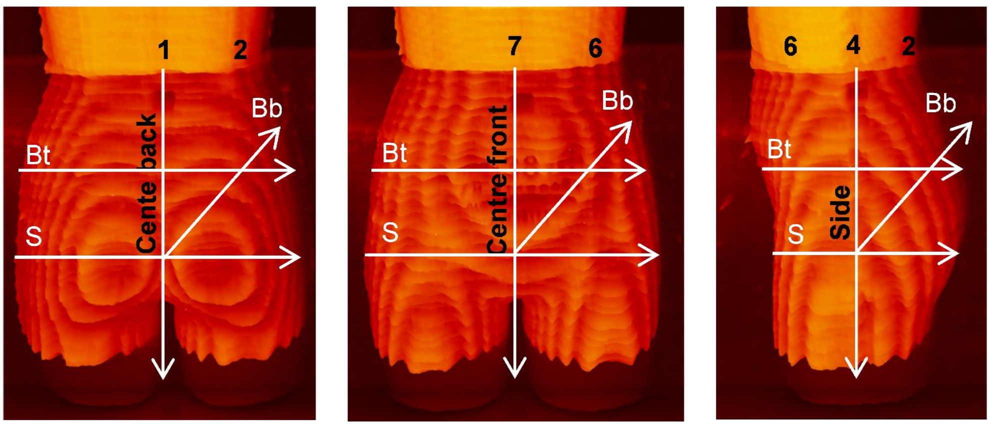

Figure 4 Intensity line profil distribution (back, front and side view)

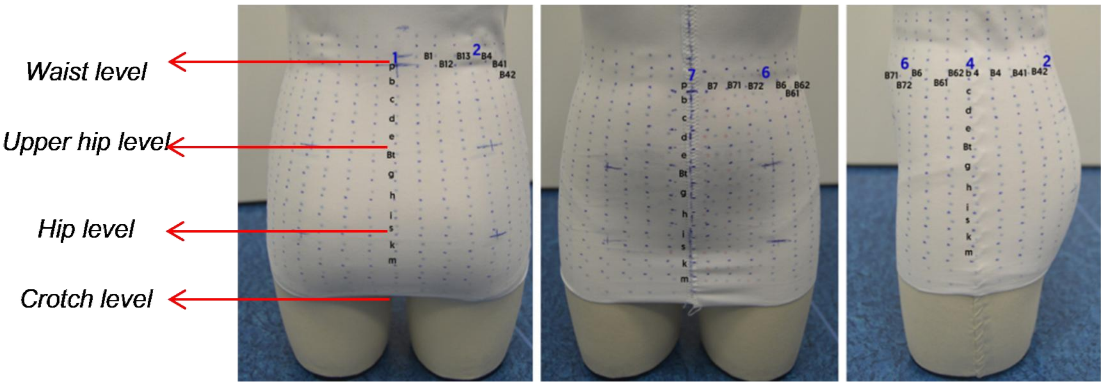

Figure 5 Measured elements on tubular knitted fabric (back, front and side part) [3]

Table 1 Dynamic effect of the measured elements

Element	Dynamic effect Δ [mm]				
	1	B1	B12	B13	2
P (Waist level)	Δ1p = 1.00	ΔB1p = 0.60	ΔB12p = 0.68	ΔB13p = 0.80	Δ2p = 0.80
b	Δ1b = 1.00	ΔB1b = 1.00	ΔB12b = 0.88	ΔB13b = 0.82	Δ2b = 0.89
c	Δ1c = 1.78	ΔB1c = 1.60	ΔB12c = 1.26	ΔB13c = 1.03	Δ2c = 1.15
d	Δ1d = 1.97	ΔB1d = 2.05	ΔB12d = 1.82	ΔB13d = 1.72	Δ2d = 1.98
e	Δ1e = 2.52	ΔB1e = 2.62	ΔB12e = 2.18	ΔB13e = 2.22	Δ2e = 2.42
Bt (Top hip level	Δ1Bt = 3.09	ΔB1Bt = 3.16	ΔB12Bt = 3.22	ΔB13Bt = 3.62	Δ2Bt = 4.24
g	Δ1g = 3.16	ΔB1g = 3.39	ΔB12g = 3.28	ΔB13g = 3.53	Δ2g = 4.12
h	Δ1h = 3.15	ΔB1h = 3.45	ΔB12h = 3.37	ΔB13h = 3.53	Δ2h = 4.47
i	Δ1i = 3.86	ΔB1i = 4.15	ΔB12i = 3.38	ΔB13i = 3.53	Δ2i = 4.27
S (Hip level)	Δ1s = 3.59	ΔB1s = 3.89	ΔB12s = 3.58	ΔB13s = 4.44	Δ2s = 3.98
k	Δ1k = 3.59	ΔB1k = 3.89	ΔB12k = 3.58	ΔB13k = 4.30	Δ2k = 3.90
l	Δ1l = 3.59	ΔB1l = 3.89	ΔB12l = 3.58	ΔB13l = 4.30	Δ2l = 3.90
m	Δ1m = 3.59	ΔB1m = 3.89	ΔB12m = 3.58	ΔB13m = 4.30	ΔB1m = 3.89

3.4 Seamless girdle construction net development

A close fitting girdle pattern block is constructed to be smaller than the body measurements and to stretch to the body shape. Some adjustments to the horizontal measurements may have made. This should be related to the stretch and relaxation of different fabrics. For this research is used 26.5% hip circumference reduction, which is static width dimension of the tubular knit width.

Experimental results are processed into the construction algorithm for a girdle pattern net design (Figure 6). Individual construction steps are listed in the Table 2.

The zoning areas in frame of the pattern constructional net are shown in the (Figure 6). The shape characteristics (in horizontal, vertical and bias direction) are match using the experimental results of image analyses of pelvic part of figurine in Figure 3.

Table 2 Construction algorithm of seamless girdle pattern net

Step	Definition		Dimension (Formula)
		Horizontal lines drafting	
1.	Centre back line	1	
2.	Waist line (**w**)	1 ⊥ w ⇒ P1	
3.	Hip line (**h**)	1 ⊥ h ⇒ S1	P1S1= 0.125 HEIGHT
4.	Upper hip line (**th**)	1 ⊥ th ⇒ Bt1	UPPER HIP DEPTH (0.5 P1S1)
5.	Hem line (**cr**)	1 ⊥ cr ⇒ R1	P1R1= BODY RISE
		Vertical lines drafting	
6.	Construction net width	Tubular width	P1P7=(0.5 WAIST) P1P7=0.5 (73.5% HIP)
7.	Centre front line	7 ⊥ w, th, h, cr ⇒ P7, Bt7, S7, R7	
8.	Side line	4 ⊥ w ⇒ P4, Bt4, S4, R4	P1P4=P4 P7 = 0.5 P1P7
9.	Back longitudinal line	2 ⊥ w ⇒ P2, Bt2, S2, R2	0.5 P1P4
10	Front longitudinal line	6 ⊥ w ⇒ P6, Bt6, S6, R6	0.5 P4P7

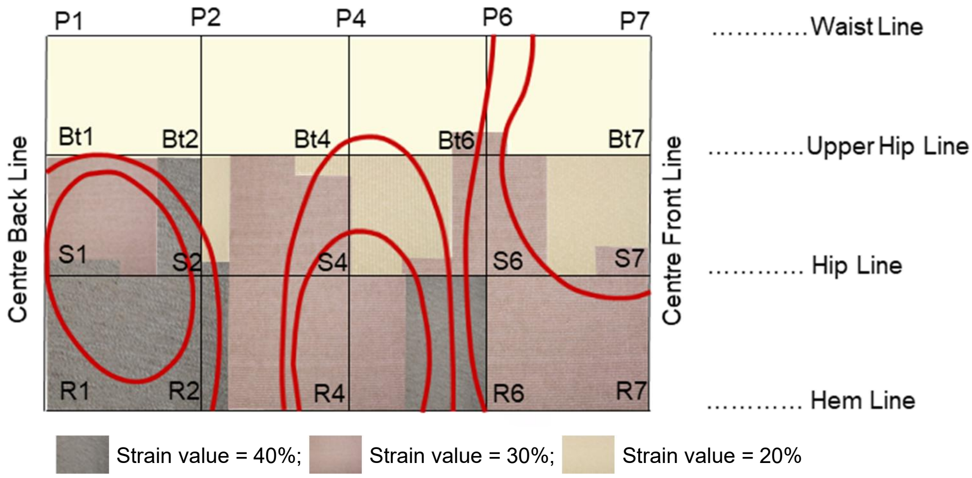

Figure 6 Seamless girdle construction net with zoning areas

4 CONCLUSIONS

Machinery that has the ability to construct garments three dimensionally, such as seamless garment, implies the possibility of creating a product that can conform to the three dimensional shape of the body. Shaping the garment is limited by the number of needles available on which to knit. The zoning areas to map the 3D body shape must commence knitting on specific needles with an exact number of available needles within each zone and between them. There are difficulties associated with knitting tubular stretch garments and its pattern construction definition of a specific zoning area shape. Therefore this presented research is concerned with the development of a construction method for tight-fit seamless garment design that covers a pelvic part of human body.

Extensive experimental pre-tests concerning to find out appropriate method to give high quality records of body morphology, and also reliable cross-sectional measurements were carried out. For experiment of this paper the technique of a shadow moiré has been applied, which is able to map a human body and create picture with a topography effect. The moiré maps were the foundations for creating zoning areas in girdle pattern constructional net of seamless circular garment. Experimental results verify the effectiveness of the moiré topography to determine geometry of a 3D human body surface to achieve information of zoning area size and shape and their location within seamless construction net.

ACKNOWLEDGEMENTS: *This work was supported by the Ministry of Industry and Trade of the Czech Republic, Programme Trio - project "Senior Tex - Smart Modular Clothing and Textile Products with Integrated Electronic Microsystems for Improving the Health Care of the Aging Population and Handicapped People", reg. no. FV10111.*

5 REFERENCES

1. Fan J., Yu W., Hunter L.: Clothing appearance and fit: Science and technology, Woodhead Publishing Limited, Cambridge England, 2004, ISBN: 1855737450
2. Hayes S.G., Venkatraman P.: Materials and Technology for Sportswear and Performance Apparel, CRC Press, Taylor & Francis, Boca Ratom, 2016, ISBN: 9781138748354
3. Hôrecká A.: Pattern construction of seamless lingerie, Bachelor thesis, TU of Liberec, 2017
4. Mandát D.: Optical contactless topographic methods (Optické bezkontaktní topografické metody), in Czech, UP Olomouc, 2012, ISBN 978-80-244-3075-1
5. Musilová B.: Prediction of the corsetry pattern construction parameters, Ph.D. Thesis, TU of Liberec, 2012
6. Song G.: Improving Comfort in Clothing, Woodhead Publishing Limited, Cambridge England, 2011, ISBN: 9780857090645
7. Vrba V.: Střihy prádla: Konstrukce a stupňování, Praha: Redakce literatury spotřebního průmyslu, 1990, ISBN: 80-03-00355-5

IMPACT OF EXTRACTION PROCESSES ON FIBER PROPERTIES OF LINSEED FLAX FIBERS

Pierre Ouagne[1], Marie Grégoire[1], Benjamin Barthod-Malat[1,2], Philippe Evon[2], Laurent Labonne[2], Emmanuel De Luycker[1] and Vincent Placet[3]

[1]Laboratoire Génie de Production (LGP), Université de Toulouse, INP-ENIT, 47 Avenue d'Azereix, Tarbes, France
[2]Laboratoire de Chimie Agro-industrielle (LCA), Université de Toulouse, INRA, INPT, 31030 Toulouse Cedex 4, France
[3]Université de Bourgogne Franche Comté, FEMTO-ST, CNRS/UFC/ENSMM/UTBM, 25000 Besançon, France
pierre.ouagne@enit.fr

Abstract: *This work of a preliminary nature has for goal to investigate the potential of the linseed flax straw for industrial valorization in technical textiles. The impact of two extraction systems ("all fiber" extraction device and a scutching/hackling device) was investigated. In a first part of the paper, it was demonstrated that it is possible to extract the fibers from the other components of the straw such as the shives and vegetal dusts. The fiber yield is of about 38% of the stem mass. This very high fiber yield is particularly interesting and is higher than the one of hemp for example. The fiber properties were also investigated. The fiber length was shown to be in the adequate range of length to be considered for the carded spinning route, and the tensile properties of the individual fibers, even if decreased by about 45% in comparison to carefully manually extracted, are still at a sufficient level of performance for semi-structural composites applications for example. When using a scutching/hackling line, the length of the fibers is preserved and the impact of the fiber extraction was shown to be lower than the all fiber extraction line, particularly for the strength. These fibers could therefore be used for higher load bearing applications. Finally, the amount of fiber that can be extracted from the linseed flax fibers is large and this could certainly be at the origin of an industrial technical textile value chain.*

Keywords: *Linseed flax, all-fiber extraction, scutching/hackling, fiber characterization, tensile properties.*

1 INTRODUCTION

To manufacture high performance composite parts, it is necessary to organize and to align the fibers. As a consequence, aligned fibers architectures such as unidirectional sheets, non-crimped fabrics and woven fabrics (bidirectional) are usually used as reinforcement. For numerous applications, it is also important that the fabric may be formed into complex shapes without the appearance of defects such as wrinkles, vacancies, tow buckles etc. [1-4]. These materials are classically constituted from synthetic fibers such as glass, carbon or aramid. However, natural fibers are now considered in Europe as a serious alternative for composite reinforcement from low load up to high load bearing applications. A consequent literature, showing the interest of different fibers extracted from different plant is available. Review papers and even book chapters summarize the different progresses in the area [5-7]. A recent very complete review on the subject was proposed by Bourmaud et al. [8]. This review paper clearly shows the high potential of plant fibers and particularly bast fibers such as flax, hemp or nettles.

If the potential of the natural fibers has widely been demonstrated in numerous publications and review papers, the conversion of this potential to reality is often a problem and this one is not necessarily maximized. The maximization of the high mechanical potential of plant fibers for composite material reinforcement is dependent on several transformation steps, from the plant to the fabric. The fiber extraction step and technology used, depending on the stem arrangement, as it is illustrated by Figure 1, is a crucial key stage. It is particularly important to pay attention to the fiber extraction so that to avoid damaging the fibers to a too large extent. Specific high performance reinforcements are required to manufacture structural or semi-structural bio-composite parts especially for the automotive industry. New flax and comingled flax/bioplastic reinforcements have been elaborated in this goal. If large panels have been realised with a good success, the feasibility to manufacture complex shape parts using a sheet forming process [9], especially with natural fibre based reinforcements without defect is still a challenge. Previous studies [10-11] demonstrated that complex shape parts could be achieved by using specifically prepared fabrics, with particular process parameters. However, this requires specific care all along the different operations leading to the part manufacture due to the use of finite length natural fibres. It is also necessary when using agro-based material to reduce the impact of the part manufacturing in comparison to synthetic technology.

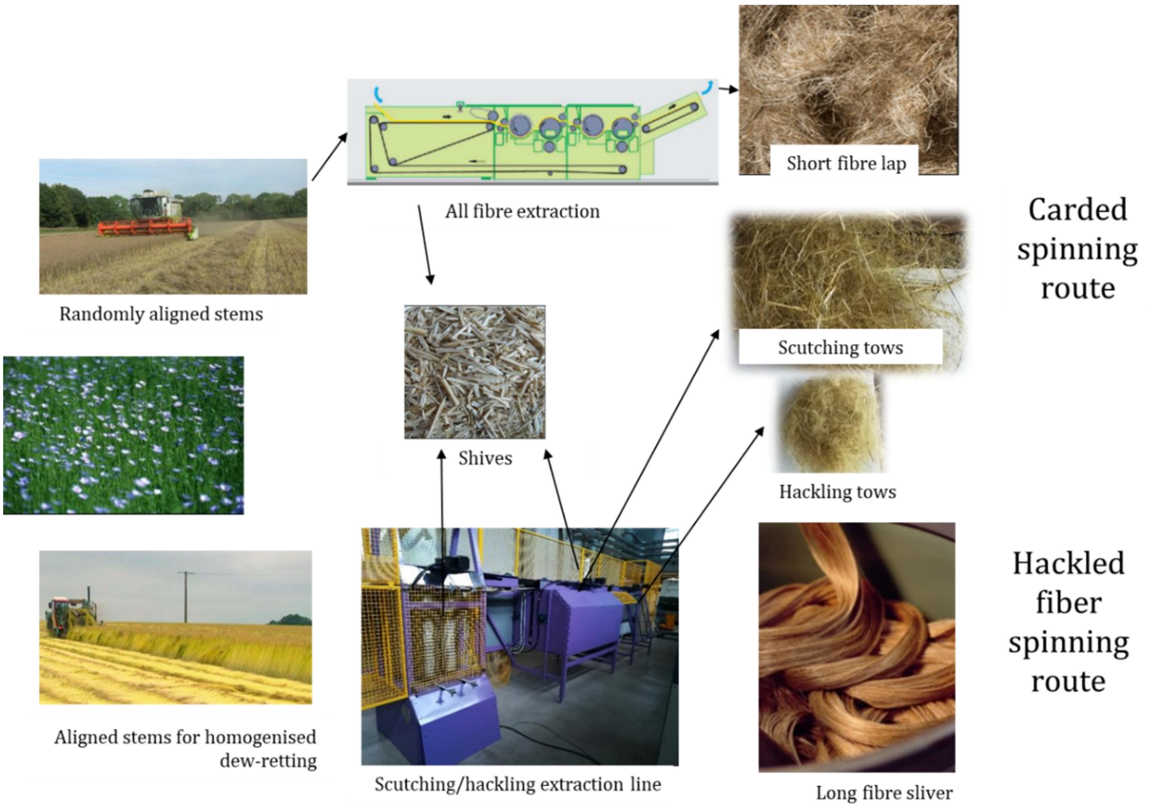

Figure 1 The fiber processing routes

The energy consumption for the production of yarn should be kept low and the possible fabric treatments should have a minimum impact on the environment. Dissanayake et al. [12] indicated that preparing composite reinforcement using natural fibers may have a higher impact on the environment than materials prepared from glass fibers if adequate manufacturing processes are not used. As a consequence, the manufacturing processes need to be adapted and optimized to reach this goal. Moreover, it is also important when considering the manufacturing processes to maximize the mechanical potential of the vegetal fibers. This means that it is important to minimize the length reduction of fibers or the appearance of defects such as dislocations or kink bands during the fiber extraction and the yarn preparation.

This paper therefore focuses on the critical and key fiber extraction stage so that to determine if the linseed flax fibers can be considered for technical textile applications. The linseed flax fibers were extracted by two different techniques and their morphological and mechanical potential characterized before and after extraction so that to determine the impact of the extraction process. Finally, the fiber yield was also studied so that to determine if an industrial value chain can be considered for the valorization of the linseed flax straw.

2 FROM THE PLANT TO THE FIBERS: IMPACT OF THE EXTRACTION PROCESSES

Within the plant, the fibers may have different roles. In flax or hemp, the bast fibers have a mechanical structural role. They contribute to the stabilization of the stems so that the plant remains vertical and that with an elongation ratio higher than the one of the highest trees. When extracted with the greatest care, the mechanical properties of the flax or hemp fibers show higher specific properties than glass fibers. However, this is only true in the case the fibers are not damaged during the different processes leading to the manufacture of the reinforcement fabric. Successive extraction and preparation processes take place before the textile architecturation into 1D (yarn) and 2D or 3D reinforcement products.

Depending on the harvesting procedures, the stems may be well ordered (textile flax or hemp in Eastern Europe) or randomly aligned (linseed flax or hemp in Western Europe). This is at the origin of different routes for the preparation of reinforcement materials. The first one, for randomly aligned stems consists in using an “all fiber” extraction line (textile fiber opener or hammer mills) that is followed by the carded preparation and spinning route. The second one is designed to receive aligned stems. It is based on the traditional well established scutching units classically used in Western Europe for flax and in Eastern Europe for hemp.

2.1 Impact of the all fiber extraction device on the morphological and mechanical properties of linseed flax fibers coming from un-retted straws.

2.1.1 The all fiber extraction device

In a preliminary study, Ouagne et al. [13] studied the potential of using an all fiber semi-industrial extraction line to extract fibers dedicated to technical applications such as semi-structural composites or geotextiles. The Laroche (France) Cadette 1000 "All Fiber" extraction opener from the AGROMAT platform (Tarbes, France), was used to extract the different vegetal fractions from linseed flax straw harvested in the south west of France. A schematic diagram of the device is presented in Figure 2.

The all fiber opening device consists of a succession of three extraction and separation modules. In each module a nailed cylinder under a rotation speed that can be up to 1700 rpm performs the fractionation of the vegetal mater into a fiber lap, shives and vegetal dusts. If the different constituent extraction is performed by the rotating nailed cylinder with the creation of a fiber lap, the shives fall on rotating belt and are sent by an aspiration system to collecting bags. In each module, a perforated cylinder extracts the fine particles through a suction process so that to separate this matter from the fiber lap. This device has the ability to process up to 175 kg of stems per hour.

2.1.2 Fiber extraction tests

Two sets of experiments were carried out on dry and rewetted by water batches. For each batch of about 25 kg of randomly aligned stem, the different fractions were weighed under similar conditions of humidity (dry state). As the fiber laps contain remaining pieces of shives trapped, these ones are removed after a mechanical sieving step and the last pieces of shives are picked up manually. Figure 3 shows the different vegetal fractions obtained at the end of the extraction process. The goal here is to evaluate the amount of fiber available from the linseed flax straws.

2.1.3 Reference material

As the goal of the study consisted in studying the impact of the extraction devices on the properties of the fibers, a reference material needs to be tested. Linseed flax fibers were extracted manually with the greatest care so that their initial potential is not decreased and represent as closely as possible the reinforcement performance of these fibers. To do so, pieces of linseed flax straws were soaked in water for 72 h under a temperature of 30°C and the fibers were extracted manually.

2.1.4 Fiber characterization: Impact of the extraction procedure on morphological and mechanical properties of technical and single fibers respectively

In a first extent, the fiber length of the technical fibers (fiber bundles) was characterized. The goal here is to investigate whether or not the technical fibers constituting the fiber lap are appropriate (sufficiently long) for a further transformation into yarns and technical textiles. The measurements were performed on about 600 fibers. To do so, one side of technical fiber was fixed and the other extremity was pulled so that to obtain a straight fiber measured between both its extremities.

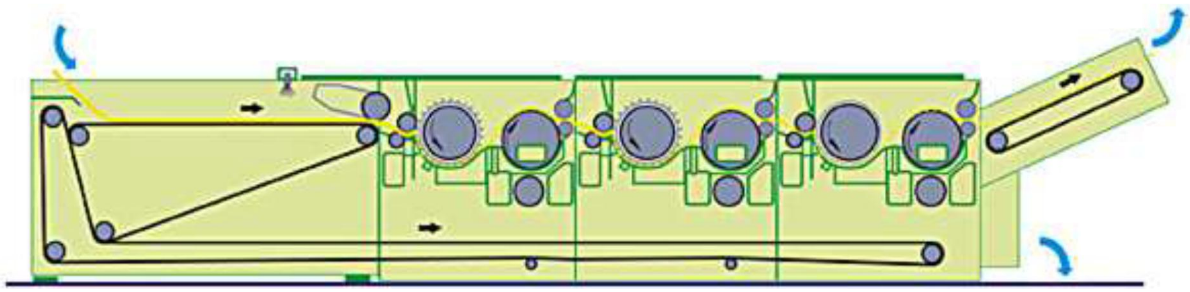

Figure 2 Schematic diagram of the three modules "all fiber" opening device

Figure 3 The three vegetal fractions

In a second extent, the evolution of the single fiber tensile properties was determined. Tensile tests on individual fibers were performed on batches of 40 fibers. The tests were performed at the FEMTO-ST laboratory following the recommendation of the NF T25-501-2 standard test method [14]. A Bose (USA) Electroforce 3230 tensile testing machine equipped with a 22 N capacity load cell was used to perform the tests. The fiber apparent diameter was evaluated using an optical microscope (Olympus PMG3-F3, France). The apparent diameters were measured at five different locations so that to calculate both tensile strength and modulus. It is assumed here that the fibers are perfectly cylindrical.

2.1.5 Results

The different vegetal fraction yields were determined after extraction processing and are presented in Table 1 for both dry and re-wetted batches.

Table 1 Fiber, shives and vegetal dust proportions after "all fiber" extraction

	Total fibre content [%]	Total shives content [%]	Total dust content [%]
Re wetted	37.5	57.6	4.9
Dry	37.8	52.4	9.8

Table 1 shows that the amount of fiber (about 38% of the stem masses) is high and much higher than what can be encountered in the literature. Indeed, the amount of linseed flax fibers in the stem is generally much lower [15]. This may be due to the fact that fiber rich stems were considered in this study, or this may be due to a different way of evaluating the fiber yields. The technical fiber lengths are presented in Table 2.

Table 2 Length of technical fibers

	Fiber bundle length [mm]
Re wetted	53±29
Dry	39±22

Table 2 indicates that the fiber bundle length is of about 40 mm for the fiber extracted from the dry stems. The fibers extracted from the re-wetted batch are longer. This suggests that it is probably interesting to re-wet the fibers before processing. This probably confers some ductility to the fibers and prevents extra breakings.

Table 3 shows the tensile properties of individual fibers manually extracted from un-processed stems and from processed bundles from the re-wetted straws.

Table 3 Tensile properties of individual linseed flax fibers

	Modulus of elasticity [GPa]	Strength [MPa]
Manually extracted	45±27	1080±640
All fiber device extration	38±17	604±409

Table 3 shows the tensile properties of the single fibers. It particularly compares the evolution of the tensile properties before and after mechanical fiber extraction with the "all fiber" device. The results indicate that the extraction has a clear impact on the tensile properties of the individual fibers. This is particularly visible for the strength with a decrease of about 45%. In the case of modulus, the decrease is more moderate (20%). This decrease in strength is probably due to the introduction of defects such as kink-bands or dislocations in the internal structure of the fibers.

2.2 *Impact of a scutching/hackling extraction device on the morphological and mechanical properties of linseed flax fibers coming from un-retted straws.*

2.2.1 The scutching/hackling device

A scutching/hackling device is shown in Figure 4. This device is a low scale version of classical industrial scutching/hackling units. It consists of successive breaking, scutching (beating), hackling (combing) units. The scutching and hackling devices are traditionally used when long fibers are expected.

Figure 4 Laboratory scutching/hackling line

In this work, non-retted aligned straws were collected manually to evaluate the potential of the linseed flax fibers and the impact of the scutching/hackling process on the fiber properties.

One of the main interest of using aligned stems in conjunction with scutching/hackling devices is the fact that the technical fiber length is not as much decreased as it is the case for the "all fiber" extraction line. In our case, the bundle length is about equivalent to the length of the collected stems, (about 300 mm). The fibers are therefore much longer than the ones extracted using the "all fiber" line. The hackled technical fibers are about six times longer. Figure 5 shows a sample of hackled linseed flax.

Figure 5 Hackled non-retted linseed flax sliver

If the breaking and scutching steps have an influence on the fiber properties, the most damaging stage is hackling. This stage is particularly important because it finishes the separation of the technical fibers from the rest of the stem components. It also contributes to the finer separation of the fiber bundles into individual fiber or small clusters of fibers.

The influence of the hackling step on the mechanical properties of individual fibers is given in Table 4 together with a comparison with the impact of the "all fiber" extraction.

Table 4 Tensile properties of hackled single fibers

	Modulus of elasticity [GPa]	Strength [MPa]
Manually extracted	45±27	1080±640
All fiber device extration	38±17	604±409
Scutching/hackling	***40±10***	***966±403***

Table 4 shows that the modulus does not decrease in a great extent in comparison to the manually extracted fiber. No statistical difference may be observed. The modulus of elasticity is surprisingly equivalent to the one obtained from fibers extracted with the "all fiber" device. The strength of fibers after hackling does not show any significant decrease in comparison to the manually extracted fibers. The result of the tensile strength is however much larger than the strength obtained from fiber extracted from the "all fiber" line. This suggests that the level of defects conferred to the hackled fibers is lower than the number of defects present on fibers extracted by the "all fiber" line.

3 CONCLUSIONS

This work of a preliminary nature has for goal to investigate the potential of the linseed flax straw for industrial valorization in technical textiles. The impact of two extraction systems ("all fiber" extraction device and a scutching/hackling device) was investigated. In a fist part of the paper, it was demonstrated that it is possible to extract the fibers from the other components of the straw such as the shives and vegetal dusts. The fiber yield is of about 38%. This very high fiber yield is particularly interesting and is higher than the one of hemp for example [15]. The fiber properties were also investigated. The fiber length was shown to be in the adequate range of length to be considered for the carded spinning route and the tensile properties of the individual fibers even if decreased by about 45% in comparison to carefully manually extracted are still at a sufficient level of performance for semi-structural composites applications for example. When using a scutching/hackling line, the length of the fibers is preserved and the impact of the fiber extraction was shown to be lower than the all fiber extraction line, particularly for the strength. These fibers could therefore be used for higher load bearing applications. Finally, the amount of fiber that can be extracted from the linseed flax fibers is large and this could certainly be at the origin of an industrial technical textile value chain.

4 REFERENCES

1. Potter K., Khan B., Wisnom M., Bell T., Stevens J.: Variability, fibre waviness and misalignment in the determination of the properties of composite materials and structures, Composites Part A 39(9), 2008, pp. 1343-1354, https://doi.org/10.1016/j.compositesa.2008.04.016
2. Ouagne P., Soulat D., Moothoo J., Capelle E., Gueret S:. Complex shape forming of a flax woven fabric; Analysis of the tow buckling and misalignment defect, Composites Part A 51, 2013, pp. 1-10, https://doi.org/10.1016/j.compositesa.2013.03.017
3. Tephany C., Gillibert J., Ouagne P., Hivet G., Allaoui S., Soulat D.: Development of an experimental bench to reproduce the tow buckling defect appearing during the complex shape forming of structural flax based woven composite reinforcements, Composites Part A 81, 2016, pp. 22-33, https://doi.org/10.1016/j.compositesa.2015.10.011
4. Ouagne P., Soulat D., Tephany C., Gillibert J.: Measurement of the appearance and growth of tow buckling defect in the frame of complex shape manufacturing process by using fringe projection technique, Strain 52(6), 2016, pp. 559-569, https://doi.org/10.1111/str.12206
5. Dhakal H.N., Zhang Z.: The use of hemp fibres as reinforcements in composites, Biofiber Reinforcements in Composite Materials, Woodhead Publishing, 2015, pp. 86-103, https://doi.org/10.1533/9781782421276.1.86
6. Mussig J., Haag K.: The use of flax fibers as reinforcements in composites, Biofiber Reinforcements in Composite Materials, Woodhead Publishing, 2015, pp. 35-85, https://doi.org/10.1533/9781782421276.1.35
7. Akin D.E.: Flax - Structure, Chemistry, Retting and Processing, Industrial Applications of Natural Fibres: Structure, Properties and Technical Applications, Wiley publication, 2010, pp. 89-108, https://doi.org/10.1002/9780470660324.ch4

8. Bourmaud A., Beaugrand J., Shah D.U., Placet V., Baley C.: Towards the design of high-performance plant fibre composites, Progress in Material Science 97, 2018, pp. 347-408, https://doi.org/10.1016/j.pmatsci.2018.05.005
9. Ouagne P., Soulat D., Hivet G., Allaoui S., Duriatti D:. Analysis of defects during the preforming of a woven flax reinforcement, Advanced Composite Letters 20(4), 2011, pp. 105-108, https://doi.org/10.1177/096369351102000403
10. Capelle E., Ouagne P., Soulat D., Duriatti D.: Complex shape forming of flax woven fabrics: Design of specific blank-holder shapes to prevent defects, Composites Part B 62, 2014, pp. 29-36, https://doi.org/10.1016/j.compositesb.2014.02.007
11. Allaoui S., Hivet G., Soulat D., Wendling A., Ouagne P., Chatel S.: Experimental preforming of highly double curved shapes with a case corner using an interlock reinforcement, International Journal of Materials Forming 7(2), 2014, 155-165, https://doi.org/10.1007/s12289-012-1116-5
12. Dissanayake N., Summerscales J., Grove S., Singh M.: Life cycle impact assessment of flax fibre for the reinforcement of composites, Journal of Biobased Materials and Bioenergy 3(3), 2009, pp. 245-248, https://doi.org/10.1166/jbmb.2009.1029
13. Ouagne P., Barthod-Malat B., Evon P., Labonne L., Placet V.: Fibre extraction from oleaginous flax for technical textile applications: Influence of pre-processing parameters on fibre extraction yields, size distribution and mechanical properties, Procedia Engineering 200, 2017; pp. 213-220, https://doi.org/10.1016/j.proeng.2017.07.031
14. ASTM D3822 / D3822M – 14. Standard Test Method for Tensile Properties of Single Textile Fibers
15. Meirhaeghe C.: ADEME Report: Assessment of natural fibre availability and accessibility for material uses in France, 2011, http://www.ademe.fr/sites/default/files/assets/documents/76290_12_evaluation_dispo_accessibilite_fibres_veg_usages_materiaux.pdf

STUDY OF THE TOW BUCKLING DEFECT DURING THE COMPLEX SHAPE FORMING OF SYNTHETIC AND VEGETAL FIBRE REINFORCED STRUCTURAL COMPOSITES

M.M. Salem, E. De Luycker, M. Fazzini and P. Ouagne

Laboratoire Génie de Production (LGP), INP-ENIT, Univ. de Toulouse, Tarbes, France

Abstract: *Fibrous reinforcements for structural composites manufacturing need to undergo in certain cases a complex shape forming process during which multiple defects could appear. These defects, such as tow buckling and tow sliding may reduce the integrity of the final part. The onset of these defects depends on the initial loading conditions, the shape of the preform and the characteristics of the textile material. While mechanisms behind the formation and development of both defects are yet to be fully understood. We focused, in this work, on investigating the buckling defect. In order to do so, we used optical field measurement techniques to monitor the kinematics of the defect appearance and predict it via an adapted analytical model of the defect appearance.*

Key words: *Composite manufacturing, preforming defects, textile reinforcement, tow buckling, full field strain measurement.*

1 INTRODUCTION

Fibre reinforced composites receive an ever growing interest, because of their interesting mechanical properties, low cost and progressively mastered manufacturing techniques [1]. The complex shape forming of fibre reinforced composites might be done using techniques such as Resin Transfer Molding or Thermoplastic-Matrix Composites Stamping to produce seamless materials [2] but it can be less productive than regular laminates and susceptible to produce defects that alter the mechanical properties of the composite [3].

Thus, it is essential to fully understand and anticipate the appearance of defects such as the tow buckling which will be the focus of this paper. In the literature, the buckling defect appears on woven reinforcements and seems to be the result of the in-plane bending of the tows coupled with initial loads and reinforcement properties. Thus a buckling device, presented in Figure 1, was designed and manufactured to reproduce those conditions in a controlled environment [4].

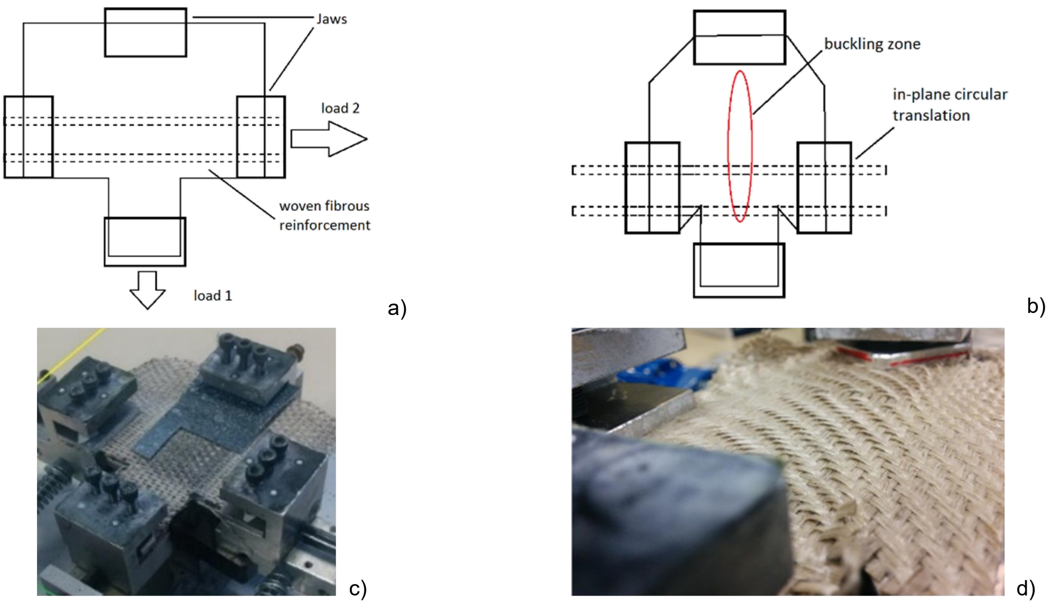

Figure 1 Buckling device principle a), b); Appearance of the buckles on the bent reinforcement surface c), d)

2 EXPERIMENTAL STUDY

2.1 Description of the buckling device

The buckling device is instrumented with two load cells, one in each direction of the weave in order to monitor the applied load. The buckling device was also equipped with a digital image correlation camera in order to record the bending angle between the tow's initial position and the bent state at any given moment. T shape samples were loaded in the device. This allowed the in-plane bending of one network (the transverse one) up to a 40° bending angle from the initial tow position (Figure 1b).

Furthermore, three full field optical systems: Various-focus microscopy (Figure 2a), Fringe projection (Figure 2b) and Stereo-Digital Image Correlation (Figure 2c), were considered and tested to assess the formation of the buckle. Three tests were performed in similar conditions as it is impossible to combine the optical systems equipments. The reconstructed surfaces of the tows from each technique are presented in Figure 2.

The profiles of the tow buckle (red lines in Figure 2) at the initial state 0° and after an in-plane bending angle of 25° are given in Figure 3 for the three reinforcements tested with the three full field optical systems. One can globally see that the three techniques indicate relatively similar profiles and thus results from each technique can be considered valid. The S-DIC was finally chosen as it allows both fast and accurate enough results plus native displacement data.

2.2 Buckling tests

Three different reinforcements, listed in Table 1, were tested. Some of their geometrical characteristics are also given in Table 1. The influence of multiple parameters, such as initial loading in both weave directions as well as the reinforcement mechanical and geometrical properties, is considered. In the following, the bending rigidity and tow's geometries were investigated. The reinforcements were subjected to a 300 N load in the fixed tows network and 20 N in the bending tows network and bent up to 40° angle. Figure 4 shows the evolution of the maximum tow elevation as a function of the in-plane bending angle.

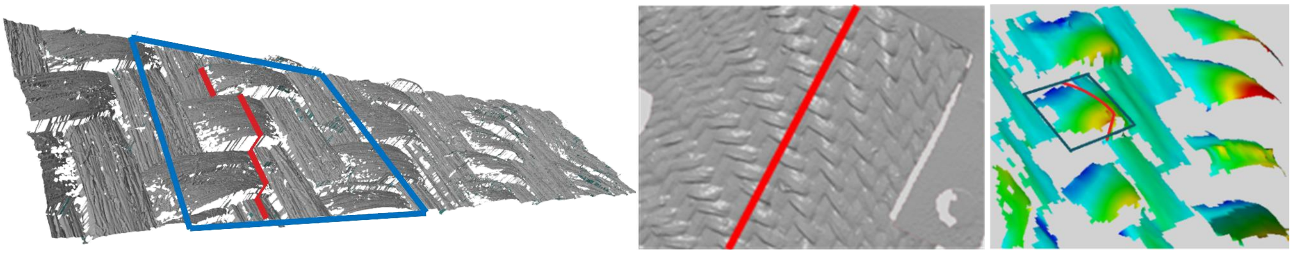

a) b) c)

Figure 2 Reconstructed surface and profile of the tows (red line) obtained by focus-variation microscopy (a), fringe projection (b) and Stereo-digital image correlation (S-DIC) (c)

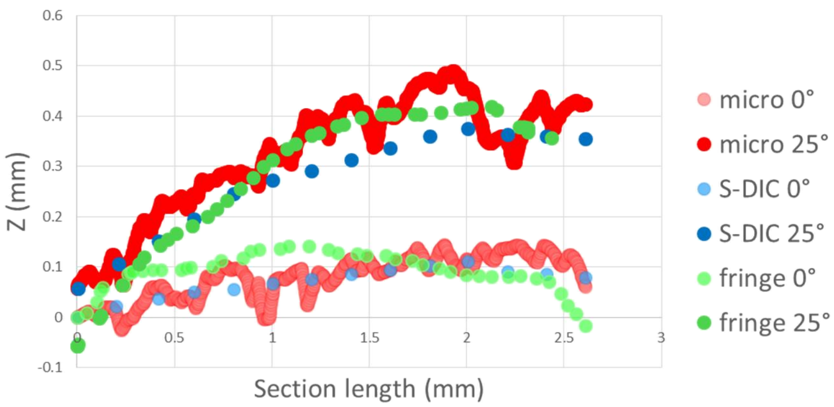

Figure 3 Buckles profiles comparison using stereo-DIC, Fringe projection and Various-focus microscopy at tow bending angles of 0° and 25°

Table 1 Characteristics of reinforcement used for tow buckling

Weave	Material	Area density [g/m²]	Warp density [m^{-1}]	Weft density [m^{-1}]	Unsupported length [mm]	Unsupported width [mm]	Tow bending rigidity [N.mm]
Twill 2x2	Sized up linen	476	380	385	6.1	2.5	1.18
Twill 2x2	De-sized up linen	465	380	430	5.7	2.4	0.72
Twill 2x2	Carbon fiber	600	380	380	6.4	2.3	7.55

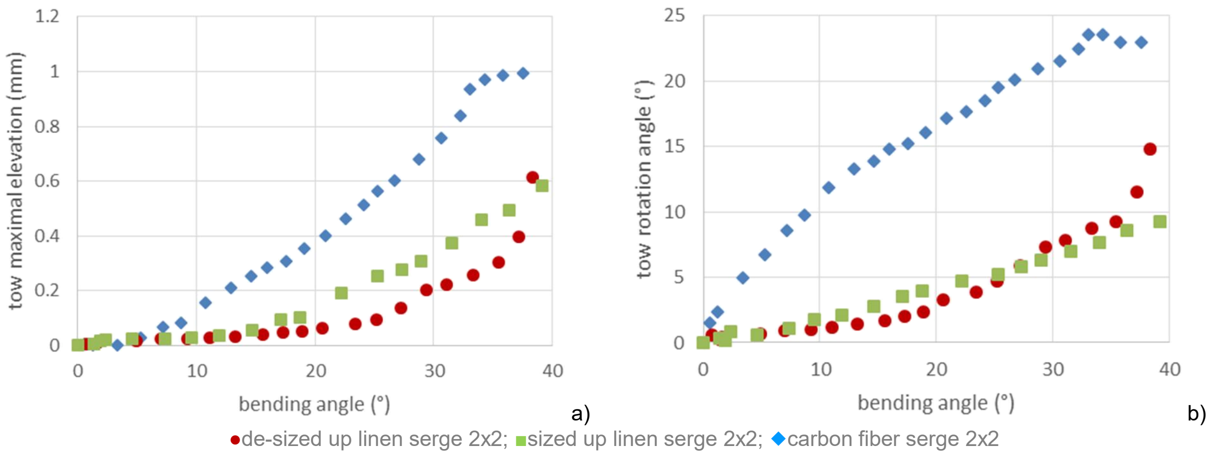

Figure 4 Maximum elevation (a) and rotation angle of the tow (b) as a function of the bending angle

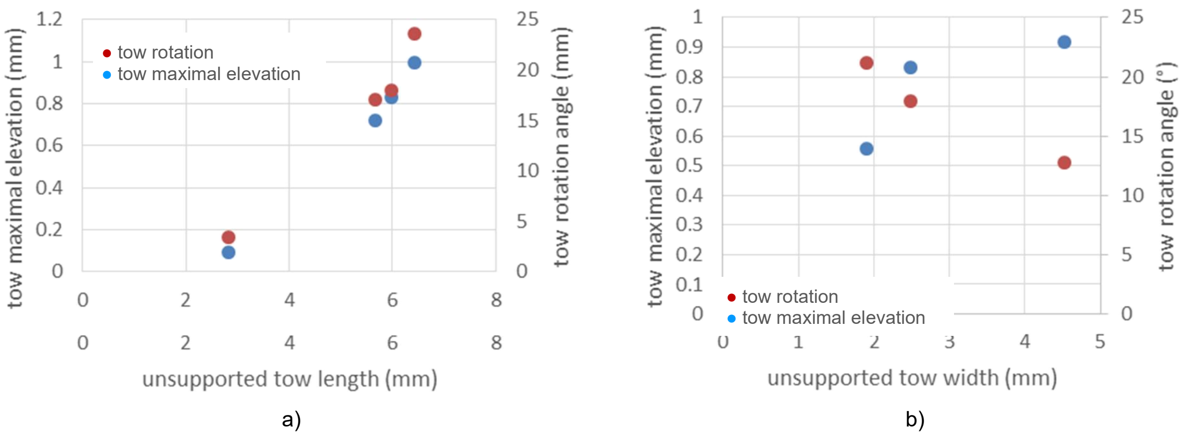

Figure 5 Maximum elevation and rotation angle of the tow as a function of the unsupported tow length (a) and as a function of the unsupported tow width (b)

One can observe in Figure 4 that the buckles appear for lower in-plane bending angles for the carbon twill weave. For the carbon reinforcement we notice the onset of the buckle at a bending angle of 5°, followed by the sized-up linen reinforcement at an angle of 10° and finally by the desized-up linen reinforcement at an angle of 13°. As the bending rigidity (measured independently on an adapted system) decreases the onset of the buckle is much more delayed and the size of the final buckle is smaller. Since the tows are under displacements constraints, the load repartition for the same bending angle is different depending on the material. More rigid tows achieve a critical buckling load for lower values of bending angles which explains the earlier buckling. Consequently, the bending rigidity of the tow for relatively similar contextures and tow geometries is therefore a key parameter that controls the appearance and the evolution of the tow buckling defect.

As for the effect of tows geometry, taking into account the variation of the unsupported length and width of the tows and using the same experimental conditions as before, we compared for a de-sized up linen based reinforcements the impact of the unsupported tow length (the length for a given architecture between two weft perpendicular tows) and the unsupported tow width (the width of the tow showing the in-plane bending (the warp tow) in Figure 5. As the unsupported length grows in Figure 5a, so does the tow deflection and rotation. This is explained by the added freedom for the buckle to rise and develop. But as the unsupported width grows in Figure 5b, the deflection grows while the rotation diminishes. This could be explained by smaller size buckles compared to the tow width, which means even if they deflect higher, the deflection compared to the tow width seems to be declining.

3 ANALYTICAL MODEL

An analytical framework based on the buckling of orthotropic homogenous plate is proposed to predict the buckling of tows inspired from a work made for tape on an elastic foundation for the buckling of steered tows in automated dry fibre placement [5]. Considering the tow as an orthotropic thin plate [6], the differential equation for plate bending, was solved by using the Rayleigh-Ritz approach. This approach allows us to determine the critical buckling load *Pcr*, for which the tow starts to deflect:

$$Pcr = \frac{\frac{24D11m^2\pi^2}{L^2} + \frac{90D22L^2}{b^4m^2\pi^2} + \frac{160D66}{b^2} - \frac{40D12}{b^2}}{6-\alpha} \qquad (1)$$

where *D11* is the bending stiffness in the longitudinal direction, *D22* is the bending stiffness in the transversal direction, *D12* is the Poisson-action bending stiffness, *D66* is the torsional stiffness, *L* is the tow length, *b* is the tow width, *m* is the buckling mode and α is the non-uniformity load coefficient which characterize the bending - tension combination (2 for pure bending and 0 for pure compression) as illustrated in Figure 6.

By equating *Pcr* to the minimal buckling load on the inner edge of the tow, P_0 defined geometrically in equation 2, the critical curvature radius for buckling, *Rcr*, was identified in equation 3.

$$P_0 = \frac{E1\,h\,b}{\alpha R} \qquad (2)$$

$$Rcr = \frac{E1(6-\alpha)bh}{\alpha\left(\frac{24D11m^2\pi^2}{L^2} + \frac{90D22L^2}{b^4m^2\pi^2} + \frac{160D66}{b^2} - \frac{40D12}{b^2}\right)} \qquad (3)$$

where *E1* is the longitudinal tensile modulus and *h* is the thickness of the tow.

As stipulated in [5], *D12* and *D22* are orders of magnitude lower than *D11* and *D22* and thus can be neglected with close to no impact on the critical radius, thus, the expression of *Rcr* becomes:

$$Rcr = \frac{E1(6-\alpha)b^3hL^2}{\alpha(160\ D66\ L^2 + 24\ D11\ \pi^2b^2m^2)} \qquad (4)$$

The bending stiffness *D11* was then evaluated using a Peirce cantilever test and the torsional stiffness was evaluated using a torsion test. α was also estimated using digital image correlation. This finally allowed us to calculate the critical buckling radius and compare it to the experimental buckling radius that was measured experimentally using ImageJ® on the previously mentioned digital image correlation pictures. *E1* was retrieved from the literature as the used tows resemble those used by Bassoumi [7] in her work. All the results are compiled in Table 2.

Table 2 Parametric results, analytical and experimental critical radii

Reinforcement	Serge 2x2 sized up	Serge 2x2 de-sized up
E1 [N/mm²]	19800	7800
L [mm]	6.1	5.7
b [mm]	2.5	2.4
h [mm]	0.4	0.4
α	2	2
m	1	1
D11 [N.mm]	1.18	0.72
D66 [N.mm]	0.44	0.17
Rcr [mm]	2082.9	1482.2
Rcr(exp) [mm]	2255	1627
Δ [%]	7.63	8.90

The analytical and experimental results seem to be in agreement with only 8.2% difference so we can assume that the model can safely predict the critical buckling radius. Yet, more reinforcement needs to be studied in order to confirm the results.

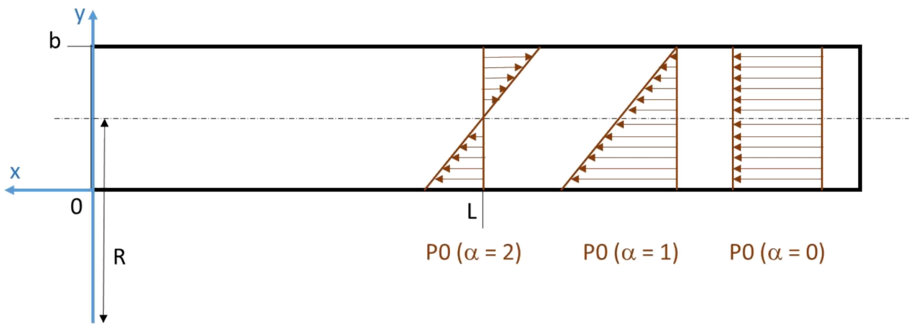

Figure 6 Tow representation from above as an orthotropic plate with compressive load P_0; representation for different values of the non-uniformity coefficient α

4 CONCLUSION

The tow buckling defect was investigated using a specifically made device and some parameters were studied. The effect of tows dimensions and tow rigidities was experimentally studied and related to the buckling. An analytical framework was adapted from the literature and was found to be able to predict the critical buckling radius so far with a need for further tests on different reinforcements to fully validate it.

5 REFERENCES

1. Pickering K.L., Aruan Efendy M.G., Le T.M.: A review of recent developments in natural fibre composites and their mechanical performance, Composites Part A: Applied Science and Manufacturing 83, 2016, pp. 98-112, https://doi.org/10.1016/j.compositesa.2015.08.038
2. Boisse P.: Mise en forme des renforts fibreux de composites, Techniques de l'ingénieur, Réf: AM3734 v1, 2004, pp. 1-10, https://www.techniques-ingenieur.fr/base-documentaire/materiaux-th11/plasturgie-procedes-specifiques-aux-composites-42474210/mise-en-forme-des-renforts-fibreux-de-composites-am3734/
3. Potter K., Khan B., Wisnom M., Bell T., Stevens J.: Variability, fibre waviness and misalignment in the determination of the properties of composite materials and structures, Compos. Part A: Applied Science and Manufacturing 39(9), 2008, pp. 1343-1354, https://doi.org/10.1016/j.compositesa.2008.04.016
4. Tephany C.: Analyse de la formabilité de renforts composites à base de fibres naturelles, PhD thesis, Université d'Orléans, 2014
5. Matveev M.Y., Schubel P.J., Long A.C., Jones I.A.: Understanding the buckling behaviour of steered tows in Automated Dry Fibre Placement (ADFP), Composites Part A: Applied Science and Manufacturing 90, 2016, pp.451-456, https://doi.org/10.1016/j.compositesa.2016.08.014
6. Florimond C.: Contributions à la modélisation mécanique du comportement de mèches de renforts tissés à l'aide d'un schéma éléments finis implicite, INSA-Lyon, 2013
7. Bassoumi A.: Analyse et modélisation du choix des renforts pour optimiser la mise en forme de matériaux composites à base de fibres végétales, PhD thesis Université d'Orléans, 2016

DETERMINATION OF OPTIMAL CONJUGATE STRESS STRAIN PAIRS

Bohuslav Stříž and Lukáš Čapek

Technical University of Liberec, Faculty of Textile Engineering, Department of Technologies and Structures Studentská 2, 461 17 Liberec, Czech Republic
bohuslav.striz@tul.cz; lukas.capek@tul.cz

Abstract: *The aim of this paper was to shown a new methodology for determining and optimal conjugated pair for Cauchy stress tensor. Methodology demonstrated in this work can be used for various materials loaded by uniaxial tension, e.g. for textiles, soft tissues etc.*

Keywords: *Stress tensor, strain tensor, conjugated pair.*

1 INTRODUCTION

In engineering practice, the mechanical parameters are usually identified in a simplified form as engineering stress and deformation. These material parameters are used worldwide since 19th century for linear tasks. When large deformation presents, as in composite materials or others, this simplified approach cannot be used any more. It is necessary to define these deformations and stress as second order tensors that are energetically conjugated. It means that their double-dot product express strain energy in the system.

When expressing derivate quantity, e.g. Young moduli, according to different conjugated pairs, different values will be obtained [1, 2]. In view of the fact that the trues stress tensor is not conjugated with any known strain tensor, it is difficult to decide about suitable conjugated pair. It will be shown, that for uniaxial loading of the specimen it is possible to determine to Cauchy stress tensor a suitable conjugated strain tensor.

2 MATERIALS AND METHODS

Let we have a specimen of an anisotropic material, loaded by a force F_1. Cartesian coordinates of points 1-4 were determined by an optical method.

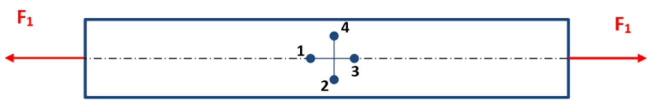

Figure 1 Testing sample

From Cartesian coordinates of points 1-4 it is possible to calculate displacements as:

$$\begin{aligned}
(1+u_{11})(x_1^{01}-x_1^{03})+u_{12}(x_2^{01}-x_2^{03}) &= x_1^2-x_1^3\\
(1+u_{11})(x_1^{02}-x_1^{04})+u_{12}(x_2^{02}-x_2^{04}) &= x_1^2-x_1^4\\
u_{21}(x_1^{01}-x_1^{03})+(1+u_{22})(x_2^{01}-x_2^{03}) &= x_2^1-x_2^3\\
u_{21}(x_1^{02}-x_1^{04})+(1+u_{22})(x_2^{02}-x_2^{04}) &= x_2^2-x_2^4
\end{aligned} \tag{1}$$

where the Langragarian coordinate system is noticed as x_i^{0j} and Euler´s coordinate system is x_i^j.

For uniaxial type of loading (symmetrical sample) the equations (1) can be simplified. Displacements u_{12} and u_{21} are zero. Thus:

$$\begin{aligned}
(1+u_{11})(x_1^{01}-x_1^{03}) &= x_1^1-x_1^3\\
(1+u_{22})(x_1^{02}-x_1^{04}) &= x_2^2-x_2^4
\end{aligned} \tag{2}$$

If we assume the lines 13 and 24 perpendicular, than only two equations can be used. For lower values of parameter x the higher scatter of coordinates x_i^j is. So that the scatter of displacement u_{11} and u_{22} is also higher.

Regarding the fact that the sample is slightly press-stress at the beginning of the measurement so that the displacement u_{11}, u_{22} will not be zero at the beginning of measurement too. Let´s suppose that displacement evaluates linearly with some constant k_1 and k_2. We can write it down as:

$$\begin{aligned}
u_{11} &= u_{11}^0+k_1x\\
u_{22} &= u_{22}^0+k_2x
\end{aligned} \tag{3}$$

It is clear that $u_{11}^0 > 0$, $k_1 > 0$, $u_{22}^0 < 0$, $k_2 < 0$, because the sample is lengthen along line 13 and shorten along the line 24.

Suppose we have a variable h as an actual thickness of the sample and h_0 as an initial thickness.

We can write the transversal displacement as:

$$\frac{h}{h_0} - 1 = u_{33} \tag{4}$$

where $u_{33} \leq 0$ due the thinning of the sample.

The deformation gradient *F* is then:

$$F = \begin{pmatrix} 1+u_{11} & 0 & 0 \\ 0 & 1+u_{22} & 0 \\ 0 & 0 & 1+u_{33} \end{pmatrix} \tag{5}$$

If we assume initial length of sample l_0, the Cauchy stress can be expressed by:

$$S_{11} = \frac{F_1}{l_0 h_0 (1+u_{22})(1+u_{33})} \tag{6}$$

which forms the first member of Cauchy stress tensor:

$$\sum = \begin{pmatrix} S_{11} & 0 & 0 \\ 0 & 0 & 0 \\ 0 & 0 & 0 \end{pmatrix} \tag{7}$$

Further we can write Biot´s stress tensor:

$$S_B = \frac{J}{2}\left[F^{-1}\sum R + R^T \sum F^{T-1}\right] \tag{8}$$

where *R* is a rotational matrix, *J* is a Jacobian and *F* a deformation gradient.

In case of uniaxial loading, we simply write an inversion of deformation gradient as inversion of diagonal matrix:

$$F^{-1} = \begin{pmatrix} \frac{1}{1+u_{11}} & 0 & 0 \\ 0 & \frac{1}{1+u_{22}} & 0 \\ 0 & 0 & \frac{1}{1+u_{33}} \end{pmatrix} = F^{T-1} \tag{9}$$

After some manipulating with expressions, we finally get a formulation of Biot's stress tensor for uniaxial loading:

$$S_{\boldsymbol{B}} = \frac{(1+u_{11})(1+u_{22})(1+u_{33})}{2}. \\ .\left[\frac{F_1}{l_0 h_0 (1+u_{11})(1+u_{22})(1+u_{33})}\right] 2 = \\ = \frac{F_1}{l_0 h_0} = C_{11} \tag{10}$$

$$S_B = \begin{pmatrix} C_{11} & 0 & 0 \\ 0 & 0 & 0 \\ 0 & 0 & 0 \end{pmatrix} \tag{11}$$

Stress tensor for conjugated pairs

In order to get a conjugated pair of stress-strain tensors, we define a exponent-generalization of different stress tensors as:

m = 2 Piola-Kirchov
m = 1 Biott
m = 0 logarithmic
m = -1 Cernych
m = -2 Hill, Almansi

$$S(m) = \frac{1}{2}\left[S_B U^{1-m} + U^{1-m} S_B\right] \tag{12}$$

Since we know all members of above equation we can simply write down a formulation for uniaxial stress tensor in a generalized form:

$$S(m) = \begin{pmatrix} C_{11}(1+u_{11})^{1-m} & 0 & 0 \\ 0 & 0 & 0 \\ 0 & 0 & 0 \end{pmatrix} \tag{13}$$

this expression is valid for Cauchy stress tensor, but with unknown parameter *m*. The strain tensor that fulfill the term of conjugation is defined by:

$$\varepsilon_{ij}(m) = \frac{1}{m}\left[U^m - I\right] \tag{14}$$

For above mentioned parameters *m*, it´s necessary to find out power of strain tensor *U*, except of m=0. In this case numerator and denominator are zero (14). Calculating limit following equation is obtained:

$$\varepsilon_{ij}(0) = \ln U \tag{15}$$

Equation (15) is valid only in the case when augmenting deformation the main axes of the tensor *U* is not rotated. When using different values of parameter m we obtained following strain tensors:

$$\varepsilon_{ij}(2) = \frac{1}{2}\left[\begin{pmatrix} (1+u_{11})^2 & 0 & 0 \\ 0 & (1+u_{22})^2 & 0 \\ 0 & 0 & (1+u_{33})^2 \end{pmatrix} - \\ - \begin{pmatrix} 1 & 0 & 0 \\ 0 & 1 & 0 \\ 0 & 0 & 1 \end{pmatrix}\right] = \\ = \begin{pmatrix} u_{11} + \frac{1}{2}{u_{11}}^2 & 0 & 0 \\ 0 & u_{22} + \frac{1}{2}{u_{22}}^2 & 0 \\ 0 & 0 & u_{33} + \frac{1}{2}{u_{33}}^2 \end{pmatrix} \tag{16}$$

$$\varepsilon_{ij}(1) = \frac{1}{2}\left[\begin{pmatrix} 1+u_{11} & 0 & 0 \\ 0 & 1+u_{22} & 0 \\ 0 & 0 & 1+u_{33} \end{pmatrix} - \\ - \begin{pmatrix} 1 & 0 & 0 \\ 0 & 1 & 0 \\ 0 & 0 & 1 \end{pmatrix}\right] = \\ = \begin{pmatrix} u_{11} & 0 & 0 \\ 0 & u_{22} & 0 \\ 0 & 0 & u_{33} \end{pmatrix} \tag{17}$$

$$\varepsilon_{ij}(0) = \begin{pmatrix} \ln(1+u_{11}) & 0 & 0 \\ 0 & \ln(1+u_{22}) & 0 \\ 0 & 0 & \ln(1+u_{33}) \end{pmatrix} \quad (18)$$

$$\varepsilon_{ij}(-2) = \frac{1}{2}\left[\begin{pmatrix} 1 & 0 & 0 \\ 0 & 1 & 0 \\ 0 & 0 & 1 \end{pmatrix} - \begin{pmatrix} \frac{1}{(1+u_{11})^2} & 0 & 0 \\ 0 & \frac{1}{(1+u_{22})^2} & 0 \\ 0 & 0 & \frac{1}{(1+u_{33})^2} \end{pmatrix}\right] = \quad (19)$$

$$= \begin{pmatrix} \frac{u_{11}+\frac{1}{2}u_{11}^2}{(1+u_{11})^2} & 0 & 0 \\ 0 & \frac{u_{22}+\frac{1}{2}u_{22}^2}{(1+u_{22})^2} & 0 \\ 0 & 0 & \frac{u_{33}+\frac{1}{2}u_{33}^2}{(1+u_{33})^2} \end{pmatrix}$$

Similarly, stress tensor $S(m)$ might be determined:

$$S(2) = \frac{C_{11}}{1+u_{11}} \quad (20)$$

$$S(1) = C_{11} \quad (21)$$

$$S(0) = C_{11}(1+u_{11}) \quad (22)$$

$$S(-1) = C_{11}(1+u_{11})^2 \quad (23)$$

$$S(-2) = C_{11}(1+u_{11})^3 \quad (24)$$

For Cauchy stress tensor following equations is obtained:

$$S(m) = C_{11}(1+u_{11})^{1-m} \quad (25)$$

$$\varepsilon_{ij}(m) = \\ = \frac{1}{m}\left[\begin{pmatrix} (1+u_{11})^m - 1 & 0 & 0 \\ 0 & (1+u_{22})^m - 1 & 0 \\ 0 & 0 & (1+u_{33})^m - 1 \end{pmatrix}\right] \quad (26)$$

Comparing relation (6) and (25) following equation is obtained

$$\frac{1}{(1+u_{22})(1+u_{33})} = (1+u_{11})^{1-m}$$
$$m = 1 + \frac{\ln(1+u_{22}) + \ln(1+u_{33})}{\ln(1+u_{11})} \quad (27)$$

Parameter m is a function of thickness defined by (4). By substituting u_{11}, u_{22}, u_{33} by terms (3) and (4) a functional dependency of parameter m on displacement x and k_3 is received:

$$m = 1 + \frac{\ln(1+u^0{}_{22+}k_2x) + \ln(1+k_3x)}{\ln(1+u^0{}_{11+}k_1x)} \quad (28)$$

Equation (28) describes formally Cauchy conjugated pair for uniaxial type of loading. It´s clear that the result is strongly influence by parameter k_3.

The requirement of dot product for equations (25) and (26) will be shown:

$$A = \int_0^{x_{max}} S(m)\frac{d\varepsilon_{11}(m)}{dx}dx = \\ = \int_0^{x_{max}} C_{11}(1+u_{11})^{1-m}(1+u_{11})^{m-1}\frac{du_{11}}{dx}dx = \quad (29) \\ = \int_0^{x_{max}} \frac{F_1}{l_0h_0}k_1dx$$

Theoretically the parameter "m" can reaches any value, but there is only one corresponds to Cauchy stress tensor. According to Hook law:

$$\overline{E_{11}}\varepsilon_{11}(m) + \overline{E_{12}}\varepsilon_{22}(m) - JC_{11}(1+u_{11})^{1-m} = 0$$
$$\overline{E_{12}}\varepsilon_{11}(m) + \overline{E_{22}}\varepsilon_{22}(m) = 0 \quad (30)$$
$$\overline{E_{11}E_{22}} - \overline{E_{12}}^2 - \overline{E_4}(\overline{E_{11}} + \overline{E_{22}} - 2\overline{E_{12}}) = 0$$

where:

$$\overline{E}_{12} = \nu(m)\sqrt{\overline{E_{11}E_{22}}}$$
$$\nu(m) = -\frac{\varepsilon_{22}(m)}{\varepsilon_{11}(m)} \quad (31)$$

Modules $\overline{E}_{11}, \overline{E}_{22}$ and $\overline{E}_4$ can be found. Poisson ratio $\nu(m)$ depends on choice of conjugated pair.

An invariant shear modulus $\widetilde{\overline{E_4}}(m)$ is given:

$$\widetilde{\overline{E_4}}(m) = \frac{1}{2}\left[\frac{1}{4}(\overline{E_{11}} + \overline{E_{22}} - 2\overline{E_{12}}) + \overline{E}_4\right] \quad (32)$$

In engineering practice following expression is often used:

$$G = \frac{\tau_i}{\gamma_i} \quad (33)$$

Where:

$$G = \frac{E}{2(1+\nu)} \quad (34)$$

$$\tau_i = \frac{1}{\sqrt{6}}\sqrt{(S_{11}-S_{22})^2 + S_{11}^2 + S_{22}^2 + 6S_{12}^2} \quad (35)$$

$$\gamma_i = \sqrt{\frac{2}{3}}\sqrt{\begin{matrix}(\varepsilon_{11}-\varepsilon_{22})^2 + (\varepsilon_{22}-\varepsilon_{33})^2 + \\ +(\varepsilon_{33}-\varepsilon_{11})^2 + 6S_{12}^2\end{matrix}} \quad (36)$$

In our case can be found:

$$\widetilde{\overline{E_4}} = \frac{\frac{1}{\sqrt{3}}S_{11}}{\sqrt{\frac{2}{3}}\sqrt{(\varepsilon_{11}-\varepsilon_{22})^2 + (\varepsilon_{22}-\varepsilon_{33})^2 + (\varepsilon_{33}-\varepsilon_{11})^2}} \quad (37)$$

This makes a system of equations that enables to find out values of "m" and u_{33}.

3 CONCLUSION

When evaluating the experimental data of a material, usually it is performed as a uniaxial tension test. What is actually measured is a force versus displacement curve, but in order to make these results independent of specimen size, the results are usually presented as stress versus strain. It is interesting that most, perhaps even all, stress definitions can be paired with a corresponding strain tensor. They come in pairs such that the product of the two will give strain energy. This does not mean that the corresponding pairs must be used together when performing structural analyses. But they must be when computing strain energy density. In view of the fact that the trues stress tensor is not conjugated with any known strain tensor, it is difficult to decide about suitable conjugated pair. It was shown, that for uniaxial loading of the specimen it is possible to determine to Cauchy stress tensor a suitable conjugated strain tensor. Methodology demonstrated in this work can be used for various materials loaded by uniaxial tension, e.g. for textiles, soft tissues, etc.

4 REFERENCES

1. Holzapfel G.A.: Nonlinear Solid Mechanics: A Continuum Approach for Engineering, Wiley, 2000, 470 p., ISBN 0471823198
2. Ogden R.W.: Non-Linear Elastic Deformations, Dover, 1997, 532 p., ISBN 0486696480

ESTIMATION OF FOLDING AND LUMINANCE VALUES OF POLYPROPYLENE BCF YARNS USING ARTIFICIAL NEURAL NETWORK TECHNIQUE AND MODELING STUDY

Emre Yakut[1], Cem Güneşoğlu[2], Emine Çot[3] and Volkan Balcı[3]

[1]Korkut Ata University, Department of Management Information Systems, 80000 Osmaniye, Turkey
[2]Gaziantep University, Department of Textile Engineering, 27000 Gaziantep, Turkey
[3]Kartal Carpets and Textile Company, Department of R&D, 27000 Gaziantep, Turkey
emine.cot@sanathali.com

Abstract: *Polypropylene (PP) yarn commonly used in the production of machine carpets in the world is called BCF (Bulk Continuous Filament) and the production process consists of extrusion - cooling - lubrication - gravitation - texturizing - winding - twisting. It is a fact that PP yarn has a disadvantage in terms of softness and brightness compared to acrylic, polyamide and polyester used in the production of machine-made carpets. Twisting is also an effective parameter on the sense of softness that the yarn gives. Therefore, various R & D studies are carried out to determine the effect of production parameters on softness, crimp and brightness values of PP yarn and / or to determine the production parameters required for PP yarn production with the highest values. In this study, it is aimed to develop an artificial neural network (ANN) algorithm which determines the crimp and brightness values of the heat set and freeze PP yarns by changing the BCF production parameters, the reverse engineering approach and the quantitative or categorical values of the production parameters for the yarn end with the target crimp and brightness values .*

Keywords: *Artificial neural network, BCF, polypropylene, estimation, crimp, brightness.*

1 INTRODUCTION

Synthetic yarns are widely used for the production of machine carpet in the world. Therefore, academic studies about the production and processing of synthetic fibers are increasing day by day. In recent years, polypropylene (PP) has led to its versatile and widely used in the carpet industry due to its low density, good processability, low cost, good elasticity, low melting point such as having superior properties [1].

Production processes of BCF yarn consist of extrusion – cooling – lubrication – drawing – texturized - winding and twisting. Raw material and masterbatch are mixed with certain ratio at dosing unit and filaments are passed through the spinneret holes in molten state. PP filaments are appropriately cooled and drawing process is carried out to product yarn in certain yarn count. Texturized (crimping) process is applied to yarn for bring needed bulkness and elasticity feature. Produced yarns are winded on the bobbins. Twisting and/or fixation processes are applied to BCF PP yarn that will be used as carpet yarn to take its final form.

As the BCF PP yarn passes through all these stages, the yarn number, cross-sectional area, number of filaments, extruder temperatures, godet temperatures and pressures are measured. Within the scope of this study, the effects of these parameter values on the brightness and twist of the yarn will be determined. These determined parameter values will be used in the artificial neural network methodology to develop a model that predicts the effect of the yarn on the brightness and crimp properties.

Artificial neural networks (ANN) are parallel and decentralized data processing structures that are inspired by the human brain. ANN have processing elements, interconnected by weighted connections, and each processing element has its own memory. In a typical ANN structure, the input layer gets the outer information and transmits the information (input) to one or more cells in the hidden layer without any change through the forward feed method. The hidden layer determines the match between input and output (weight function) by trial and error method (learning). In cases where the specified output values and the target output values are incompatible, the weighting functions are updated with error diffusion method. The general principle diagram of an artificial neural network model is given in Figure 1.

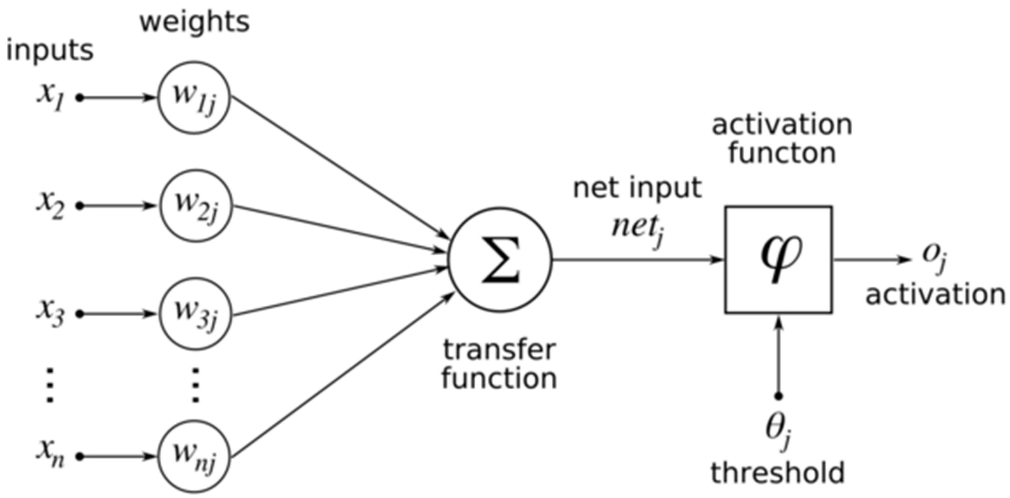

Figure 1 Artificial neural network model

2 EXPERIMENTAL

When consumer demands are evaluated in the carpet market, it seems that there is an increasing demand for softer, brighter and better resilience yarn and carpets to be produced from these yarns. In studies conducted for PP BCF yarns it is observed that changes in production parameters generally concern properties such as strength, elongation and compressibility.

Kebabcı reported that the rate of change in the spinning speed of the BCF PP yarn production and the cross-sectional shape of the yarn have a significant effect on the yarn count, strength, breaking length and the amount of spin finish oil taken by yarn [1].

Sarkeshick et al. examined the changes that the heat set process brings to nature in BCF PP yarns. Heat set operation reduces tenacity, modulus, bending rigidity, crimp and tensile values while increases the linearly density of yarns. As a result of the changes at the end of the process, the resilience values of BCF PP yarns are improved and become more suitable for carpet pile yarn. The results of the heat set effect will be used to compare the results obtained with the ANN algorithm [2]. Dadgar has studied on the estimation of heat-set PP yarn properties by artificial neural network method. It has been shown that yarn twist, yarn count and process temperature are effective on the final yarn count, yarn tension, crimp and packaging factor [3]. Demiryürek reported that the properties of polyester/viscose blended open-end rotor yarn Artificial Neural Networks (ANN) for estimation of production before production and statistical models. In conclusion, both ANN statistical models can be used for the prediction of yarn properties, however, the predictions of ANN gave more reliable results than statistical models [4].

2.1 Brightness and biological properties of BCF PP yarns

When consumer demands are evaluated, demands for softer, brighter and better resilience yarns and carpets to be produced from these yarns seem to be increasing day by day. The upgrading of the bending and compression module (increasing the softness) of the textile materials used in the carpet and the improvement of the resilience feature can be presented as a solution to the expectation in question. This viewpoint has led to various studies in order to improve the brightness, crimp, resilience and softness properties of PP BCF yarns.

BCF PP yarn of heat set, frieze or shaggy type is generally used as pile yarn in machine cases produced with wilton type face-to-face weaving technique. They affect the mechanical properties such as resilience, thickness, abrasion resistance, appearance preservation grade. Every stage of the production process has inputs that affect these properties. Their effects on yarn and carpet properties are made by collecting long-rolling production experiences and traditionally by trial and error. However, the abundance of data, the absence of a specific system for evaluation and the lack of standards in determining production parameter values have led to a lack of industrial practice following BCF yarn production. In particular, BCF PP yarn production parameters such as curl and brightness, such as extremely high commercial value of yarn properties cannot be estimated, the production parameters are changed according to the finished yarn properties are carried out by changing the process. These preliminary studies in production cause time and cost loss. All these imperfections necessitate the passage of ANN study.

2.2 Artificial neural network method

In this paper, MATLAB18 will be used for creation ANN algorithm and as the ANN algorithm feed-forward, back propagation, momentum learning rate rule, sigmoid transfer function models will be applied. The constituted ANN models for each yarn property, the model with the smallest error rate will be chosen as the best successful model. With the obtained regression equations it enables to forecast the yarn properties by the constituted models. According to the optimum BCF production conditions heat set and frieze BCF yarns will be produced and will be used for pile yarn of the sample carpets. Then the mechanical properties of the sample carpets and the current production carpets will be compared. Also it can be possible to evaluate the effect of a new spinneret flat section design to brightness of yarn.

3 RESULTS AND DISCUSSION

In this study, the BCF PP production parameters of Kartal Carpet Company were used for the data. Firstly the drawing ratio, yarn number, filament number, fixed heat, cooling heat, frieze heat and etc. were used by Meta-analyze as the scope of this Project (Table 1).

An analysis was made by MINITAB to determine the more effective parameters at the crimp value of heat set and frieze BCF yarns. As a result of this analysis the regression value is found 95.78% the effective five parameters are determined as number of twist, number of filaments, fixed heat, extruder exhausted temperature and drawing rate. Values are shown at Table 2.

Once the ANN input set was determined, the number of data variations was determined and samples were generated. The ANN module was operated until the optimal output result was achieved.

MATLAB18 software from Mathworks and the accompanying Neural Network Toolbox were used in the design and operation of the network. A feedforward back-propagation artificial neural network having two intermediate layers is formed to estimate the model with five input variables and an output variable. In Figure 2, there were 5 processor elements that provide input variables to the network and input layer contains 1 processor element which has network output of the dependent variable. As a result of the experiments performed for the number of processor elements in the intermediate layers, it was decided to have 2 hidden layers and 10 neurons.

Table 1 Parameter values of BCF PP yarn

DTex	PP	Number of twist	Number of filaments	Crimp number	Extruder exhausted temperature [°C]	Cooling temperature [°C]	Shooting rate	Texture temperature [°C]	Texture press [bar]
2600	25.9	145	255	4.74	238	19	3.2	160	7
2400	24.5	145	240	4.42	238	19	3.2	160	7
1750*2	24.5	170	160	5.67	238	18	3.3	155	7
2400*2	25.5	170	240	6.88	238	19	3.2	160	7
5000*2	24.5	140	255	9.52	238	19	3.2	160	7
2220	25.5	145	240	10.59	238	19	3.2	160	7

Table 2 MINITAB Results

Source	DF	Adj SS	Adj MS	F-Value	P-Value
Regression	8	1472.45	184.056	1178.20	0.000
PP	1	0.06	0.060	0.38	0.536
Number of twist	1	79.87	79.867	511.25	0.000
Number of filaments	1	5.63	5.629	36.03	0.000
Fixed heat	1	5.46	5.465	34.98	0.000
Extruder exhausted temperature [°C]	1	39.71	39.710	254.20	0.000
Cooling temperature [°C]	1	0.73	0.733	4.69	0.031
Fixed time [s]	1	0.91	0.911	5.83	0.016
Shooting rate	1	17.96	17.956	114.94	0.000
Error	415	64.83	0.156		
Lack-of-fit	57	15.74	0.276	2.01	0.000
Pure error	358	49.09	0.137		
Total	423	1537.28			

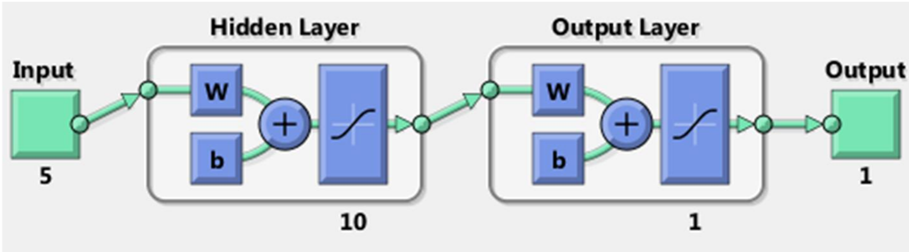

Figure 2 Artificial neural network architecture

The parameter values of the network were estimated based on the results of the experiment which gives the best error value. The selected parameter values of the network are shown in Figure3. In addition, learning and momentum coefficients, according to the results of the test that gives the least error; 0.01 for momentum and 0.09 for momentum.

After the creation of the model's architecture, the training process was started. At the beginning of the training process, the connection weights of the network are assigned randomly. 420 data was used as a training set for the training process. The remaining 150 data were separated as test data.

As a result of the experiments, a minimum error has been obtained. Since the training process is completed with a very small error rate, when the actual values and the estimated values were shown in the same graph, the values were almost overlapping. This relationship is shown in Figure 4.

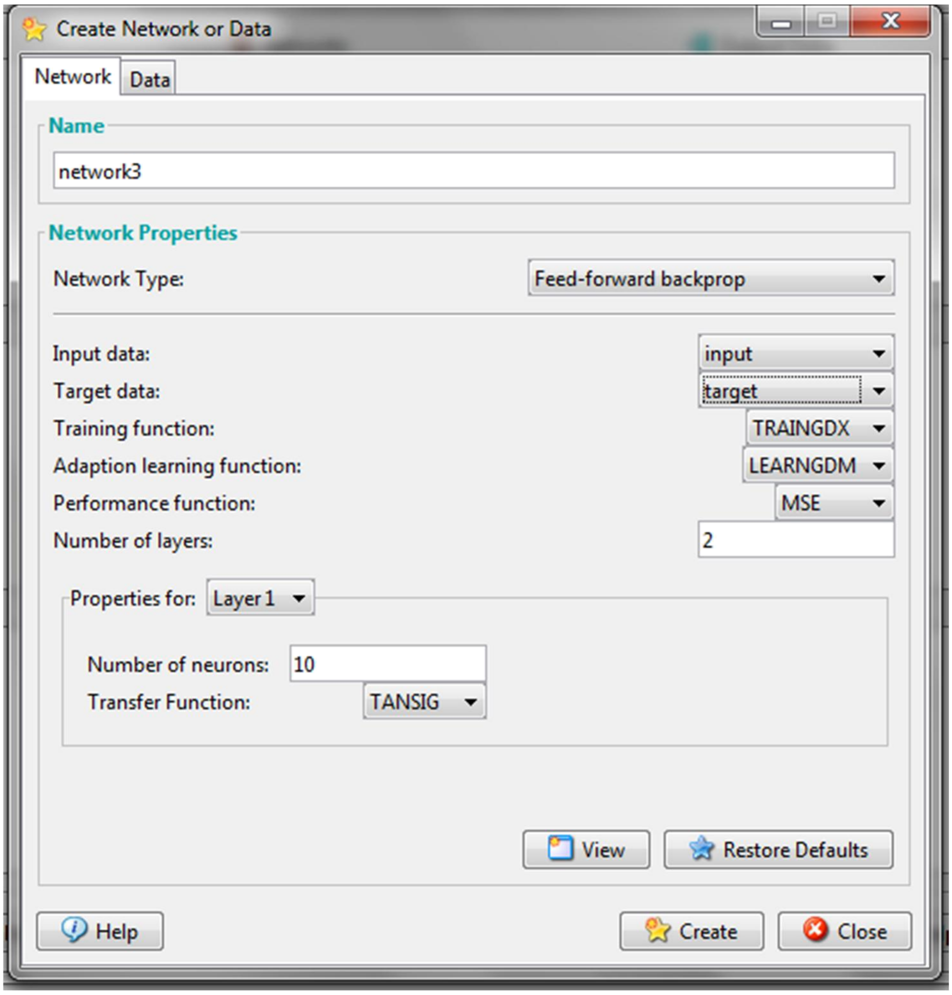

Figure 3 ANN parameters

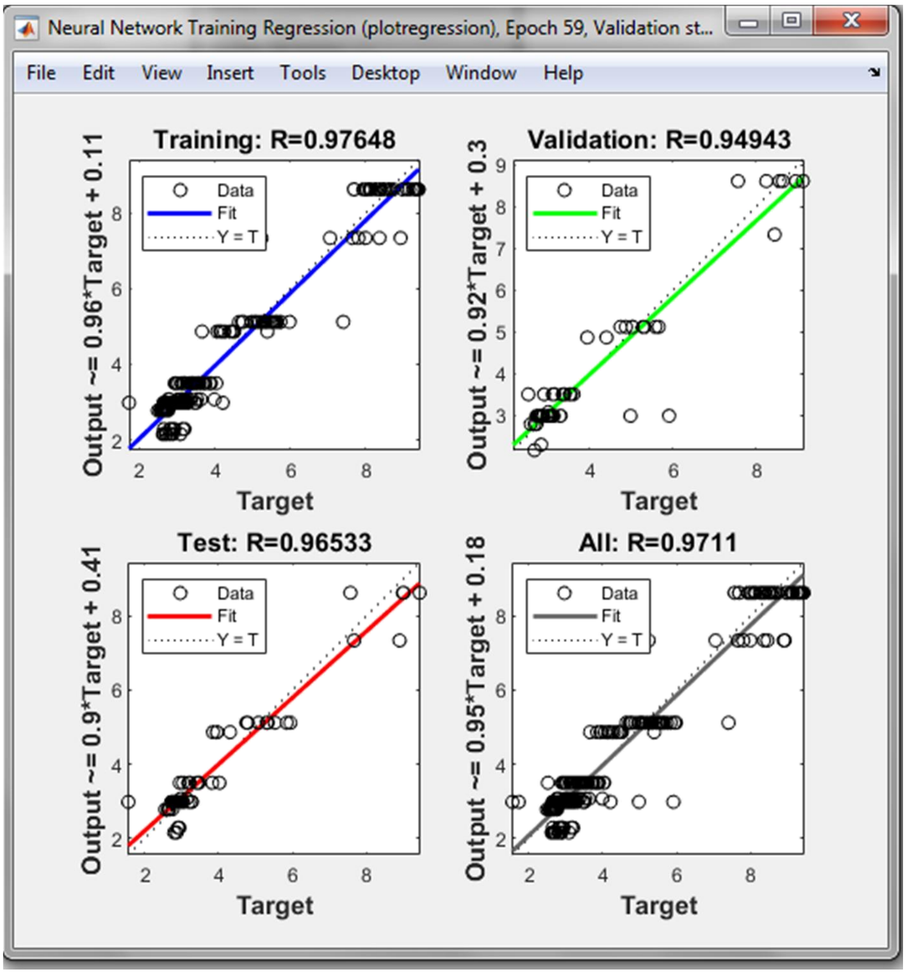

Figure 4 The regression results of ANN

Finally, the artificial neural network was asked to produce the result data for the 5 input variables that were not previously seen. The actual data and the results of the artificial neural network are shown in Table 3.

Table 3 Comparison of actual values with ANN output

Actual values	Estimated values	Difference	MSE values
2.87	2.99	-0.12	0.02
4.31	4.31	0	0.00
5.13	5.31	-0.18	0.03
4.44	4.25	0.19	0.03
5.62	5.31	0.31	0.10
3.73	2.99	0.76	0.54
2.94	2.99	-0.05	0.00
3.74	2.99	0.75	0.56
3.84	3.42	0.42	0.18

As seen in Table 3, the artificial neural network is very close to the actual values and produced results consistent with the actual values.

4 CONCLUSIONS

In this study, as a result of the evaluation of ANN algorithm, categorical and numerical data, it is ensured that outputs are obtained quickly and production parameters are optimized. In the study, 2017 data were used as network learning data, and the data for the first three months of 2018 were used in the estimation of the network.

In the study, the criteria used in the current structure were taken into consideration and the criteria which were of greater importance over the results were selected through the MINITAB program.

Then, the determined parameters the feed nets which are the most widely used in the neural networks and which give successful results were selected and the resulting error was minimized.

Thus, it is ensured that the yarn production of the BCF yarn parameters is determined by estimating the crimp values before the yarn production.

In the continuation of the study, it will be ensured that the yarn brightness data is collected in sufficient level. Then, the data will be estimated in the ANN module.

5 REFERENCES

1. Kebabci M., Babaarslan O., Hacioğullari S.O., Telli A.: The effect of drawing ratio and cross-sectional shapes on the properties of polypropylene CF and BCF yarns, Tekstil ve Mühendis (Journal of Textiles and Engineer) 22(100), 2015, pp. 47-53, https://doi.org/10.7216/1300759920152210006
2. Sarkeshick S., Tavanai H., Zarrebini M., Morshed M.: An investigation on the effects of heat-setting process on the properties of polypropylene bulked continuous filament yarns, The Journal of the Textile Institute 100(2), 2009, pp. 128-134, https://doi.org/10.1080/00405000701692429
3. Dadgar M., Varkiyani S., Merati A.: Comparison between artificial neural network and response surface methodology in the prediction of the parameters of heat set polypropylene yarns, The Journal of The Textile Institute, 106(4), 2015, pp 417-430, https://doi.org/10.1080/00405000.2014.924656
4. Demiryurek O.: Estimating polyester/visconized open-end rotor yarn properties by setting artificial neural networks and statistical models, Scientific Research Projects of Cukurova University, MMF.2005.D9, 2009

INSTRUCTIONS FOR AUTHORS

The journal ,,**Vlákna a textil**" (**Fibres and Textiles**) is the scientific and professional journal with a view to technology of fibres and textiles, with emphasis to chemical and natural fibres, processes of fibre spinning, finishing and dyeing, to fibrous and textile engineering and oriented polymer films. The original contributions and works of background researches, new physical-analytical methods and papers concerning the development of fibres, textiles and the marketing of these materials as well as review papers are published in the journal.

Manuscript

The original research papers are required to be written in English language with summary. The advertisements will be published in a language according to the mutual agreement.

The first page of the manuscript has to contain:

The title of the article (16 pt bold, capital letters, centred)

The full *first name* (s) and also *surnames* of all authors (11 pt, bold, centred).

The complete address of the working place of the authors, e-mail of authors (9 pt, italic, centred)

Abstract (9 pt, italic)

Key words (9 pt, italic)

The manuscript has to be written in A4 standard form, in **Arial, 10 pt**.

The text should be in ***double-column format*** *(width 8.1 cm)* ***in single line spacing***.

Page margins: up and down 2.5 cm; left and right 2.0 cm.

Do not number the pages and do not use footnotes. Do not use business letterhead.

Figures, tables, schemes and photos (centered) should be numbered by Arabic numerals and titled over the table and under the figure or picture.

Photos and schemes have to be sufficiently contrastive and insert in text as pictures.

Figures, tables, schemes and photos, please, send in separate file.

Mathematical formulae should be centred on line and numbered consecutively on the right margin.

Physical and technical properties have to be quantified in SI units, names and abbreviations of the chemical materials have to be stated according to the IUPAC standards.

References in the text have to be in square brackets and literature cited at the end of the text. References (9 pt), have to contain names of all authors.

[1] Surname N., Surname N.: Name of paper or Chapter, In Name of Book, Publisher, Place of Publication, YYYY, pp. xxx-yyy

[2] Surname N., Surname N.: Name of paper, Name of Journal Vol. (No.), YYYY, pp. xxx-yyy

[3] Surname N., Surname, N.: Title of conference paper, Proceedings of xxx xxx, conference location, Month and Year, Publisher, City, Surname N. (Ed.), YYYY, pp. xxx-yyy

[4] Surname N., Surname N.: Name of Paper, Available from http://www.exact-address-of-site, Accessed: YYYY-MM-DD

The final template of manuscript is available on **http://www.vat.ft.tul.cz**

Authors are kindly requested to deliver the paper (in Word form) to be published together with information about at least 3 recommended reviewers from institutions others than the parent (name, e-mail, institution, department) by e-mail: marcela.hricova@stuba.sk

After successful review procedure there is charged fee (article processing charge) of EUR 100. All articles after review process are freely available online and this fee helps to cover the costs of taking a manuscript and turning it into a finished article.

Address of the Editor Office:

Marcela Hricová

Faculty of Chemical and Food Technology,

Slovak University of Technology in Bratislava

Radlinskeho 9

812 37 Bratislava,

Slovakia

TECHNICAL UNIVERSITY OF LIBEREC
Faculty of Textile Engineering

23rd International Conference STRUTEX

Structure and Structural Mechanics of Textiles

December 2 - 4, 2020
Liberec, Czech Republic

Registration and abstract: June 30, 2020
Notification of acceptance: July 31, 2020
Submission of full text: September 30, 2020

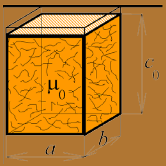

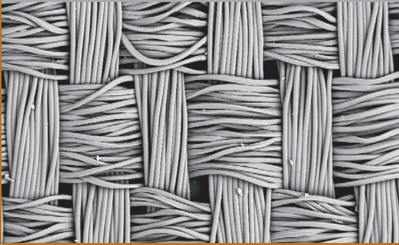

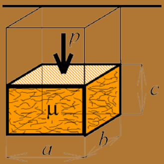

strutex.ft.tul.cz